Biomechanical Contribution of the Long and Short Heads of the Distal Biceps to Elbow Flexion and Supination Strength: Analysis of the Intact and Surgically Repaired Tendons

By

Hakim Louati

Thesis submitted to the Department of Mechanical
Engineering in conformity with the requirements
for the degree of Master of Applied Science

Carleton University
Ottawa, Ontario
August 18, 2014

Abstract

Introduction

Distal biceps tendon (DBT) tear or rupture is an acute injury in middle-aged men usually resulting from heavy-lifting activities or when the arm is used to break one's fall. Conservative and surgical treatment of full and partial tears often results in diminished elbow flexion and supination (rotation) strength. This deficiency may be attributed to treating the DBT as a singular unit. Recent anatomic studies have shown that the DBT is comprised of two distinct tendons, a short head (SH) and a long head (LH), with each having discrete attachments on the radius. The individual contribution of each of the two heads, and hence their importance to elbow function, has not been well defined. There were two major objectives of this study. Firstly, to experimentally measure the intact contribution made by each of the heads to elbow flexion and supination and secondly, to assess the effect of anatomic and non-anatomic repair following rupture of the intact tendons.

Methods

Eight fresh-frozen cadaveric arms were mounted on an in-vitro elbow simulator developed for this project, while controlled static loads were applied to the individual biceps tendons. Isometric supination torque and flexion force were individually recorded with the forearm in 45 degrees supination, neutral rotation and 45 degrees pronation. This was done with the tendons intact to assess their native contribution and then repeated after a complete rupture was simulated and repaired both anatomically and non-anatomically.

Results

In the intact biceps, the SH contributed 14% more than the LH to flexion for all forearm positions. In pronation and neutral positions the SH contributed 11% more than the LH to supination torque. In the supinated forearm, the LH contributed 2% more than SH to supination torque. When comparing anatomic and non-anatomic repairs, there was no difference in the supination torque when the forearm was in pronation. With the arm in neutral and supinated rotation, the non-anatomic repair generated less supination torque (15% and 40% less than intact, respectively). Anatomic repair reliably reproduced intact level supination torque in all forearm positions.

Discussion and Conclusion

This study demonstrates that the SH of the biceps is an especially important flexor, contributing 14% more to flexion force for the same load. The SH is also an important forearm rotator of the arm when it is in pronation and neutral rotation, with the LH playing a slightly larger role when the arm is in supination. Anatomic repair reliably restores distal biceps tendons function throughout the forearm range of rotation. If the tendon is repaired non-anatomically, the biceps will not be able to generate its full supination torque in neutral and supinated positions.

Acknowledgements

I would like to first thank my supervisor Hanspeter Frei. Your general enthusiasm and pragmatic nature were infectious throughout this process. I always left our meetings motivated to get things done.

To Andrew Speirs, my colleague and friend, many thanks for your help and support during your tenure at the Orthopaedic Biomechanics Laboratory. Your problem solving skills and knowledge are second to none.

To Philippe Poitras, thank you for kindling my interest in research and giving me my first opportunity at the OBL. I will always remember your continued support and encouragement as well as your genuine personality.

To Marc Purd'homme Foster, orthopaedic resident and friend, the early mornings and long nights spent dissecting specimens and working on the simulator are among the fondest memories of this experience.

To J W. Pollock, Steve Papp, Geoffrey F. Dervin, Peter Lapner and to the staff at the Division of Orthopaedic Surgery, I am grateful for your continued support.

I would like to dedicate this thesis to my parents, Mariem and Ali Ben Amor, in recognition of their numerous sacrifices and limitless love and support.

Table of Contents

List of Figures

List of Tables

Glossary

Avulsion – An injury in which a body structure (in this context, tendon) is forcibly detached from its normal point of insertion (bone), usually as a result of trauma or severe overloading.

Contralateral – A reference to the side of the body opposite to that on which a particular structure or condition occurs.

Distal – Farther away from a point of reference such as the midline of the body, a joint or point of attachment.

Eccentric loading – Muscle elongation while under tension due to an opposing force greater than the muscle force generated (e.g. lowering a dumbbell in a controlled manner).

Extension – The opposite of flexion, movement that straightens and increases the joint angle between any two parts. In the elbow it involves moving the forearm away from the shoulder

Flexion – The bending movement that decreases the joint angle between two parts. In the elbow it involves moving the forearm towards the shoulder.

Frontal plane – A plane that is parallel to the long axis of the body and perpendicular to the sagittal plane; it separates the body into front and back portions.

Insertion – Distal attachment site of a muscle, tendon or ligament that it "inserts" into after spanning the joint and which moves when the muscle contracts.

Isokinetic loading – Variable resistance to a muscle contraction or elongation so that movement takes place at a constant speed regardless of muscle force generated.

Isometric loading – Loading of the muscles such that muscle length does not change during tensioning, the muscle force is generated while the muscle and joint are in a static position.

Joint Stability – The Ability of a joint to withstand mechanical loading and movements without becoming dislocated, displaced or injured. Stability is provided by the bones of the joint and the soft tissues surrounding it.

Origin – The proximal, static attachment site of a muscle, tendon or ligament from which it "originates" on the bone.

Pronation – The opposite of supination, internal rotation of the forearm resulting in the palm turning backward or downward.

Proximal – Nearer to a point of reference, such as the midline of the body, a joint, or point of attachment.

Rupture /Tear – Refers to a full tear or separation of the soft tissue such as muscle or tendon. A tear can also be a partial discontinuity rather than a complete separation of the tissue.

Supination – External rotation of the forearm turning the palm forward or upward.

Sagittal plane – A plane that is parallel to the long axis of the body and perpendicular to the frontal plane; it separates the body into left and right portions.

Tuberosity – A large prominence or outcropping on a bone, serving for the attachment of muscle, tendon or ligament. A tuberosity acts as cam which improves mechanical leverage by increasing the muscle moment arm around a joint.

Valgus – Oblique displacement or outward angulation of a limb away from the midline of the body.

Varus – Oblique displacement or inward angulation of a limb toward the midline of the body.

1. Introduction and Objectives

Distal biceps tendon (DBT) rupture and avulsion are traumatic but uncommon injuries. They have a relatively low incidence rate of 1.24 per 100,000 population per year. However, they primarily affects active, middle aged men who either use their arms for physical labor (such as carpenters and mechanics), or those frequently engaging in athletic activity.[1] The rupture or tear is usually a result of forceful eccentric loading, extending the elbow, as done during a "biceps curl" or when breaking a fall with the arms.[2] The trauma most often results in either a full rupture or avulsion of the tendon at the insertion, with partial tearing of the tendon being less common. In all cases, elbow function, in the form of flexion and supination strength, is impaired.[3]

1.1 The Distal Biceps Tendon

The reason that the anatomy and mechanics of the DBT is not well understood is due to the lower occurrence of rupture-based injuries when compared to the proximal tendons injuries of the biceps. Until recently, it has been suggested that the muscle originates as two proximal heads that merge below the shoulder, forming a single distal muscle belly. This muscle belly produces a single distal tendon that twists from a predominantly frontal plane to a sagittal plane before inserting into the radial tuberosity on the proximal radius.[4] The radial tuberosity protrudes medially from the radial shaft creating a cam that extends the attachment of the biceps away from the forearm rotation axis. The rotation axis begins at the center of the radial head proximally; shifting the attachment site away from the center of the radius increases the biceps moment arm (Figure 1).

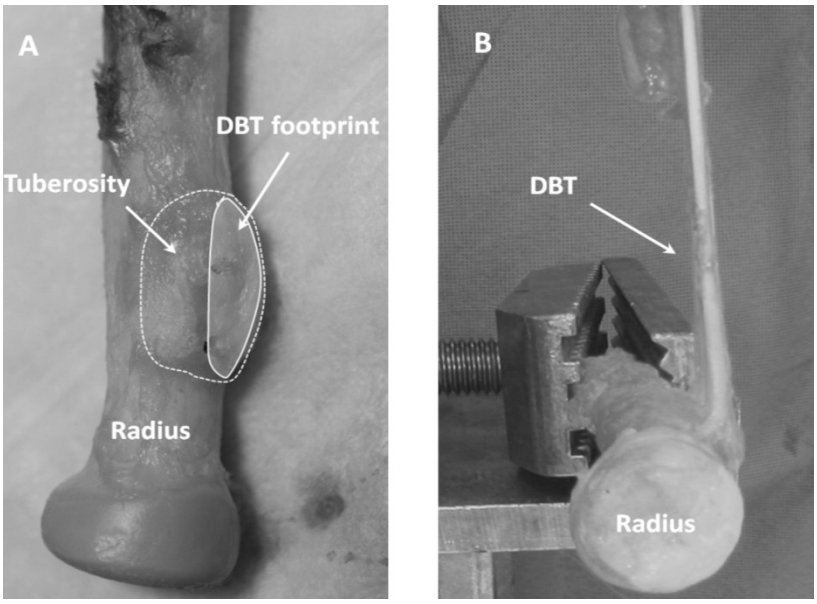

Figure 1. A – Anterior view of proximal radius highlighting the location of the radial tuberosity. B – Axial view of the proximal radius with the biceps tendon intact.[5]

Recent anatomic studies have indicated that the distal anatomy is more nuanced than previously understood and that the DBT may actually remain as two distinct anatomic and functional tendon bundles at the level of insertion into the bone.[5,6] These studies have characterized and quantified the individual head locations and insertion areas on the radial tuberosity. The short head (SH) usually has a more distal and radial attachment. The long head (LH) crosses under the SH and has a slightly more proximal and anterior insertion on the tuberosity (Figure 2).

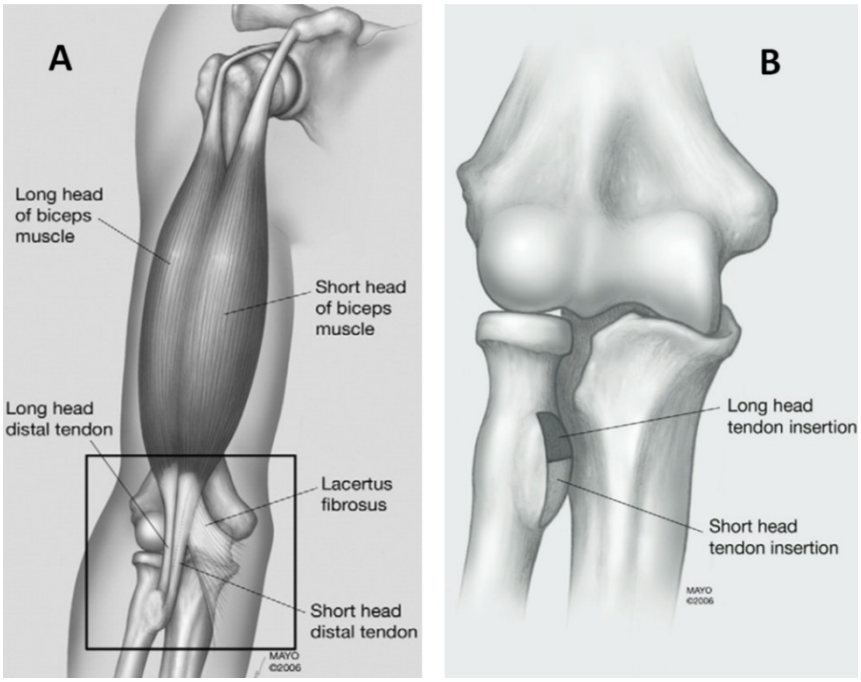

Figure 2. A – Anatomy of the biceps brachii indicating the continuous separation of the LH and SH. B – Close up of the insertion footprints of the LH and SH of the biceps onto the radial tuberosity.[5]

1.2 DBT Repair

DBT ruptures are treated in either a conservative manner with rehabilitation and rest or by surgical repair that reattaches the tendon. Non-operative treatment often results in diminished function and weakness of the elbow. Elbow flexion and forearm rotation are both affected, with reports of 30-50% loss of supination strength and 20% loss in flexion strength when compared to the contralateral limb as measured through in-vivo isokinetic testing.[7]

The primary goal of surgery is to restore normal strength to the elbow. One of two surgical approaches is typically used to repair the compromised DBT: a 1-incision (non-anatomic) or a 2-incision technique (anatomic). With the non-anatomic repair technique, the tendon is re-attached to the anterior aspect of the radial tuberosity. In the anatomic technique, the tendon is re-attached

more closely to its original anatomical insertion, on the posterior aspect of the tuberosity (Figure 3). Each repair technique has specific advantages in terms of surgical exposure, ease of tendon reattachment and rates of complication. To date, only one study has sought to assess and compare the functional results of the two techniques directly.[8–11] Henry et al. did not find a significant difference between the repairs. However the investigators did not study the DBT as the two headed complex that the recent studies indicate it is. Rather, the distal attachment was treated a as singular unit with no distinction between the two heads.

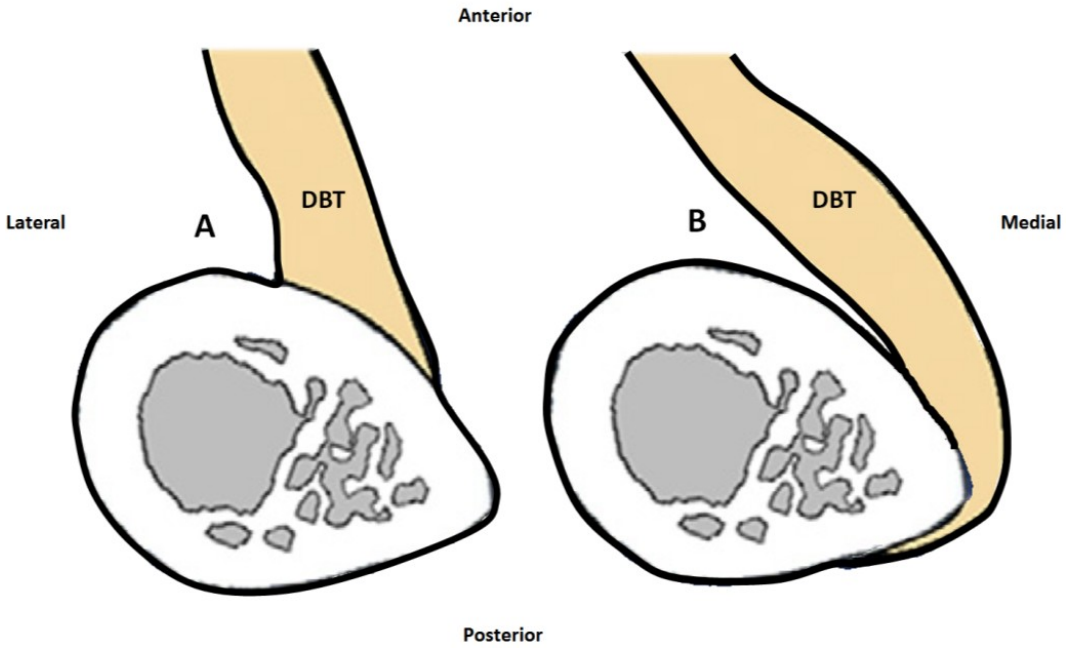

Figure 3. Axial view of the radial tuberosity and insertion of the DBT. A – Non-anatomic attachment of the DBT anterior to the tuberosity apex. B – Anatomic reattachment of the DBT, posterior to the apex.[2]

It is suspected that failure to surgically restore the discrete attachments of the LH and SH of the distal biceps may account for reduced post-operative supination strength associated with the 50%

partial rupture surgical recommendation.[12] In light of the new characterization of the DBT, understanding and restoring the anatomy of the distal biceps insertion is essential to optimizing patient functional outcomes.[13]

1.3 Clinical Relevance and Rationale

Based on anatomic studies, it appears that the SH and LH have discrete distal attachments on the radial tuberosity. The SH attaches distally and therefore may function as a stronger flexor, whereas the LH attaches more proximal and ulnar, and may have a greater contribution to supination. The individual contribution of each of the two heads to flexion and supination has not been defined. Therefore, the aim of this study is to directly measure the contribution of the SH and LH of the biceps to elbow flexion and forearm supination, and provide biomechanical evidence for what is inferred in recent anatomical studies. This project has several points of clinical relevance. It will help determine the amount of weakness expected following a partial biceps tear affecting only one of the distal tendons and if repair of a partial biceps tendon rupture (SH or LH) is indicated. The study will also help clarify the importance of an anatomic repair footprint.

The current understanding of the function of the SH and LH of the biceps at the elbow is based purely on anatomic location. At the time of starting this project there were no existing biomechanical studies quantifying the contribution of the SH and LH of the biceps tendon to supination and flexion strength. Review of the literature indicated that all relevant biomechanical studies have approached the distal biceps tendon as a singular, homogenous unit.[14–20] While the project was underway, Jarrett et al. published a study investigating the SH and LH contributions

to elbow function as proposed in this study. [21] Both studies were conducted in a parallel and blinded manner. The Jarrett results will be used in comparison with the current study findings.

1.4 Objectives

There are three primary objectives of this project.

a) To quantify the contribution of short and long heads of the bicep tendon to total biceps flexion force. This is measured at the level of the wrist while the forearm is in pronation, at neutral and in supination.

b) To quantify the contribution of short and long heads of the bicep tendon to total biceps supination torque. This is measured at the level of the wrist while the forearm is in pronation, at neutral and in supination.

c) To compare the anatomic and the non-anatomic repair of individual distal biceps tendons and their ability to restore normal elbow flexion and forearm supination torque. An anatomic repair has a footprint which is re-established posterior to the apex of the radial tuberosity while a non-anatomic repair approximates the tendon anterior to the apex.

2. Background

The relevant elbow anatomy as a whole is described in this chapter, followed by the typical range of motion and discussion of relevant biomechanical and kinematic considerations. This will drive the experiment and elbow loading design. In order to precisely describe the anatomy and position, the anatomic coordinate system will be used throughout this thesis. Figure 4 below is provided as reference to this convention.

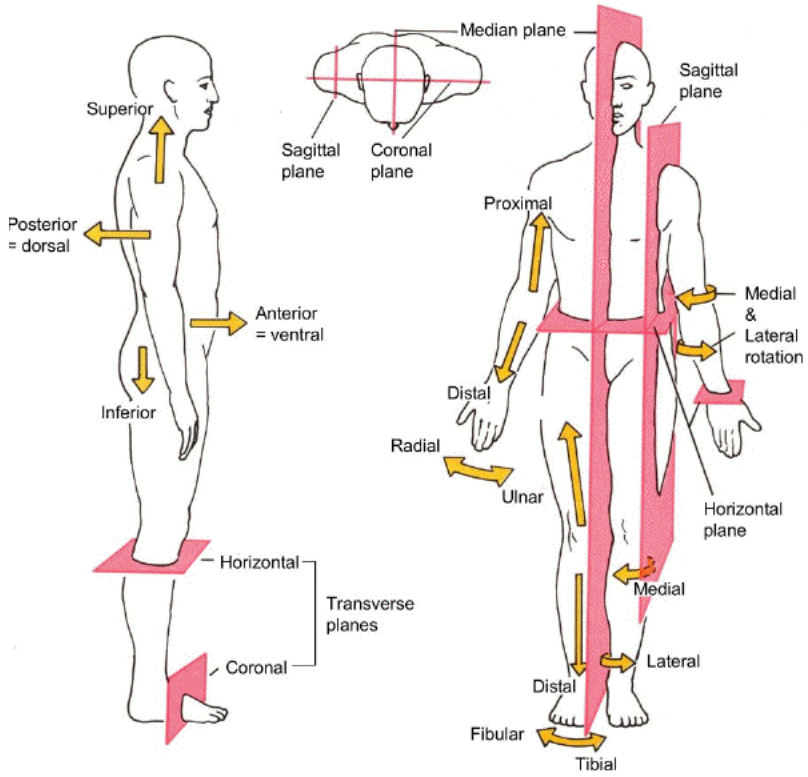

Figure 4. Anatomic definitions and coordinate system.[1]

[1] http://doctorsgates.blogspot.ca/2011/02/terms-of-position-direction-and-main.html

2.1 Elbow Joint Anatomy

Flexion and rotation of the elbow are a result of the bone geometry as well as soft tissue interactions. In order to load the biceps and study the effects of the contributions of the SH and LH and compare the repairs of DBT rupture, elbow anatomy and kinematics are reviewed in the subsequent chapters. This was done in order to identify the necessary constraints and criteria that will help drive the design of the experiment.

2.1.1 Bones of the elbow

The elbow joint is comprised of three bones: The humerus, ulna and radius. The humerus is the longest bone of the arm (Figure 5). It has a large ball-like head at its proximal end that articulates with the glenoid of scapula (shoulder blade). The distal articulating surfaces of the humerus are the trochlea and capitulum. The trochlea resembles a pulley onto which fits the trochlear notch of the ulna which swings when the elbow is flexed. The capitulum is a ball of bone that is lateral and adjacent to the trochlea on which the radial head articulates during elbow rotation. The trochlea and capitulum are bounded on either side by boney processes called the medial and lateral epicondyles respectively. Slightly superior to the trochlea are depressions on the anterior side and posterior side called fossae. Anteriorly, the coronoid and radial fossae allow for deep flexion of the elbow, while posteriorly the olecranon fossa allows for near full extension by accommodating the olecranon of the coronoid. The fossae contribute to the stabilization of the elbow by providing boney constraints to elbow motion at the extreme ranges of motion (Figure 5).[22]

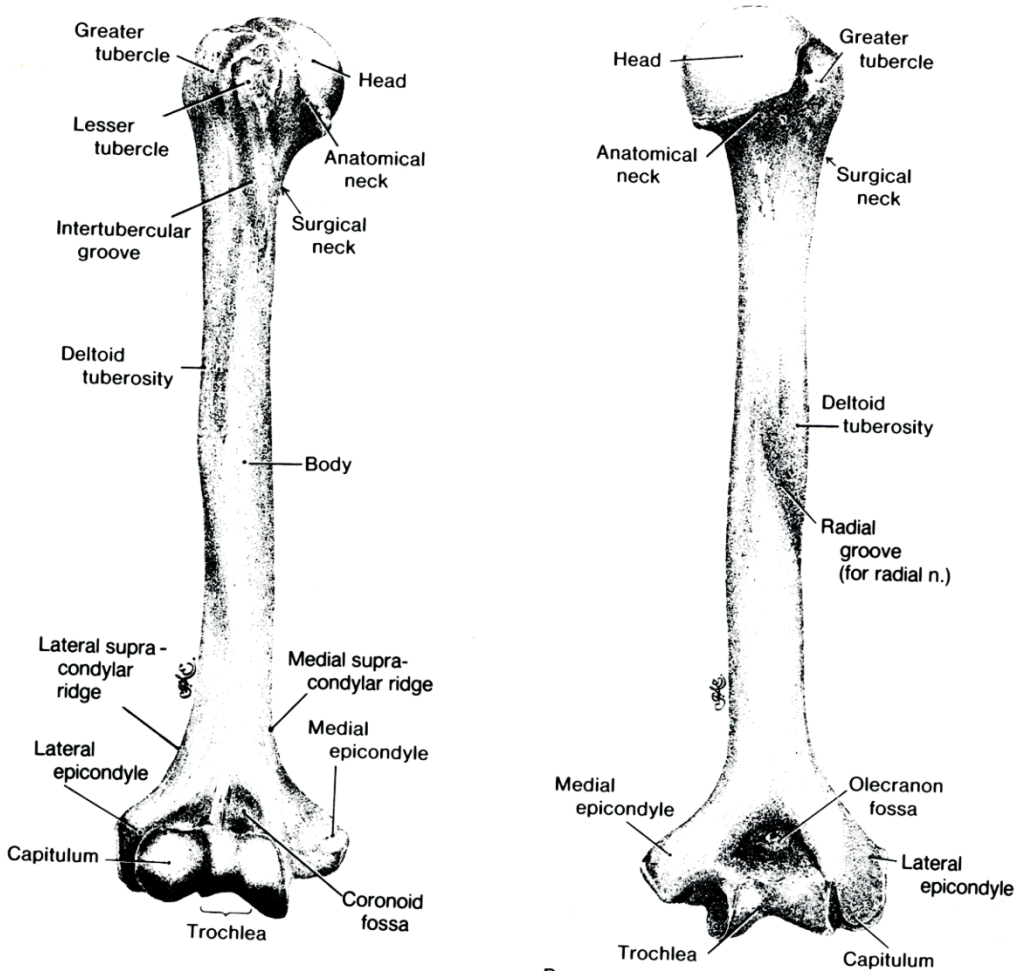

Figure 5. Anterior and posterior views of the humerus.[22]

The ulna is shaped like a "pipe wrench". The olecranon, located at the proximal end of the ulna is a prominent boney process that forms the "upper jaw" of the wrench while the coronoid process forms the "lower jaw" (Figure 6). These jaws clasp the trochlea on the humerus forming the very stable hinged elbow joint. The proximal ulna has two articular surfaces, the radial notch which articulates with the proximal radius and the trochlear notch which articulates with the trochlea on the distal humerus. The ulna is thicker at its proximal end becoming slender and smaller towards to the distal rounded ulnar head. Lateral to ulnar head is a prominent process called the ulnar styloid.[22]

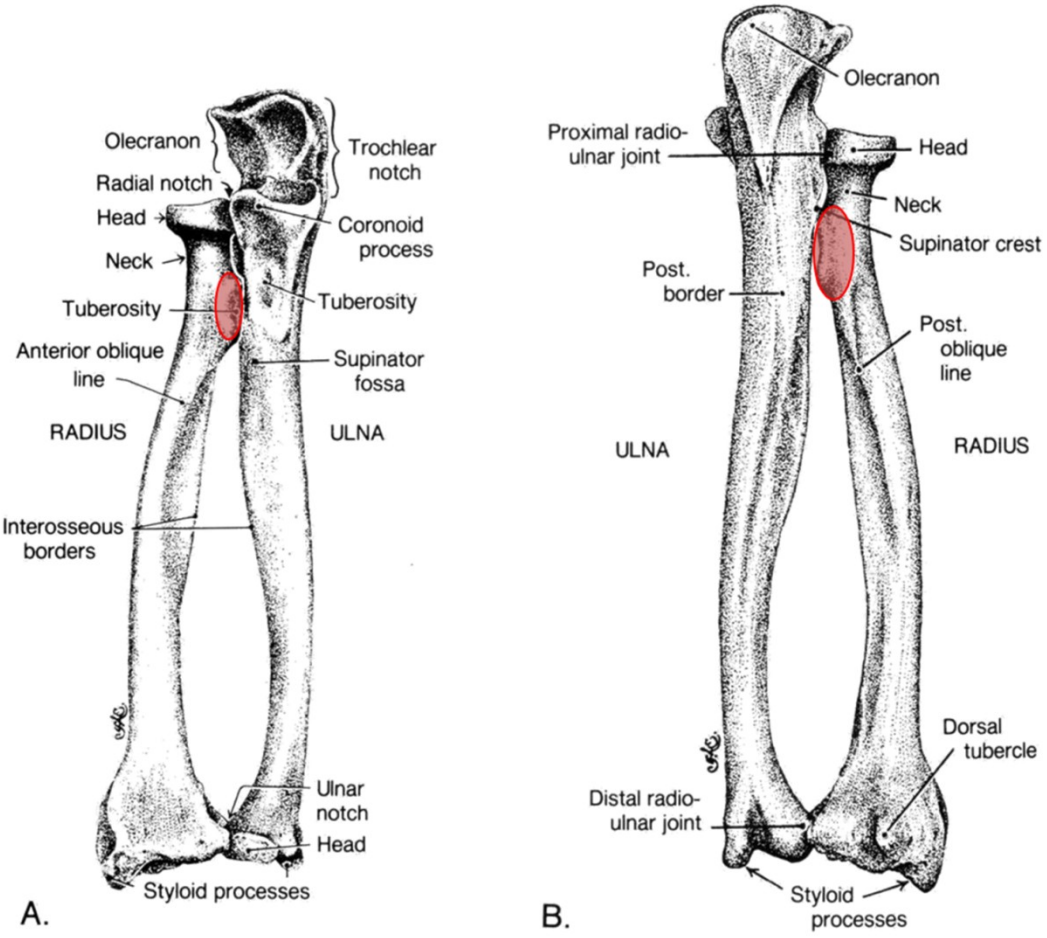

Figure 6. A – Anterior view of the ulna and radius, B – Posterior view of the ulna and radius.[22]

The radius is the shorter bone of the forearm. The proximal end of the radius has a circular, slightly concave surface, resembling a shallow dish that is congruent to and articulates with the capitulum on the humerus. Slightly distal to the radial head is the radial tubercle, a bony outcropping which serves as the insertion of the biceps tendon, as a result the radial, or bicipital tuberosity, is of particular importance this study. The tuberosity extends the biceps attachment away from the long axis of the radius making the tuberosity a "cam" that increases the moment arm and muscle efficiency of the biceps as previously discussed (Figure 3).[3] Distally the radius broadens and increases in size. It has a medial notch that articulates with the head of the ulna.

Laterally at the distal radius there is a prominent pyramidal process called the radial styloid (Figure 6).

2.2.2 Ligaments of the elbow

The elbow is a highly stable joint due to the tight congruency of the articulating surfaces, particularly as a result of the trochleo-ulnar bony constraints which stabilize elbow flexion. The joint is further stabilized by a highly fibrous joint capsule and the medial and lateral ligament bundles (Figure 7). The ligaments serve to limit non physiological joint motion. The medial bundle is comprised of the anterior, posterior, and transverse ligaments which limit valgus elbow motion. While the lateral bundle is comprised of the radial and ulnar collateral ligaments, which limit varus movement of the elbow, and the annular and accessory ligaments which stabilize the radius anterio-laterally, maintaining the radial head congruent with the capitulum and in contact with the ulna.[3]

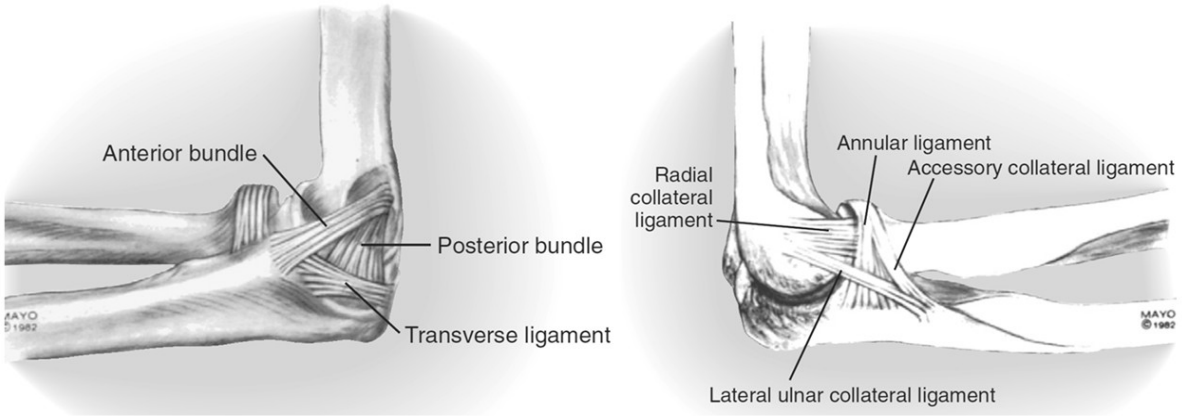

Figure 7. Medial and lateral ligament bundles of elbow.[3]

2.2.3 Muscles of the elbow

The muscles of the elbow are best categorized and described according to their roles and contributions to elbow motion. These four muscle groups are the flexors, extensors, pronators and supinators

The biceps brachii, brachialis and the brachioradialis are the main flexors of the elbow joint (Figure 8B). The biceps has two heads that originate at the scapula and span both the shoulder and elbow joints. The two distinct heads merge as they approach the insertion on to the radial tuberosity on the proximal radius. The biceps is a significant contributor to elbow flexion as a result of its large cross-sectional area despite the relatively short moment across the elbow joint. The brachialis is another significant contributor to elbow flexion. Originating on the mid-to-distal third of the humerus and inserting at the ulnar tuberosity, it has the largest cross-sectional area of any of the flexors. As a result is the greatest contributor to elbow flexion, particularly with the forearm in pronation when the biceps contribution is diminished as a result of the distal biceps tendon wrapping around the radius and reduction in its flexion moment arm. The brachioradialis is a weak flexor even though it has the longest moment arm across the elbow, due to its relatively posterior origin on the humerus and its small cross-section when compared to the biceps and brachials.[3,23]

The elbow is extended primarily by the triceps (Figure 8A). As per its name the triceps has three heads, the lateral head originates on the lateral proximal aspect of the humerus, the medial head has a broad origin on the medial aspect of the humerus and the long head spanning the shoulder joint as well as the elbow and originating on at the base of the scapular glenoid. All triceps heads insert onto the proximal ulna bone, on the supra posterior surface of the olcranon

process. The triceps is a second example of a two joint spanning muscle and as such contributes to elbow as well as shoulder extension. The second elbow extensor is the anconeus though owing to its small moment and cross section it is a weak contributor to extension compared to the triceps and serves primarily as a joint stabilizer.[3]

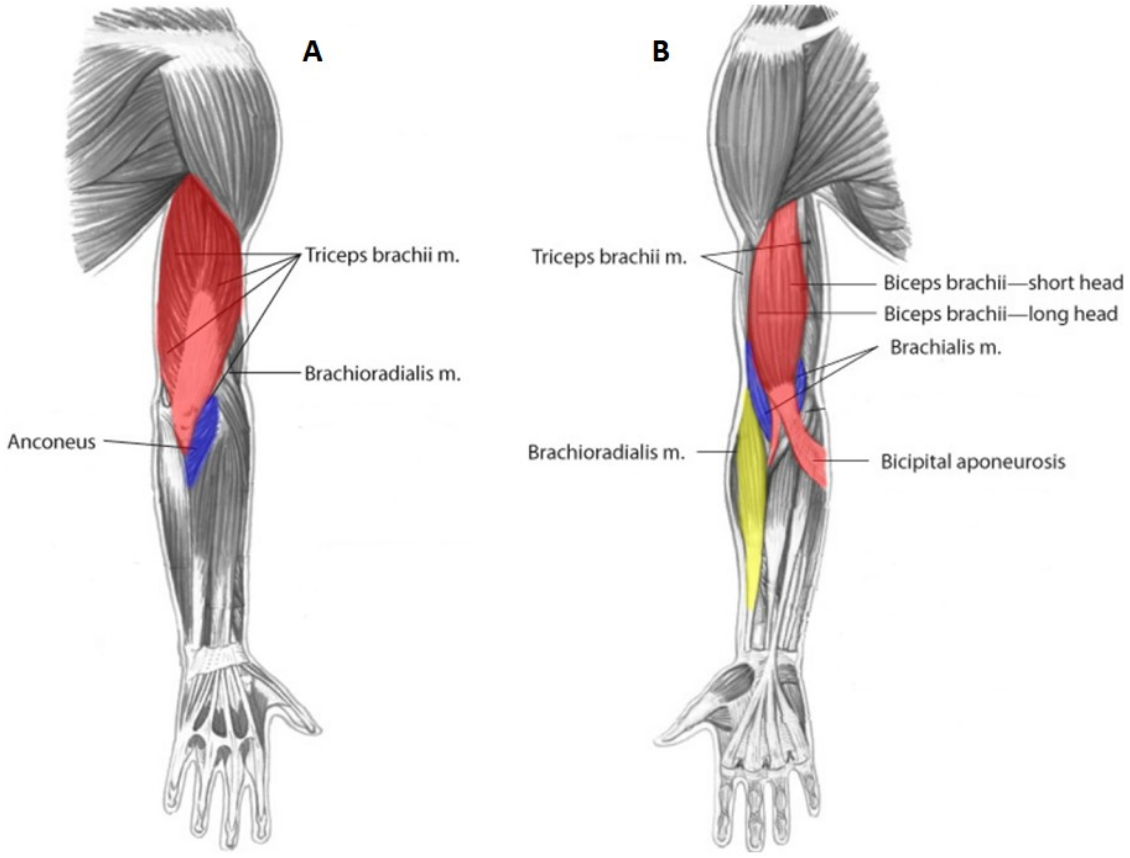

Figure 8. A – Posterior view of the arm highlighting elbow extensor muscles, B – Anterior view of the arm highlighting elbow flexor muscles.[23]

The primary pronators of the forearm are the pronator quadratus and the pronator teres. The pronator quadratus is a broad short muscle that originates on the distal ulna and inserts on the distal radius. The pronator teres has two origins, one at the medial epicondyle and a second at the

coronoid process of the ulna and inserts in the proximal third of the radius. Its line of action across the elbow makes it a weak contributor to flexion and a strong pronator (Figure 9). The brachioradilis also contributes to pronation once the arm is past neutral and in supination.

Forearm supination is driven primarily by the contraction of the supinator and the biceps brachi1with contribution to supination by the brachioradialis when the arm is in pronation. The supinator muscle originates on the lateral epicondyle and has a broad insertion into the proximal third of the radius just inferior to the radial head. While smaller in size than the biceps, the resulting line of action of the supinator and its singular role makes it a powerful contributor throughout the elbow flexion range. The biceps is another powerful forearm supinator. This is due to the wrapping of the tendon around the cam like radial tuberosity which extends its line of action away from the forearm rotation axis and increases its moment arm. Elbow motion is driven by the combination of aforementioned bones, ligaments and muscles (Figure 9).

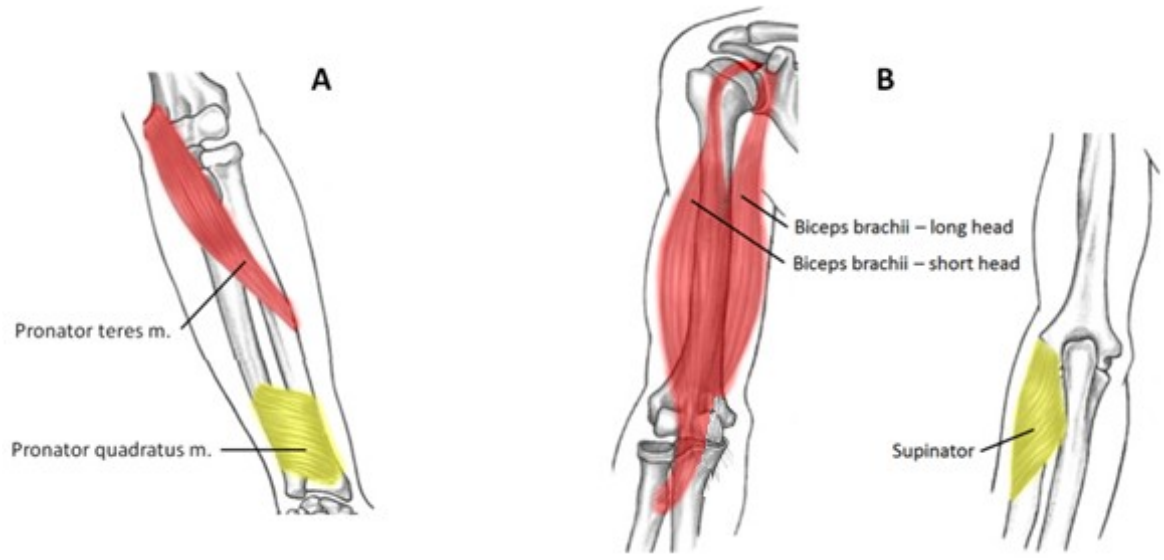

Figure 9. A – Elbow pronating muscles, B – Elbow supinating muscles.[23]

2.2 Elbow Kinematics

The elbow is considered a trochoginglymoid joint. The ulnohumeral joint is a cylindrical hinge (ginglymus) joint, allowing for motion only one plane (in this case the sagittal plane). The proximal radioulnar and radiohumeral joints are cylindrical pivoting joints (trochoid) that allow for rotation and twisting of the ulna and radius about an axis parallel to the long axis of the bones. The combination of these three articulations gives the elbow two degrees of freedom and motion: flexion-extension and supination-pronation (forearm rotation).[3] Elbow flexion is defined as the movement of the arm anteriorly bringing the wrist up towards to the shoulder while extension is the movement of the arm posteriorly (Figure 10). The normal range of motion in most subjects is from full extension or 0 degrees of flexion to 150 degrees.[3] The flexion axis of the elbow is anterior to the humeral shaft and runs through the centers of the capitulum and the trochlear groove.[24] Furthermore, the medial lip of the trochlea is larger than the lateral lip and extends farther distally; consequently the trochlear groove has a spiral contour running anteriolateral to posteriomedial. The ulnohumeral joint has a variable rotation axis rather than a singular, fixed hinge axis and elbow flexion-extension follows an oblique helical trajectory. The increasing oblique angle formed by the long axes of the humerus and ulna as the forearm extends and rotates about the spiral trochlear groove is called the carrying angle. The carrying angle is generally greater in females ranging 15-20 degrees while in males it ranges 5-15 degrees. (Figure 11).[25]

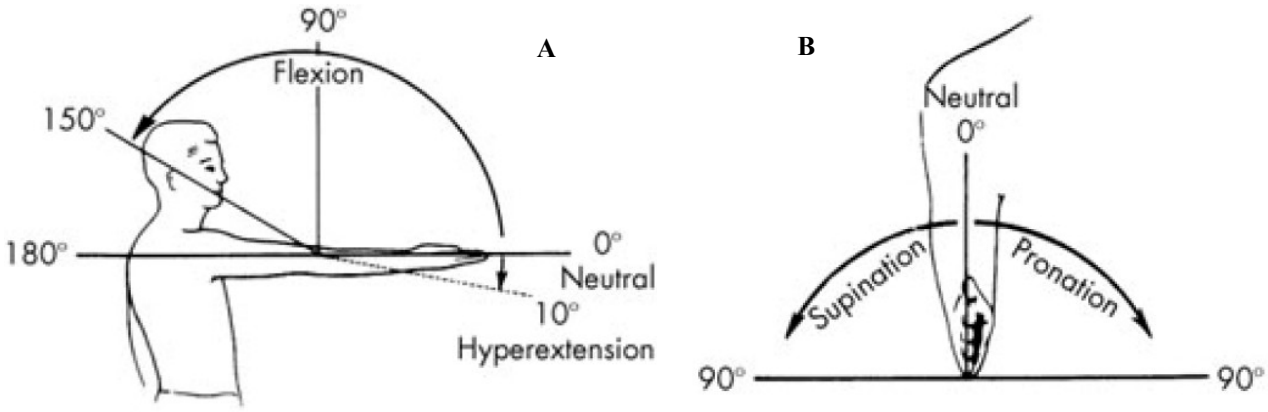

Figure 10. Elbow range of motion. A – Flexion-extension arc of the forearm bones, B – Pronation-supination radial rotation at the wrist

The reference neutral orientation for the forearm is with the wrist parallel to the sagittal plane of the body. Forearm rotation is best described at 90 degrees of elbow flexion where it is isolated from the rotation contribution of the shoulder.[3] In this position external rotation of the forearm turning the wrist upward is defined as supination while internal rotation turning the wrist downward is defined as pronation (Figure 10). Supination is a product of rotation of both the elbow and the wrist (proximal radioulnar joint and distal radioulnar joint). In the forearm the ulna is largely stationary while the radius rotates around it. The forearm rotation or pro/supination axis runs from the center of the radial head to the center of the distal ulnar head. The motion of the radius is circumferential about the ulnar head while at the proximal end, within the elbow joint, the radius pivots about it radial head. A normal subject can obtain 150-160 degrees of forearm rotation with 80 degrees of supination from neutral and 80 degrees of pronation from neutral.[3] The radius has been shown to move axially as well during forearm rotation, moving proximally with pronation and distally with supination.[26]

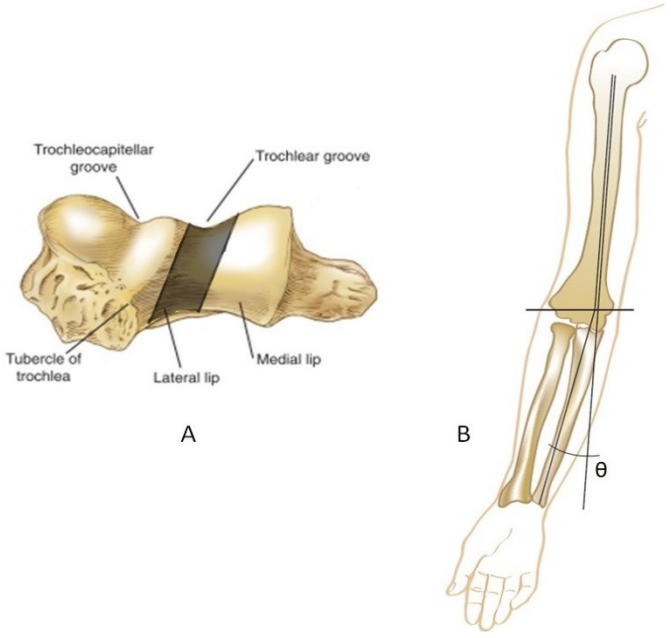

Figure 11. A – Axial view of the trochlea with the oblique angle of the trochlear groove highlighted. B – The elbow carrying angle.[3]

As can be seen from the above descriptions, while the gross joint motion can be approximated by a combination of a hinge and pivot joint, elbow joint motion in reality is more nuanced with off-axis rotations and translations that must be carefully considered when designing clamping and positioning fixtures and mechanisms. Constraining the natural kinematics of joint can result in undue stresses and reaction forces that would compound the studied variables.

3. Simulator Development

This chapter describes the design and development of the elbow load simulator. First, a literature review of relevant fixtures and simulator designs are presented. The design criteria used to drive the simulator development are then defined. The final design and modifications based on a pilot study on four specimens are then detailed. Finally, the loading and tracking capabilities of the simulator as used for the subsequent study are summarized

3.1 In-vitro loading and Elbow simulators

The primary technique for evaluating elbow muscle function has been through in-vivo assessment of isokinetic strength testing. These clinical studies are typically conducted post-surgery to assess the patient strength and the contralateral limb is used as the control for comparison. These studies continue to be of primary importance to determining surgical outcome. However due to their in-vivo nature they tend to provide a "blackbox" measure of strength. This provides limited insight into the individual muscle contributions and repair mechanics since the muscles synergize and often compensate for individual muscle deficiencies through the training effect.

In-vitro, some studies have investigated the biomechanics of various DBT repairs. The focus has largely been on evaluating the strength of the tendon repair either with sutures, suture anchors, cortical button, and interference screws[8,27–29]. However these studies tend to focus on the mechanical repair strength, and isolate and constrain the proximal radius and biceps, testing the intact or repair strength in a direct, uniaxial manner. These tests are invaluable in optimizing

technique and method of repair at time of surgery. However, they give little insight into the function and mechanics of the biceps in its role as a primary elbow flexor and supinator.

At the time of this study's conception and development, only one in-vitro study, done by Henry et al. had investigated repaired biceps supination strength by assessing the effect that attachment location has on functional outcome of the repair.[18] Henry et al. tested biceps reconstruction through a 1-incision anterior or 2-incision anterior and posterior position using bone tunnel suture fixation in cadaveric elbows. In the experiment they measured flexion and supination force at the level of the wrist arising from loading the distal biceps tendon after each repair. The distal humerus was pinned in place to stabilize the joint while the elbow was maintained at 90 degrees of flexion for the duration of the experiment. To test flexion force, the radius and ulna were then pinned together in full supination with a load cell placed at the level of the distal radioulnar joint. A 100N force was applied to the proximal biceps tendon and the resultant elbow flexion force was measured. To determine forearm supination torque, the forearm pin was removed, and the ulna was pinned at 90 degrees to the humerus. The radius was placed in neutral rotation, and a pin was inserted through the distal radius, parallel to the load cell such that supination would result in the pin applying a compressive force on the load cell (Figure 12). The 100N force was again applied to the proximal biceps tendon. The measured supination force was then multiplied by the distance from the center of the distal radius to the center of the load cell to calculate torque. While no direct justification is provided for the selected muscle force of 100N, it is a physiologically relevant load as it is 25-30% of the ultimate failure load of the intact biceps tendon (ranging from 250-360N) .[30]

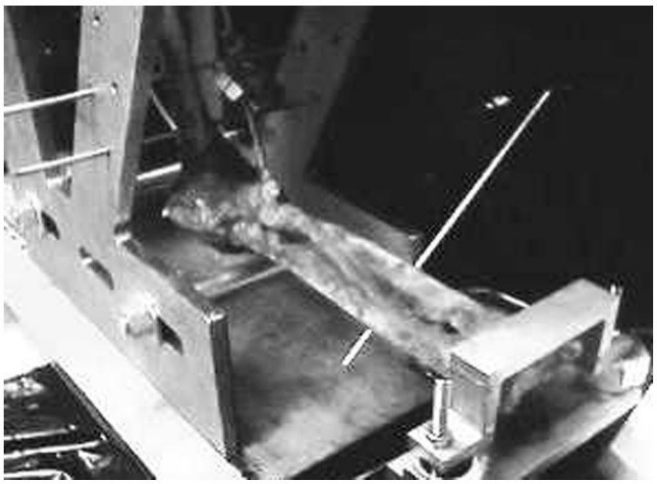

Figure 12. The Henry et al. testing apparatus showing the fixed humerus and pinning of the radius to the ulna for flexion force measurement.[18]

Many aspects of the Henry experimental design were adopted for this project. For example, Henry et al. fix the position of the humerus, the elbow joint is not externally constrained in this model and as such, no artificial reaction forces are imposed on the ulna or radius during the relevant function testing. Also testing at 90 degrees of flexion is a good design decision as it represents the angle at which biceps contribution to flexion is maximized and hence differences in the moment arm arising from the LH and SH footprint locations would be most detectable.[19]

More advanced in-vitro simulators have been developed with the aim of studying elbow motion. The University of Western Ontario (UWO) Elbow Simulator and the Allegheny General Hospital (AGH) Elbow Simulator were designed to study elbow joint motion in-vitro (Figure 13 and Figure 14).[31,32] As a result they adopt a more comprehensive approach to loading the elbow joint by loading multiple joint spanning muscles and maintaining natural joint biomechanics.

The simulators reproduce elbow motion through tensioning of elbow muscles. Both simulator designs allow for the elbows to be mounted and loaded in the vertical, varus, or valgus

orientations with the UWO Elbow Simulator also allowing for horizontal mounting and loading. Varus and valgus loading are of particular importance to the study of the elbow ligaments and stability as they are often compromised following joint trauma.[31]

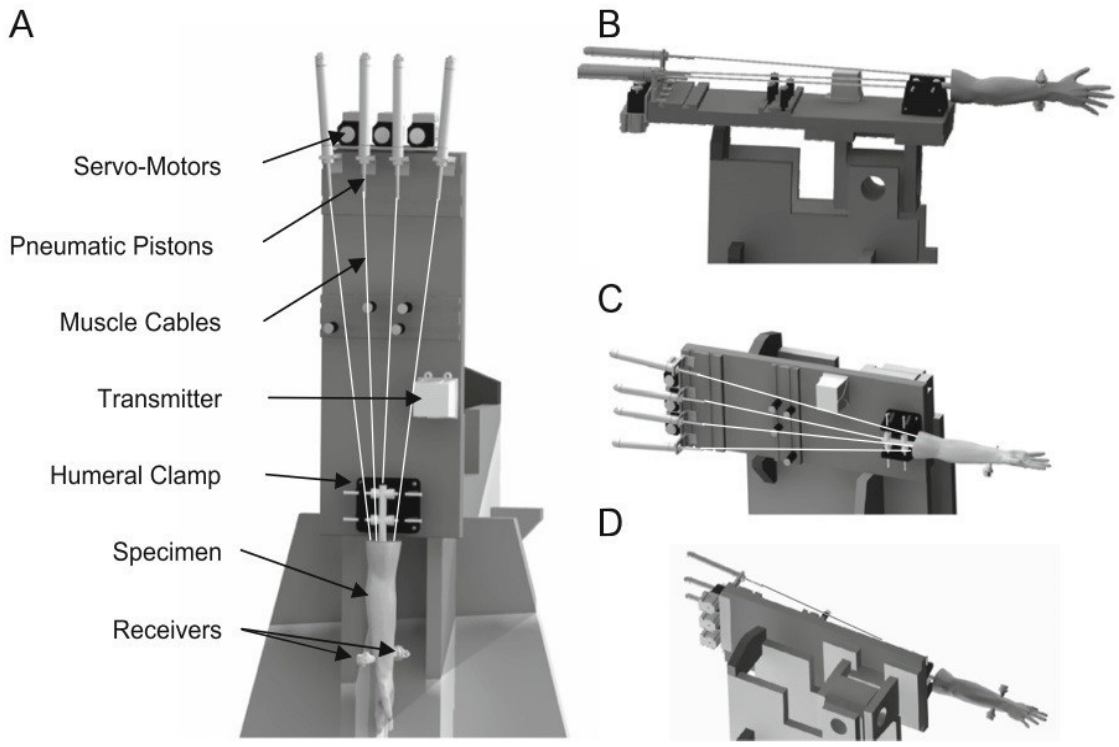

Figure 13. The University of Western Ontario Elbow Simulator shown with the elbow in A – Vertical-dependent, B – Horizontal, C – Valgus and D – Varus positions.[31]

The simulators use a combination of pneumatic actuators and servo motors to apply quasi-static or continuous loads to the various elbow flexors and extensors. The cables that attach to each tendon are routed in their respective load frames to reproduce each muscle's physiological line of action. In order to load the elbow muscles and reproduce in-vivo motion, both simulators rely on a "prime mover" loading scheme. With this technique, a single flexor or extensor is selected for direct displacement-control. A load cell is interposed in-line with the cable driving the prime

mover to provide feedback of the muscle force. This force is then proportioned to the other, load controlled muscles using set ratios. The ratios of the load through the muscles are determined through a combination of muscle cross-sectional area (CSA) and electromyographic (EMG) data. This is done to resolve the indeterminate loads in the individual muscles spanning the elbow joint. This technique has also been successfully used in shoulder joint simulators where the deltoid is designated the prime mover while the rotator cuff muscle loads are resolved as ratios of the load in the deltoid.[33,34]

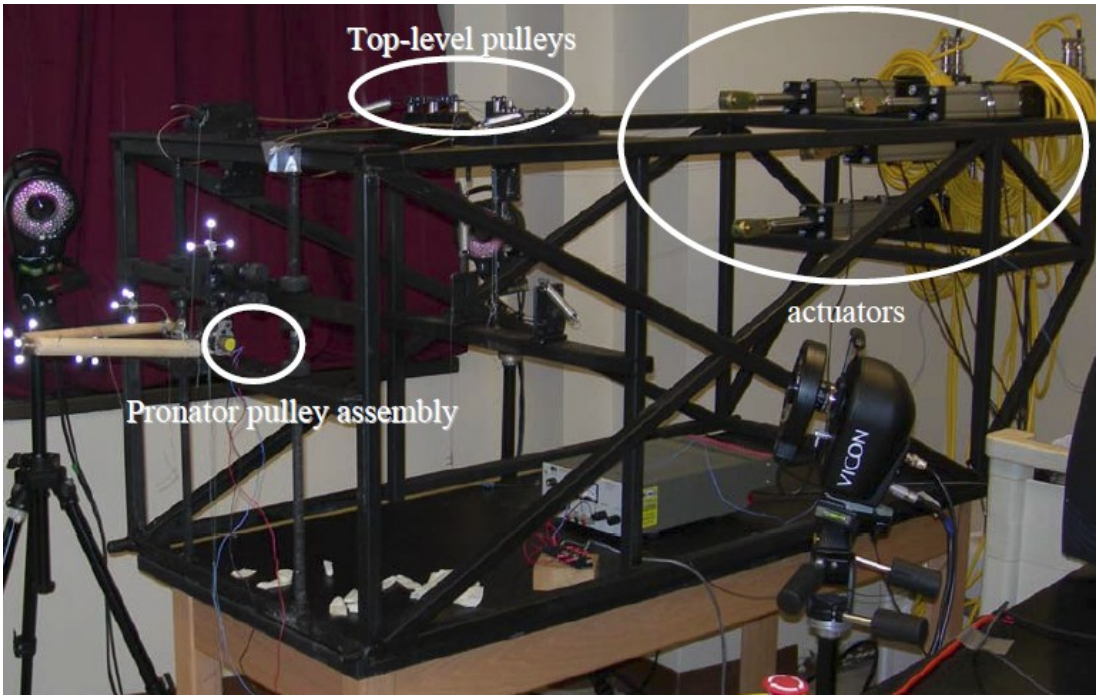

Figure 14. The Allegheny General Hospital Elbow Simulator shown in with the elbow in vertical-dependent position.[32]

Both systems employ non contacting joint tracking technology to record elbow kinematics. The UWO Elbow simulator employs an electromagnetic solution while the AGH Elbow Simulator

uses a passive tool optical tracking system. The electromagnetic system used on UWO simulator has the advantage of not requiring direct line of sight between the central transmitter and the tracked receivers that are fixed to the bones. However the system is susceptible to electromagnetic noise and interference from metallic objects in the tracking volume.[31] The optical tracking system used on the AGH simulator does not suffer from these interference issues however the required line of sight between the camera and tracked markers has posed a few technical challenges in tracking large rotations on small prosthesis components placed in the confined spaces of the elbow.[32]

Developing a similar active, feedback controlled and dynamic elbow simulator is not necessary to study the intact and repair flexion and supination force and torque. The aim of this project is to measure isometric force and torque at the level of the wrist therefore no dynamic motion simulation is required. Furthermore, developing such a simulator is beyond the scope of the project, with both the UWO and the AGH elbow simulators requiring a decade of dedicated development of the various subsystems, from the frame and cable routing, to motion tracking and load control schemes.[31,32,35] Additionally, as previously stated, both simulators measure joint kinematics as the outcome measure and neither simulator was designed to measure the loads in the distal forearm resulting from muscle loading.

However the above simulators serve as inspiration for the design of the isometric static load simulator developed for this study. Many aspects of the UWO and the AGH simulators transfer and guide the development of the proposed elbow simulator. For example, clamping the specimen, cable routing and stabilizer muscle loads are adopted from the UWO design while joint kinematics is tracked optically as done with the AGH simulator. The “prime mover”

technique for resolving muscle loads is also adopted to load the triceps and brachialis joint stabilizers.

The simulator developed for the distal biceps investigation in this thesis will be used as a "stepping stone" in beginning the development of a full motion dynamic elbow simulator. As a result, the simulator design is made with the aim of making it modular, interchangeable and easily adaptable to incrementally expanding its capabilities with subsequent projects.

3.2 Design of Elbow Simulator

The simulator design is inspired by the fixture design described by Henry et al. the UWO and AGH simulators, and the shoulder simulator developed by Poitras et al. at the Orthopaedic Biomechanics Laboratory.[31,32,34] The primary criteria used to guide the design of the simulator are derived from the requirements of the current biceps investigation and are as follows:

- the design must allow for the independent loading of the two distal heads of the biceps in order to assess the individual contributions of the SH and LH;
- the simulator must be adjustable and accommodate for anthropological variations in cadaveric specimens;
- the simulator must accurately reproduce the muscle lines of action as they cross the elbow, they should be adjustable and specific to each specimen's morphology;
- the elbow joint should not be externally constrained in order to closely mimic the unconstrained in-vivo biomechanics;

- the simulator design should allow for the evaluation of isometric flexion and supination force distal at the level of the wrist; and

- to reduce the cost and development time, the design should incorporate static weights for loading.

In future research, this first generation simulator can be modified to incorporate active and automated loading and joint motion simulation. To this end, a set of secondary criteria were identified that were deemed important to consider during this first version of the design. They are as follows:

- the simulator should incorporate a reliable technique for tracking joint kinematics. While not a requirement for the biceps investigation such a system is an invaluable tool in biomechanics research;

- the simulator design must allow for the in-situ radiographic imaging of the elbow.

- the simulator must be reasonably portable and lightweight to allow for easy integration with preexisting laboratory hardware; and

- the design should be modular, allowing for incremental upgrading and improvements to the loading and tracking systems.

With the design requirements identified, a solid model of the humerus, ulna and radius were downloaded from the Université Libre de Bruxelles (ULB) human anatomy library[2] and imported into Autodesk Inventor 2009 (Autodesk Inc., San Rafael, CA) to facilitate the design of the simulator. Detailed engineering drawings of the all the parts and assemblies can be found in Appendix G. The final simulator assembly is comprised of five subsystems or assemblies, the simulator frame, the arm fixture assembly, the load cell assembly, cable routing system and the loading assembly (Figure 15). A description of the main components and assemblies as well as design details and modifications done during the pilot phase are provided in the following paragraphs.

[2] http://homepages.ulb.ac.be/~anatemb/welcome.html (2009)

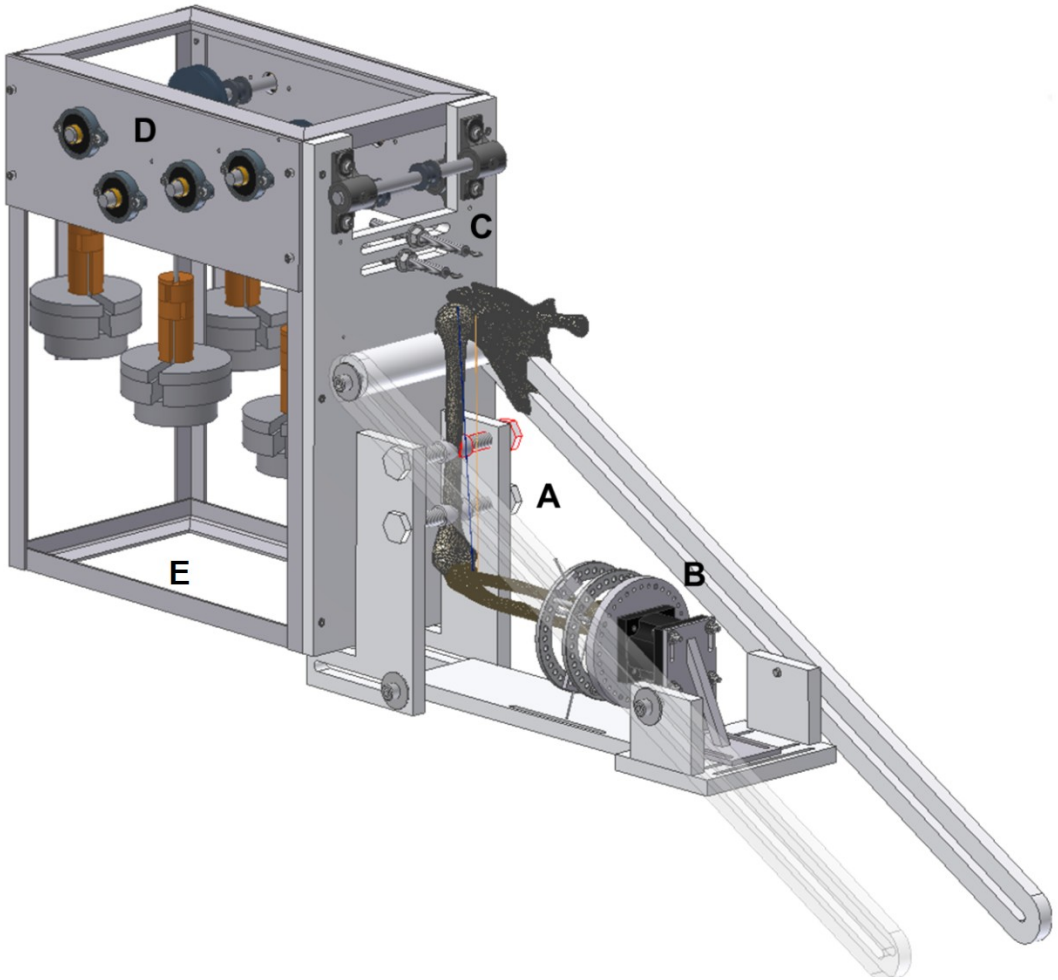

Figure 15. CAD Model of Elbow Load Simulator. A – Arm fixtures assembly, B – Load cell assembly, C - Cable routing system, D – Loading assembly and E – Simulator frame.

3.2.1 Simulator frame

The simulator frame is made from welded 6061 aluminum angle for corrosion resistance to the wet lab environment where it will be exposed to saline during the test and harsh chemicals during the cleaning and disinfection protocol following testing. It is designed to be light weight because the simulator assembly cannot be permanently attached to the multi-use load frame base, while providing the structural strength and anchorage points for the loading assembly, the arm fixtures assembly and the load cell assembly.

The frame is also designed to accommodate a clinical fluoroscopy C-arm. The frame is spaced such that the C-arm detector can be positioned right behind the Arm fixtures assembly back plate (Figure 16 A). This provides the best possible images for future investigations involving diagnostic imaging of the elbow joint during simulated loading and allows for acquisition of images at any oblique angle (Figure 16 B).

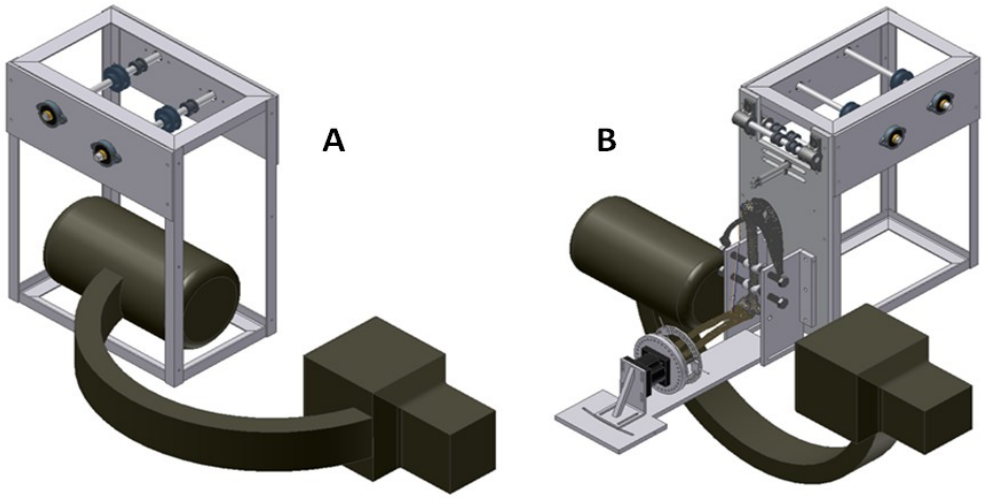

Figure 16. Frame C-Arm accommodation. A – AP projection, B – Lateral projection.

3.2.2 Arm fixture assembly

The arm fixture assembly is comprised of the humerus clamp, the main back plate, forearm base and load cell braces (Figure 17).

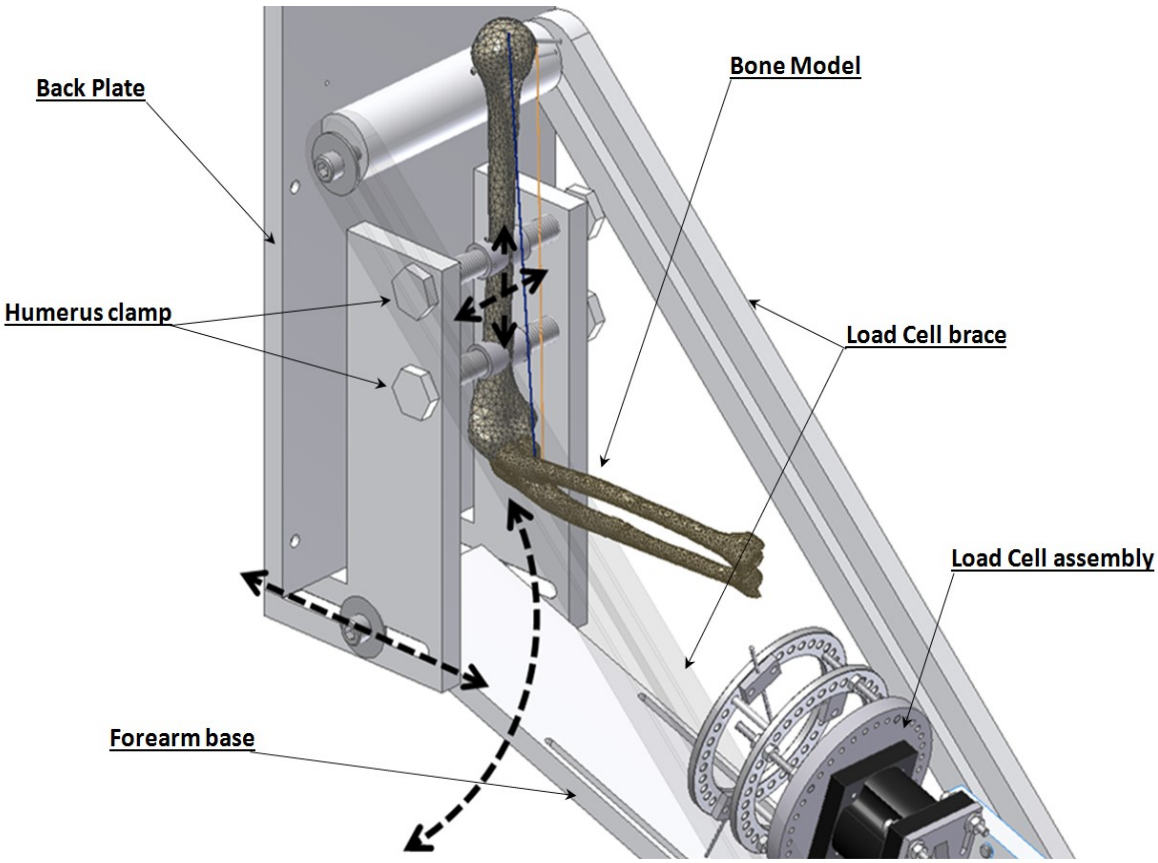

Figure 17. Arm fixtures assembly.

The assembly is mainly machined from Delrin. Delrin was selected due to its radiolucency which would allow for unobstructed radiographic imaging. It also has excellent machinability and corrosion resistance. The arm is attached to the simulator by self-adjusting clamps. The humerus is typically attached midshaft and at its distal third by the four serrated aluminum tipped screw clamps. The screw clamp assembly allows for medial-lateral and superior-inferior adjustment of the humerus (and hence whole arm). At its proximal end, the forearm base attaches to the base clamp side walls. The design allows for the forearm brace pivot point to be translated backwards and forwards to accommodate the large variation is forearm length. The translating pivot allows for the forearm brace to track with the arm through its 150 degree flexion arc. The load cell

assembly is attached to the distal end of the forearm brace. The weight of the load cell assembly is supported by the load cell braces on either side of the forearm base. The load cell assembly can be fixed to the forearm brace at a wide range of rotations and translations to accommodate the flexion angle dependent carrying axis in both left and right arms and the variations in valgus and varus due to forearm rotation (Figure 18). This feature is critical to ensuring no external stress is applied to the elbow when the load cell is in contact with the forearm.

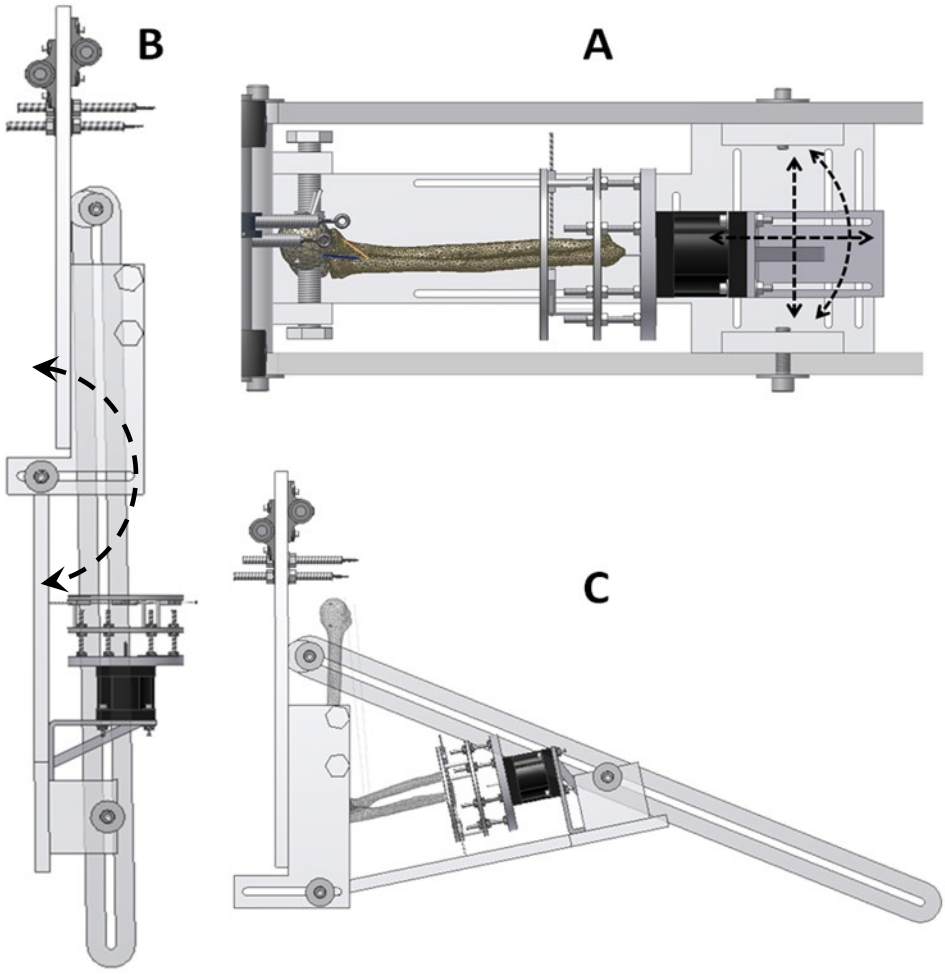

Figure 18. A – Top view of forearm brace indicating the wide range of angles and lengths at which the load cell can be positioned, B – Simulator at full extension showing the need for a translating forearm base pivot, and C – Simulator at an acute flexion angle.

3.2.3 Load cell assembly

The load cell assembly is positioned at the distal end of the forearm. It is comprised of an external fixator, a load cell adapter, a six axis load cell and the load cell bracket (Figure 19). The flexion and supination forces at the distal ulna and radius are transferred to the load cell by an external carbon fiber Ilizarov fixator. This fixator is typically used to stabilize bone fractures but in the load cell assembly, it is used because it allows for flexible guiding and positioning of the radius and ulna in the simulator. As discussed in Section 2, the distal radius rotates about the stationary ulna during pronation and supination. The fixator rings have a total of 32 equidistant 7 mm holes. This allows for the reproducible positioning of the radius at the required measurement rotation angle. In the current study, the supination torque was measured at three different forearm orientations under three different distal biceps conditionings. Therefore, it is essential that the radius orientation is reproduced for each of the three different conditions (intact, following anatomic repair and following non-anatomic repair). The load cell adaptor is used to transfer the forces on the external fixator to the load cell. A 4 mm center hole is drilled into the load cell adaptor that is aligned with center of the load cell and allows for the measurement of pure reaction forces. This was an essential modification as off-axis loading of the load cell produces significant cross talk and compounds load cell readings (Appendix C).

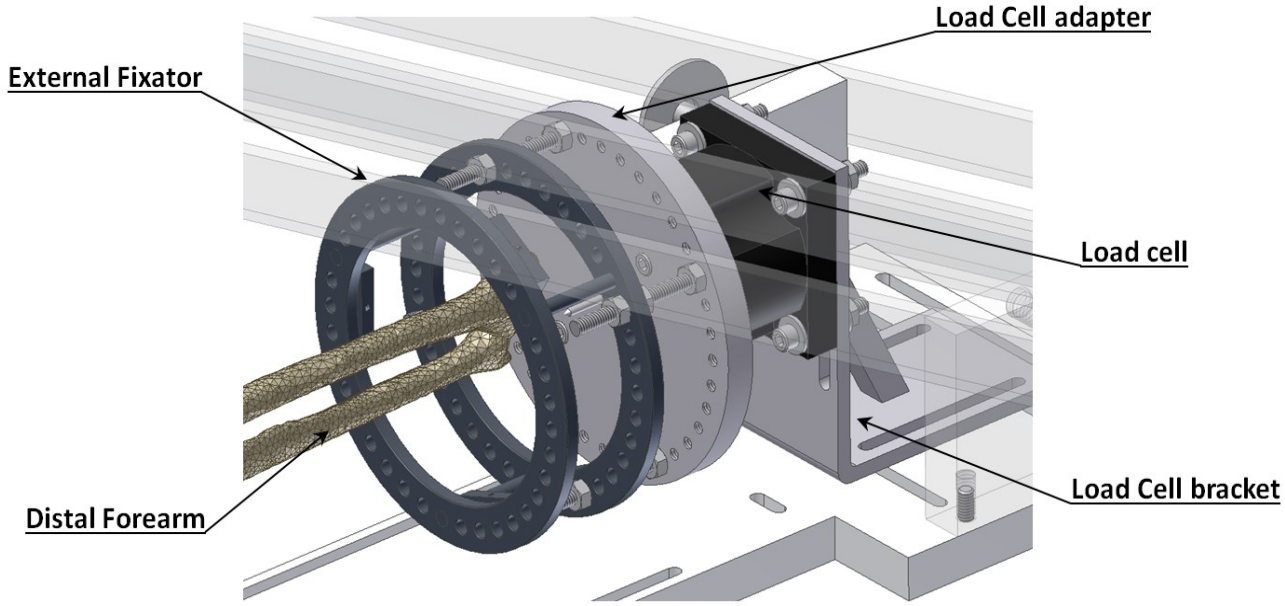

Figure 19. Load cell Assembly.

An MC3A-100 six axis load cell (AMTI, Watertown, MA, USA) is used to measure the resultant forces at the level of the wrist due to muscle loading with the simulator. The load cell is designed to resolve forces and moments along the three Cartesian axes. The 100 series load cell has a force and torque range of 222N and 11Nm respectively. The load cell and attached fixtures are secured to the forearm brace with an aluminum reinforced L-bracket which mitigates the cantilevering effect. The load cell assembly as a whole is designed to be a self-contained module that can be positioned independent of the forearm brace and other simulator components, in order to accommodate the wide range of variability is specimen morphology.

The flexion force and supination torque were measured separately since the initial, combined and constrained loading introduced significant experimental error during the piloting phase (Appendix C). The final methods for unconstrained flexion force and supination torque transfer are described in Section 3.2.3.1 and 3.2.3.2.

3.2.3.1 Unconstrained Flexion Force Measurement

For evaluating muscle contribution to flexion force, the radius was first pinned to the ulna in the required supination angle (Figure 21). A 100 mm long 3 mm diameter pin was drilled into the medullar canal along the long axis of the ulna, leaving 2cm protruding distally. The protruding end of the rod was than inserted into the 4 mm center hole in the load cell adapter (Figure 22). This served to align the load cell with the long axis of the ulna and reduced the load transfer connection to a simple pin connection transferring only forces and eliminating any reaction moments. The axially unconstrained design also eliminated any axial loading and other off-axis loads by aligning the load cell assembly with the long axis of the humerus.

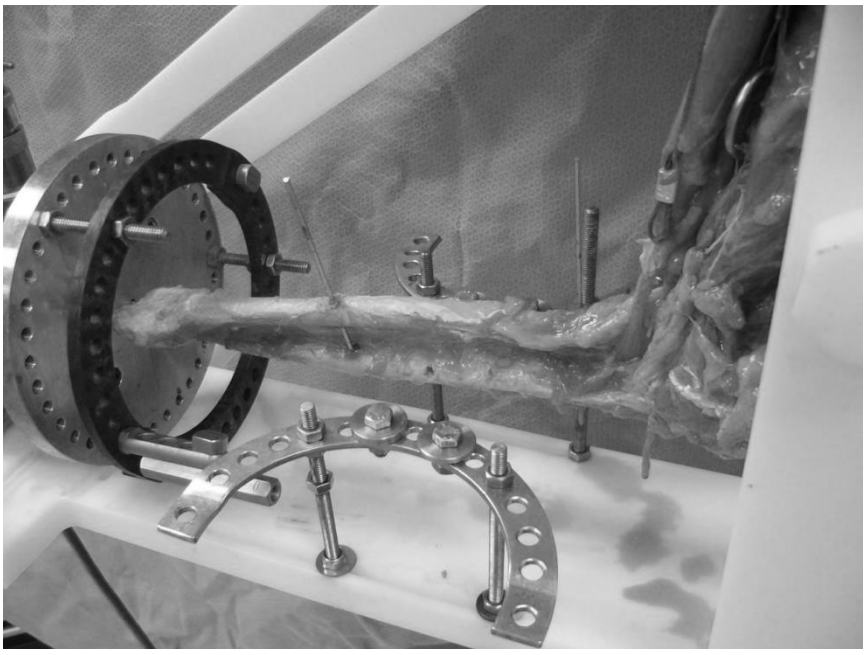

Figure 20. Radius pinned to the ulna when measuring flexion force.

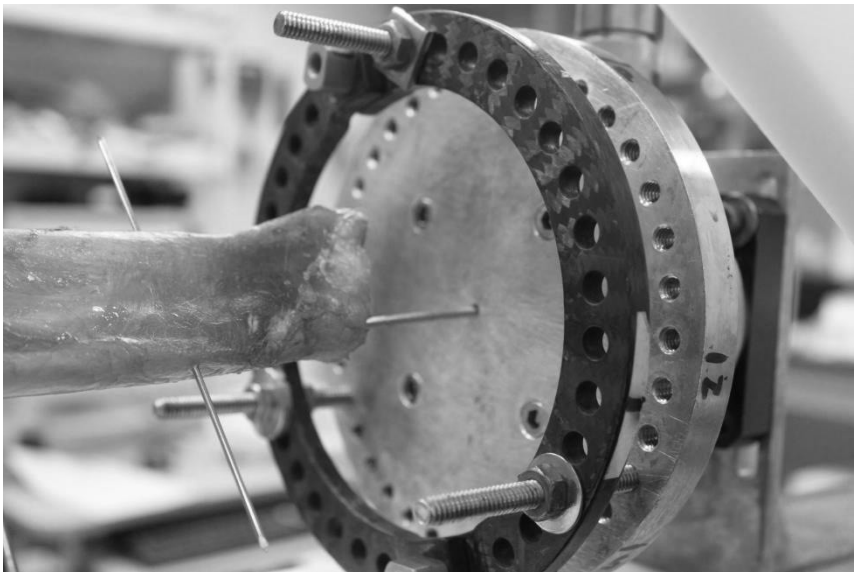

Figure 21. Ulna is attached to the center of the load cell adapter with a sliding pin for flexion force measurement.

3.2.3.2 Unconstrained Supination Torque Measurement

In the modified design, supination torque is measured directly at the distal radius by unpinning it from the Ulna. The supination effect of the biceps is isolated by fixing the ulna to the forearm base such that the flexion force component is eliminated. The load cell is centered about the ulna using the same ulnar pin used for flexion measurement; however, it is backed out of the adapter hole so that no force is transmitted through it. A transverse pin is drilled through the radius bisecting the distal radius at the level of the radial styloid. Two opposing posts are erected on the external fixator corresponding to the forearm rotation angle to be assessed. The free ends of the transverse pin are then balanced on the erected pins. Loosening the load cell assembly from the forearm base then allows it to self-align, such that the torsion load is balanced across both opposing posts and off-axis forces are diminished (Figure 22).

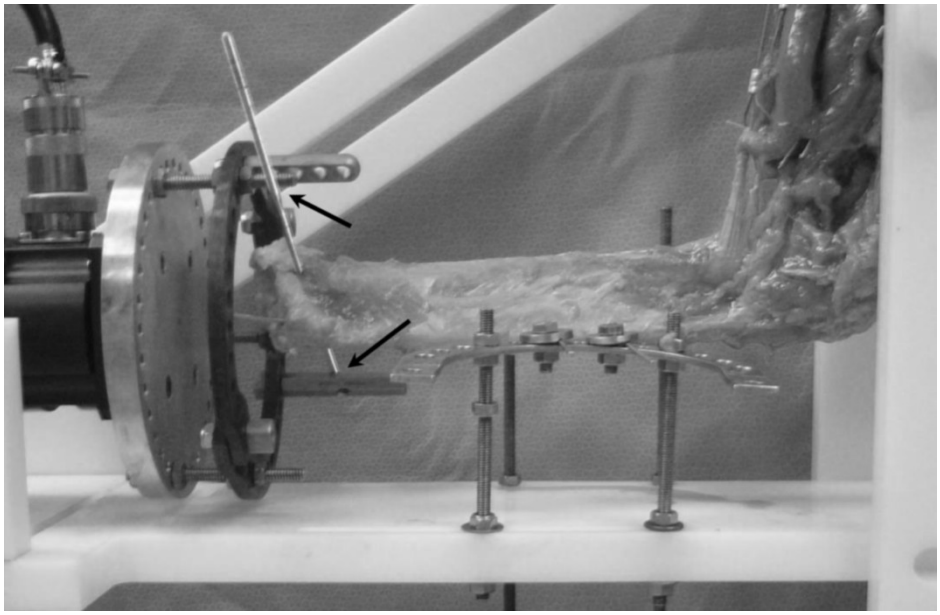

Figure 22. Transverse radial pin transfers supination torque by balanced loads on the fixator posts. The black arrows indicate the balanced contact points on the load cell.

3.2.4 Cable routing system and muscle loading assembly

The cable routing system is comprised of an eyelet that is screwed into a threaded rod and an alignment shaft and pulley for each muscle that is loaded (Figure 23).

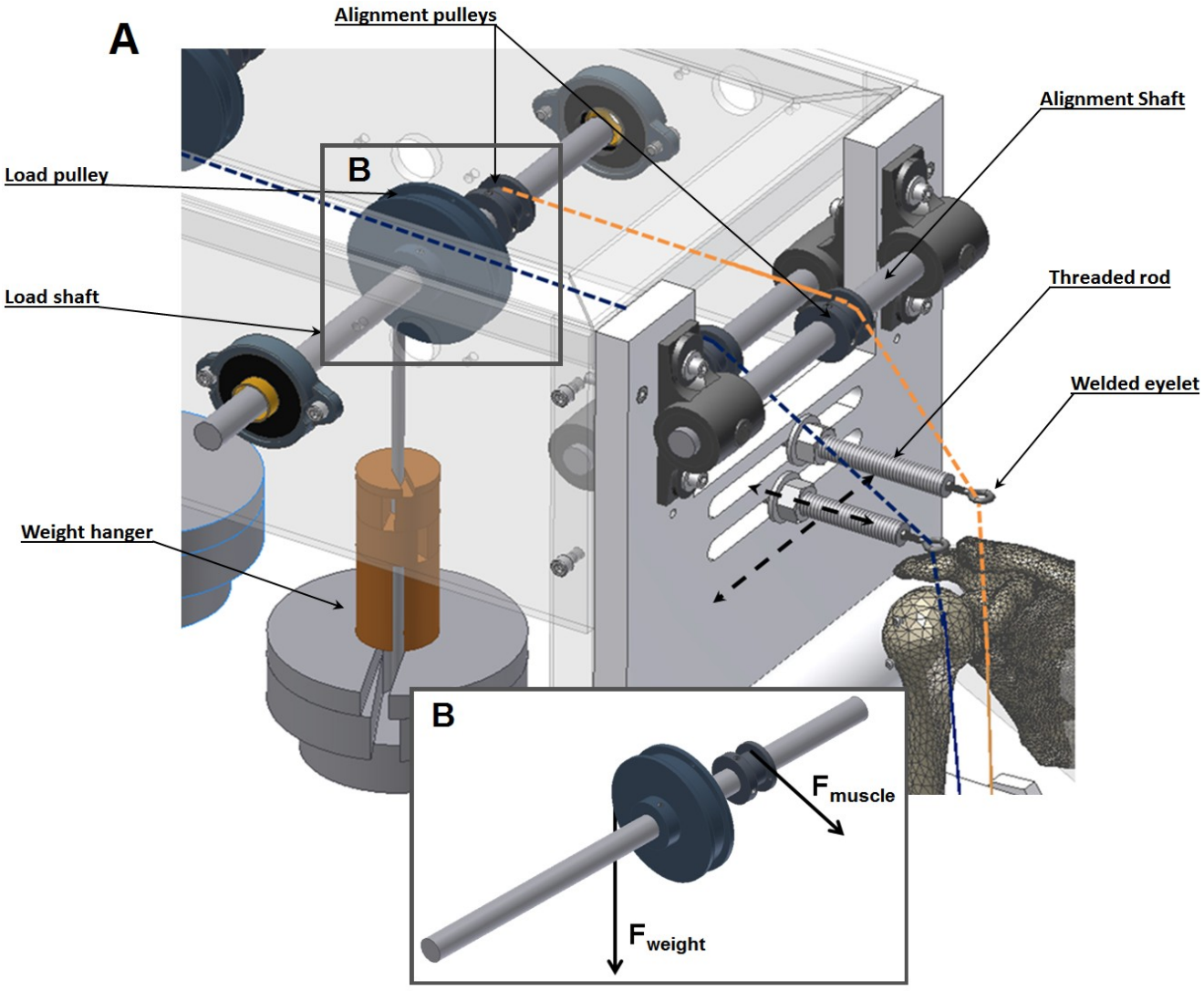

Figure 23. A – Cable routing and muscle loading assembly. B – Load shaft assembly.

Polymer coated aircraft cables, 1/16" in diameter, are used to load and route the muscle forces. Each muscle cable is routed through the alignment pulley and threaded through its own respective eyelet prior to attachment to the muscle tendon. The back plate is slotted to allow for medial-lateral adjustment of the alignment rods. The threaded alignment rods can also be backed or advanced. This gives the eyelet complete planar freedom of motion to match the muscle load vector in the specimen (Figure 24). The eyelet loops are welded to ensure a smooth sliding

interface and minimize friction. A post study analysis of the friction losses was conducted and is described in the limitations (Section 6.4).

Figure 24. Cable alignment reproducing the proximal LH and SH of the biceps vectors.

The alignment shaft and pulley direct the cable to the load shaft. Two pulleys are mounted on each stainless steel load shaft. The shaft rotates on bearings (eccentric collar locking type, SA202-10, KML Bearing Canada Inc, Dorval, QC) mounted to the side walls of the elbow simulator. The alignment pulley is adjusted along the length of the shaft with set screws to align its center with the alignment shaft of the respective muscle. On the load shaft assembly, the outer diameters of the load and alignment pulley are designed for an effective ratio of 2:1 to reduce the required static weights (Figure 23 B). Each muscle is loaded via calibrated weights on a weight hanger (Troemner, Thorofare, NJ).

In its current iteration the simulator accommodates loading the biceps LH and SH separately. Additionally the triceps as the primary elbow extensor and the brachialis as the primary elbow

flexor are also loaded to stabilize the joint. The biceps loads used for this study were chosen to allow for comparison with Henry et al. and are 25-50% of the ultimate failure load of the biceps (80, 120, and 160N distributed evenly between the SH and LH, compared to the 100N on both heads used in the Henry study). The support muscles loads are calculated as ratios of the biceps loads based on their EMG activation and muscle cross-sectional area.[36,37] Specifically, the biceps load is used as the "primary mover" and the support muscles are 1:1.2 and 1:3 of the biceps load for the brachialis and triceps respectively.

The adjustments to distal forearm loading and joint stability as well as other smaller modifications to the design were made during the piloting phase of the simulator design. The final simulator as used for this biceps investigation is pictured in Figure 25.

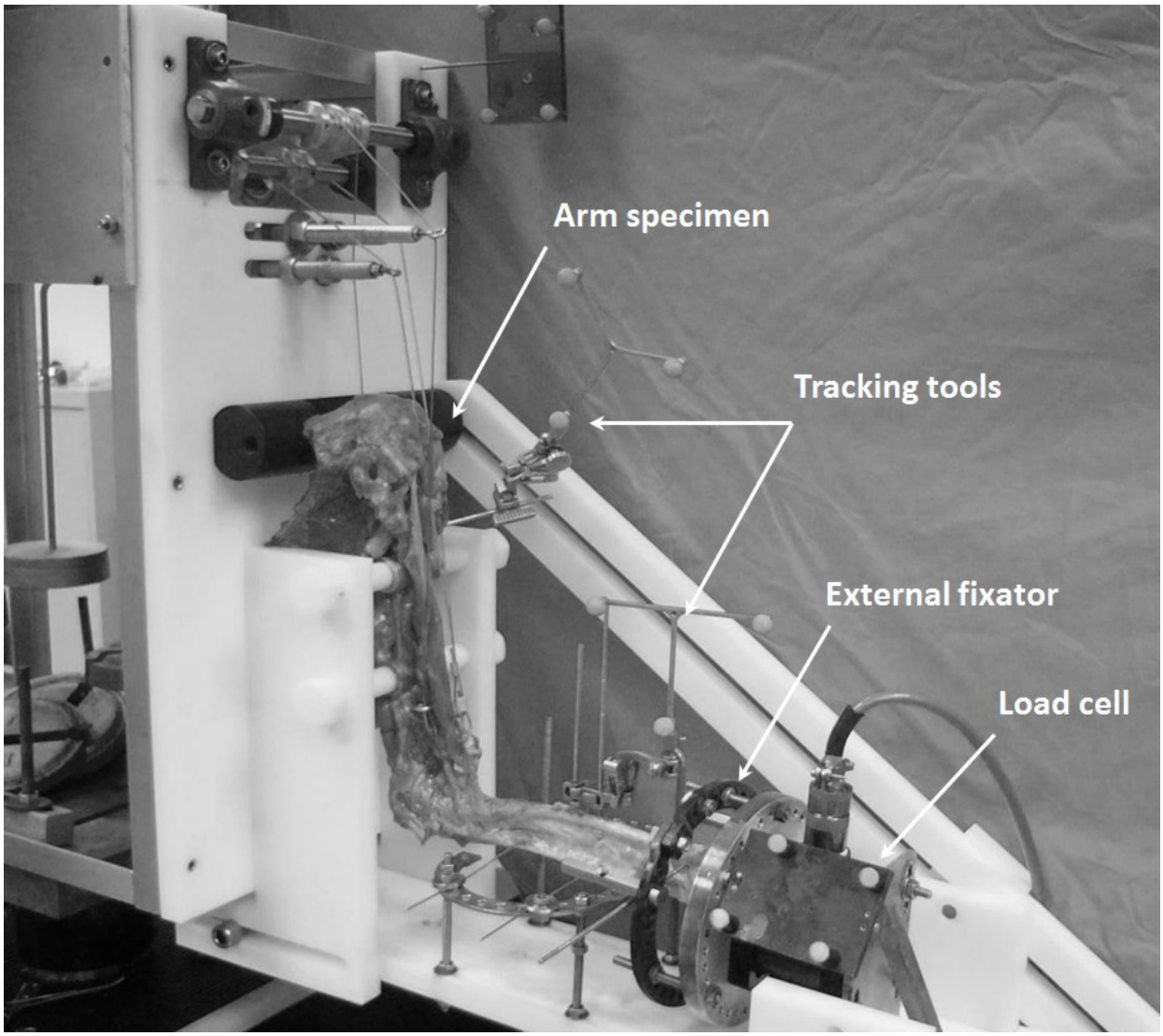

Figure 25. Elbow Simulator with a mounted specimen and optical tracking markers.

3.3 Elbow Joint Kinematics Definition and Tracking

As part of simulator development an experimental protocol and Matlab routines were developed for kinematics tracking. The tracking system and algorithms are briefly described in this section. The final tracking Matlab code and more details are included in Appendix D. The tracking system was required for this study in order to verify joint elbow stability under load by tracking the radial head, SH and LH insertion positions. The current biceps investigation was done in isometric, static positions that did not require angular tracking of the elbow bones. However, the fixed orientations, as verified by a goniometer, were tracked by the developed system for validation purposes in one specimen. The ISB recommendation for joint coordinate systems and motion tracking are adopted for this investigation (Figures 42, 43 and 44).[38] The ISB system recommended coordinate system is an example of an anatomy derived coordinate system where in joint function and motion is expected to follow joint form (i.e. geometry and congruency).[39]

For this study, motion is tracked using the Polaris passive marker optical tracking system (Polaris, NDI, Waterloo, ON). Three tracking tools, as depicted in Figure 25, were used to track the humerus, radius and ulna. The protocol involves first registering landmarks in each bone to define the local coordinate systems for each segment. The elbow is then positioned and loaded as required for the experiment and a "snapshot" is taken of the joint in its new orientation by the Polaris system cameras. The bone positions and joint angles are resolved through a series of transformations from initial reference instance to final instance. The resulting rotation matrices for each bone are then solved for the flexion/extension and supination/pronation angles while the translation vectors are used to calculate bone displacement.

3.4 Repeatability of Elbow simulator loading and joint tracking

The repeatability of resulting flexion and torque measurement at the level of the wrist was determined from the repeated loading trials following the experimental loading protocol described in Section 4.4. Load repeatability was calculated as the average of the range of the force or torque for all loading conditions (i.e. 3 repeated trials, loading both heads, loading LH only or SH only, with 80N for each head). Angular tracking repeatability was determined by tracking the flexion and pro/supination angles as the arm was oriented in the various angles described in the protocol. The angular positions were tracked in 3 repeated trials. Table 1 summarizes the simulator repeatability as evaluated in the final pilot specimen.

Table 1. Load and tracking repeatability of the simulator.

Repeatability	Range	
	Mean	SD
Flexion force (N)	0.66	0.35
Supination torque (Nm)	0.05	0.02
Flexion angle (Degrees)	5.7	3.0
Pro/Sup angle (Degrees)	4.8	2.1

3.5 Joint Stability

The radial head and biceps insertions translation due to loading were tracked to assess elbow joint stability. With only the biceps tendons loaded, there was a visually apparent shifting of the proximal radius anteriomedially with increasing loads during the piloting phase. Displacement of

the proximal radius under load results in a shift of the moment arm about the joint rotation axes. Therefore, instability of the proximal radius results in inaccurate measurement of the SH and LH contributions to flexion and supination torque, particularly when both heads are loaded when compared to loading only one of the heads. To stabilize the proximal radius and reduce the error associated with the proximal radius displacement, the triceps and brachialis muscles were loaded. These muscles provide muscular stability to the joint through compression as it would be in the in-vivo scenario.

The proximal radius motion under loading was tracked in one specimen subsequent to modification of the simulator to include stabilizing muscles. First, both the biceps heads are loaded as per the original design and the radial head and LH and SH insertion translation was recorded. Then the triceps and brachialis muscles were loaded as joint compressors and stabilizers and then the landmark displacement was tracked. The results of loading the stabilizing muscles on proximal radius motion are summarized in Table 2 below.

Table 2. Proximal radius stability under load.

Landmark	Average Displacement in (mm)		% Reduction
	Biceps Only	Bi+Bra+Tri	
Radial Head	3.61	0.59	84
LH insertion	3.62	0.49	86
SH insertion	3.49	0.47	87

3.6 Stress and creep analysis

A stress analysis was conducted for the Delrin braces and the stainless steel load shafts. The Delrin components were deliberately oversized to facilitate easy handling during experimentation as well as to ensure that they were not excessively stressed during the experiment. The back plate is anchored directly to the aluminum frame at multiple points and as a result provides minimal direct structural support. The analysis was conducted for the load cell braces used to support the modular load cell assembly and the forearm base (Appendix E). The downward weight of the load cell assembly is greater than the upward flexion force generated when the muscles are loaded; therefore the stress on the braces is at a maximum with the arm unloaded. The results of the analysis are summarized in Table 3 below. The applied stress and strain are negligible when considering the mechanical properties of the Delrin polymer used for the design (DuPont Delrin 100BK602).

Table 3. Delrin brace stress analysis summary.

Mechanical Design Parameters	Value	Unit
Tensile Modulus	3000	MPa
Yield Stress	72	MPa
Yield Strain	23%	%
Nominal strain at break	40%	%
Applied stress	0.02226	MPa
Applied strain	0.00074	%
Yield stress safety factor	>1000	
Yield strain safety factor	>1000	

The loading trails for each tested condition required approximately 10 minutes to complete under the final experiment protocol (Section 4). From the creep curves in Figure 26, the experimental stress (~22KPa) also resulted in negligible creep for the duration each of the loading trials as they were conducted under room temperature.

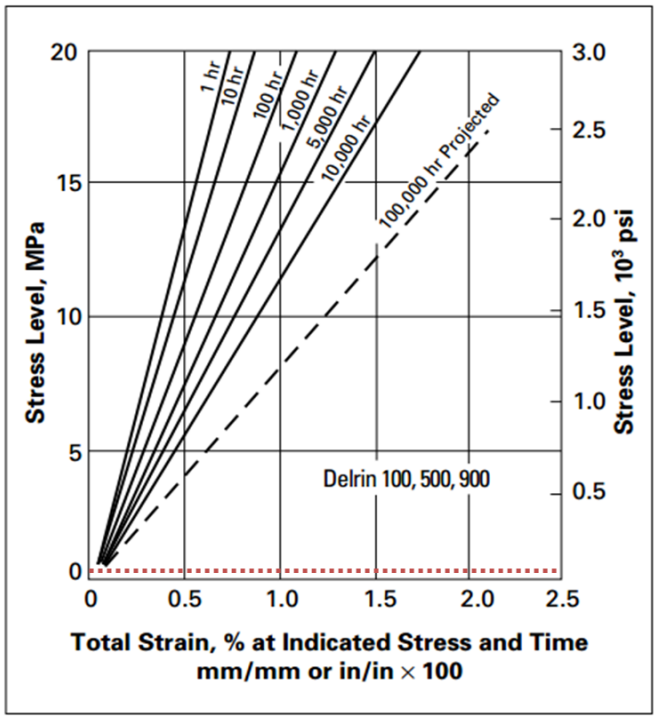

Figure 26. Creep behavior of Delrin under load at 23°C.[3]

The stainless steel shaft stress analysis was done for the triceps shaft as it is subjected to the highest loads. The summary of the results are presented Appendix E. Once again the normal and

[3] http://www2.dupont.com/Plastics/en_US/assets/downloads/design/DELDGe.pdf

shear stress safety factors are substantial (at 46 and >200 respectively). As well, the shaft deflection is limited to less than 1 mm and the angle of twist is less than 0.15 degrees.

3.7 Elbow Simulator Discussion

Loading the triceps and brachialis effectively stabilized the joint, reducing the displacement of the tuberosity by more than 80% and reducing the displacement under combined loading to ~0.5mm on average. This is within in-vivo variation range and near the limit of the accuracy of the tracking tools.[3] The triceps and brachialis are by far the most active during flexion and extension, and they are the largest muscles spanning the elbow joint. It is therefore expected that they provide the greatest contributions to muscular elbow stabilization. Furthermore, the muscle ratios employed were experimentally verified as they caused the elbow to remain at stable 90 degrees of flexion prior to loading the biceps.

The loading repeatability of the simulator is acceptable for this study as the flexion force at the wrist typically falls between 10 and 20N and the supination torque ranges between 1.6 and 1.0 Nm when both muscles are loaded with 80N per head (Appendix A). This translates to roughly 5% error in experimental loading.

Kinematic tracking data was only from one specimen. The angular tracking repeatability is somewhat lacking since a difference of up to 5 degrees was measured for the same arm position. This may be attributable to the imprecise nature of landmark registration which relies on singular points to define the different bone processes and landmarks. As well, it can be a result of the assumptions made when developing the coordinate systems. The accuracy of the tracking system however does not affect the evaluation angles used for the biceps analysis. Elbow flexion and forearm rotation were standardized by pin holes and the load cell simulator posts such that each

configuration was reproducible for each of the tested conditions, i.e. 45 degree pronation, neutral and 45 degree supination. Furthermore, the stability assessment was not affected by the error in the elbow joint coordinate system definition and approximations as they were not required for this study. Only the radial tool position and orientation were tracked and transformed from local to global references and hence the accuracy is limited only by the Polaris system itself (i.e., 0.35 mm RMS).

4. Research Methods

Once the elbow simulator design was completed and validated, the experimental biceps investigation was initiated. The methods used to evaluate intact SH and LH contribution to flexion and supination, and to compare anatomic and non-anatomic repair following simulated rupture are described in this chapter. The testing protocol is outlined in Figure 27 below.

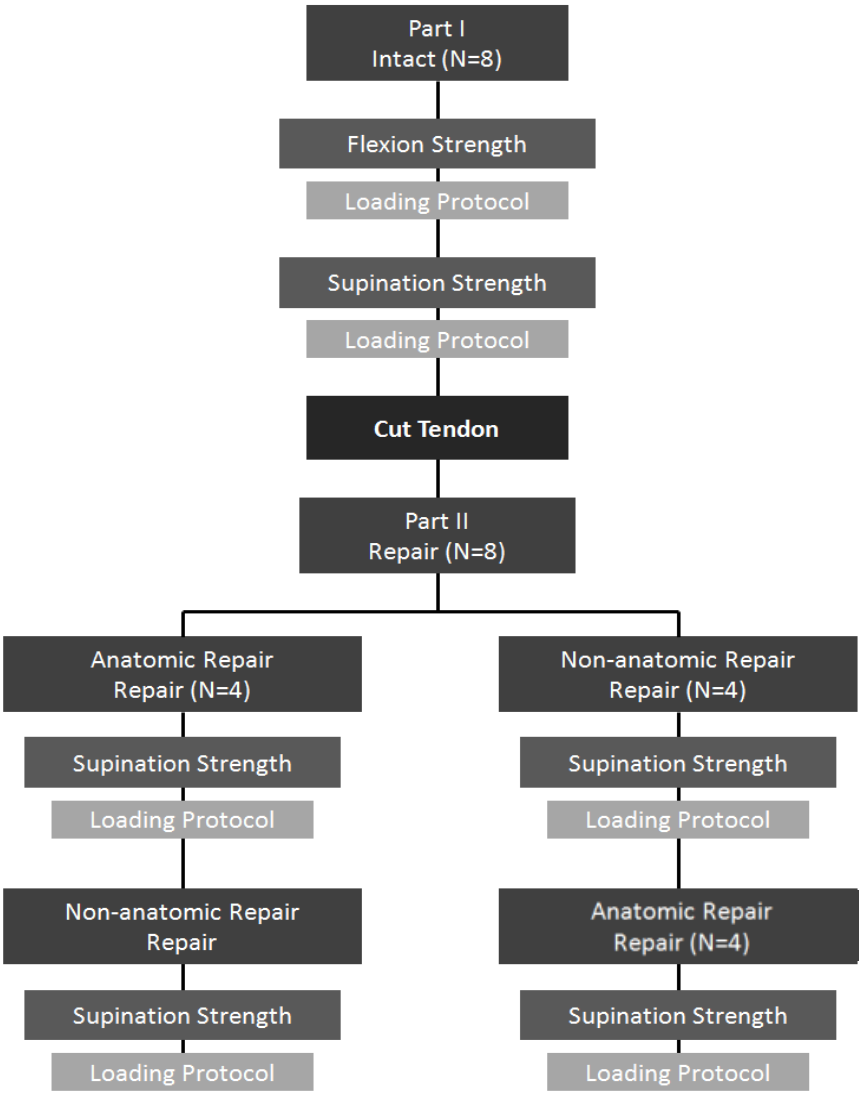

Figure 27. Biceps experiment protocol.

4.1 Specimen preparation

A total of twelve fresh-frozen cadaveric arms were acquired from the Anatomy Laboratory, Faculty of Medicine, at the University of Ottawa following ethics approval. Four specimens were used for piloting and methods development in the preceding chapter and eight were used for the study. The specimens were thawed for twenty-four hours at room temperature and then dissected to preserve the elbow capsule and ligaments, proximal and distal biceps tendon attachments, triceps and brachialis attachments and the flexor and extensor muscles of the elbow and forearm. The average age of the study specimens was 81 (SD 10.6, range 59-92, 5 Male and 3 Female) and specimens with evidence of upper extremity joint pathology or previous surgery were excluded. The specimen tissue was kept moist throughout testing using normal saline. All specimens were tested with the biceps tendons intact for flexion and supination force and torque before simulating rupture of the distal LH and SH tendon at the insertion into bone and performing the subsequent repair. Each specimen was randomly assigned to an anatomic or non-anatomic repair first, group. Following repair the specimen was tested for supination torque only. Once tested, the initial repair was cut and followed by the alternate repair to eliminate sequencing effects. Hence, each specimen underwent the loading protocol a total of three times.

4.2 Test setup

The elbow load simulator was used to orient the arm and apply controlled loads on the individual biceps tendons. Testing was performed in the vertical (dependent) position with the long axis of the humerus oriented perpendicular to the ground. The humerus was rigidly secured in the simulator using the self-adjusting clamps, while the forearm remained unconstrained with the

only point of contact at the distal radius or ulna. Sutures were secured to the distal tendons of the SH and LH at the respective myotendinous junctions (Figure 28). The sutures were then attached to load cables that passed through the adjustable alignment guides to reproduce the anatomical biceps lines of action across the elbow and shoulder joints. This was determined by preserving biceps origins on the scapula during specimen mounting.

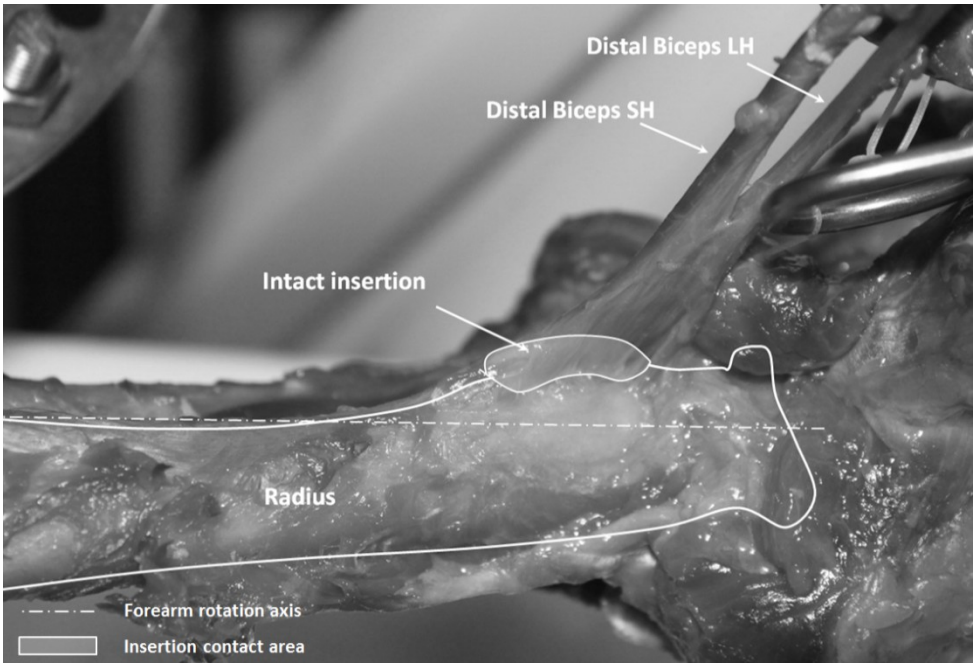

Figure 28. Anterior view of the loaded intact biceps tendon showing LH and SH inserting along the apex of the tuberosity.

The initial study design included testing at three biceps load levels (40, 60 and 80N). This would span the biceps loads used by Henry et al. while also providing insight into any changes resulting from load variation. However, during piloting it was found that due to the time consuming nature of the static loading load protocol (requiring 16 hours to dissect, mount and run the various loading protocols for each specimen), the experimental protocol could only be completed for one

load level. The 80N per head load (160N with both loaded) was selected as it represented approximately 50% of total biceps failure load and would therefore not compromise or rupture the tendon during the intact testing phase.[30] At the same time, at this load level, differences in resultant forces at the wrist would be proportionally larger and easier to detect than at the 40 and 60N load levels. The final muscle loads and corresponding weights used are summarized in Table 4.

Table 4. Muscle loads and applied weights.

Muscle	Muscle Load (N)
Biceps LH	80
Biceps SH	80
Biceps Total	160
Triceps	480
Brachialis	192
Muscle	**Pulley Weights (kg)**
Biceps LH	4.08
Biceps SH	4.08
Triceps	18.00
Brachialis	7.20

For flexion force testing, the radius was pinned to the ulna. A 3 mm K-wire was drilled into the medullar canal of the ulna and used to apply the resultant flexion force on the load cell adapter. This allowed for testing of unconstrained elbow flexion. For supination torque testing, the radius

was left unconstrained from the ulna. A Steinman pin was drilled transversally into the distal radius at the level of the styloid process. The pin was balanced on both ends on posts erected on the external fixator attached to the six-axis load cell. This allowed for measuring of unconstrained supination torque at level of the wrist (Figure 22). The triceps and brachialis muscle loads were balanced as ratios of the biceps load, such that the elbow remained at equilibrium at 90° throughout the experiment for all loading protocols and test conditions.

4.3 Biceps Repair

Once the testing of the intact biceps was complete, the distal biceps tendon was cut, simulating a complete rupture (Figure 29). The biceps insertion was divided into four quadrants as shown in (Figure 30). The tuberosity apex was used as the bisector separating the non-anatomic, more radial repair locations, from the anatomic, more ulnar locations. The centroid of each quadrant was then used as the location for anchor placement. Suture anchors were used to affix the tendon onto the bone in both repair scenarios (Figure 31). The non-anatomic repair contact area or footprint was on the anterior side of the radial tuberosity (Figure 32). The anatomic repair footprint was more posterior, wrapping over the radial tuberosity apex (Figure 33). Two 2.3 mm Ultra-fix anchors were used (ConMed Linvatec, Largo, FL, USA) for each repair, one for each head of the distal biceps. The biceps was repaired using a sliding locking modified Krackow technique with number 2 Hi-Fi™, Ultra High Molecular Weight Polyethylene Suture (ConMed Linvatec, Largo, FL, USA) in all cases .[3] Once the loading protocol was completed, the repair was cut and the alternate repair technique was tested.

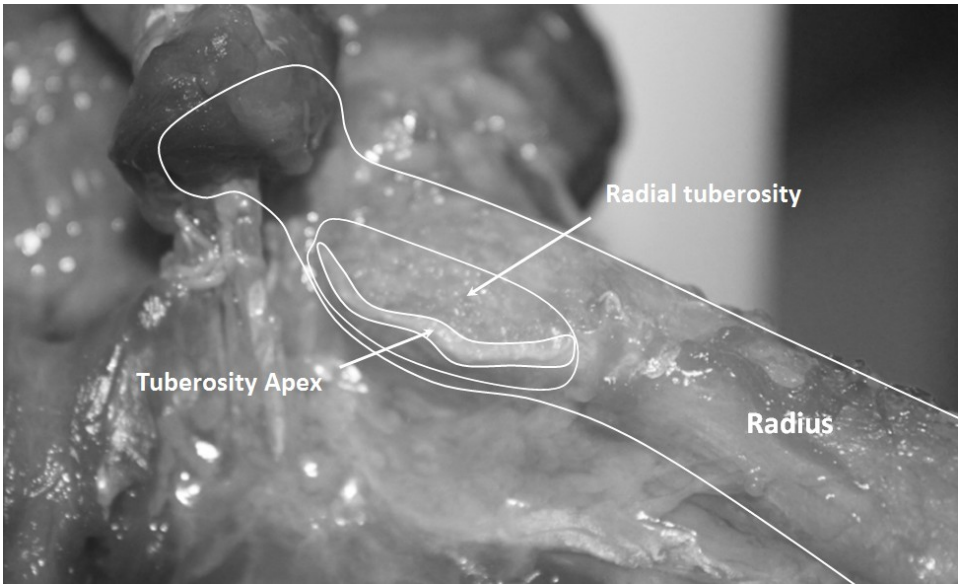

Figure 29. Medial view of the radial tuberosity following simulated biceps tendon rupture by lifting the insertion off the bone.

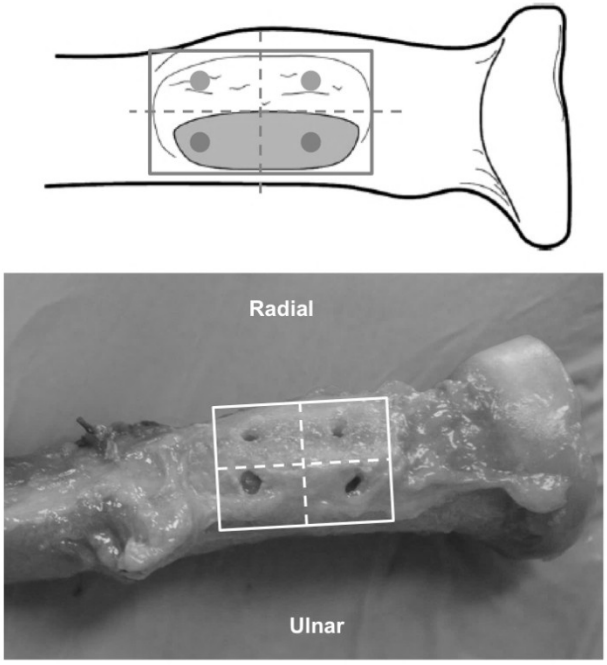

Figure 30. The distal biceps tendon radius repair schematic and actual specimen. The radial anchor holes were used for non-anatomic repair of the LH and SH while the ulnar holes were made for the anatomic repair.

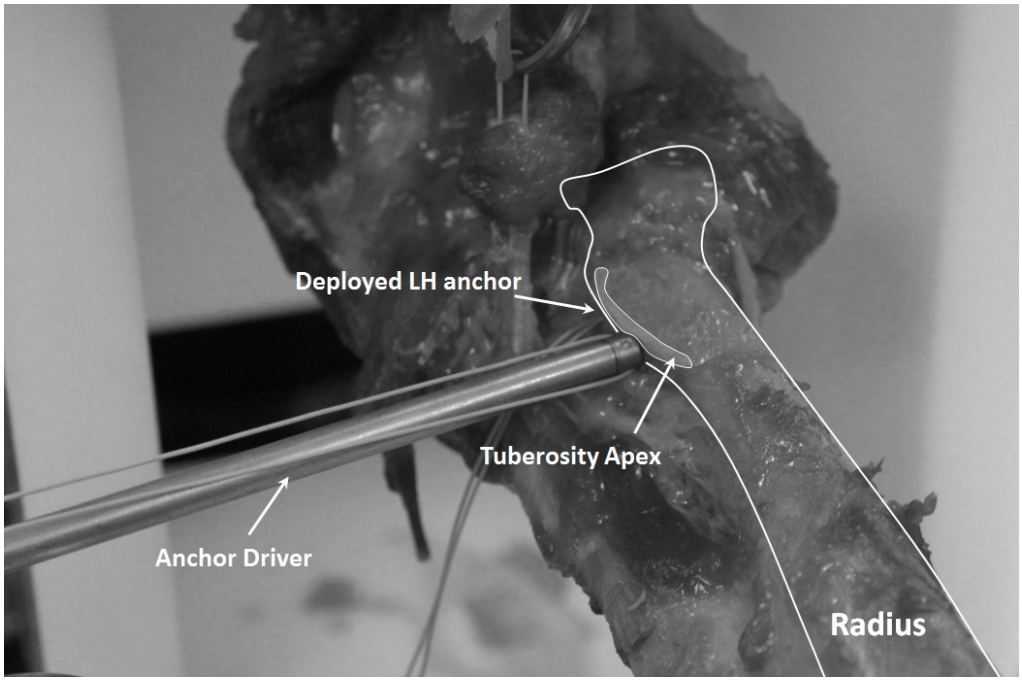

Figure 31. Anchor fixation employed for both anatomic and non-anatomic repair.

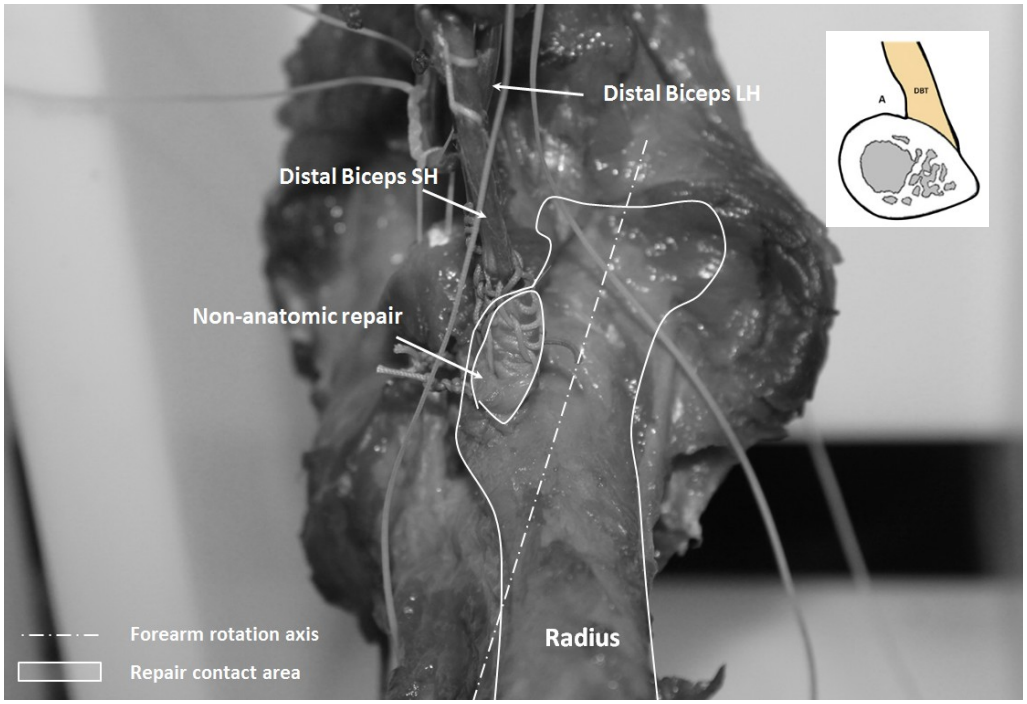

Figure 32. Completed non-anatomic repair with the SH and LH attached anterior to the tuberosity apex.

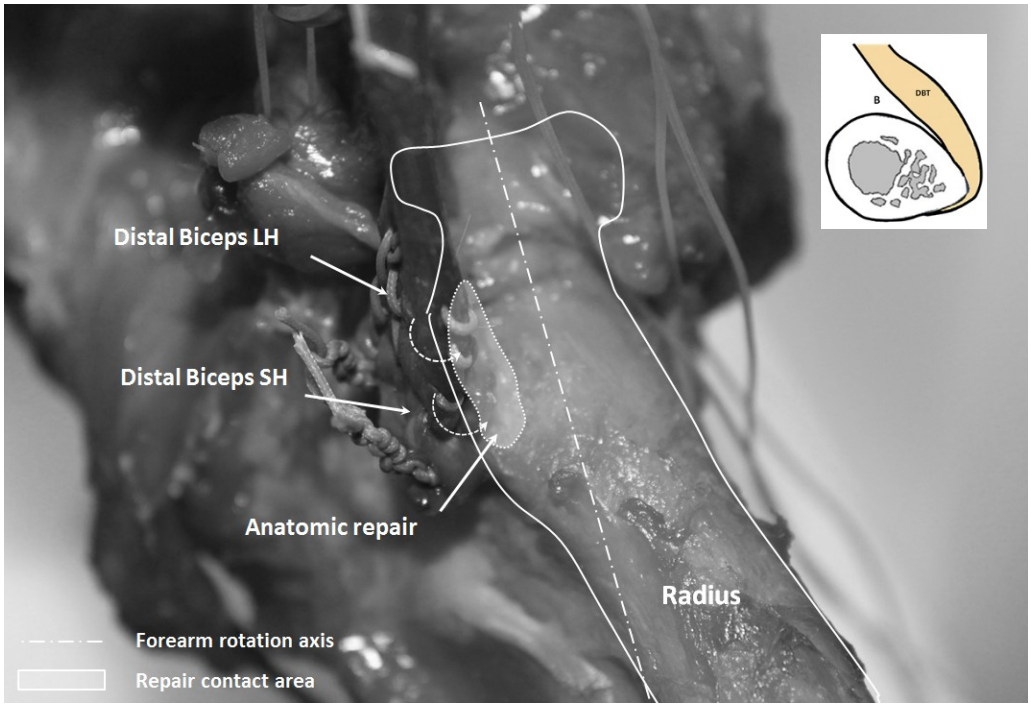

Figure 33. Completed anatomic repair with the SH and LH attached posterior to the tuberosity apex.

4.4 Loading Protocol

Once the arm was secured to the elbow simulator, all tendons were ramped to their full testing load and unloaded three times to precondition the tissue and tension all attachments before beginning the loading protocol. Isometric flexion force and supination torque were recorded with the forearm at 45 degrees supination, neutral rotation and 45 degrees pronation.

At each of the arm configurations, three loading trials were completed. Testing consisted of randomly loading only the LH or only the SH, or both simultaneously and recording the resulting load at the distally attached load cell (Appendix B). These tests established the intact contributions of the biceps LH and SH to forearm rotation at the three forearm positions. Following intact testing, the loading protocol was repeated for either the anatomical or non-anatomic repairs to assess repair supination torque.

The primary outcomes were force (N) and torque (Nm) at the distal ulna and radius under the various LH and SH loading configurations. The tables in the results section summarize the force data. For the intact contribution comparison of the LH and SH to flexion and supination, the SH and LH are normalized to the both heads loaded condition. For the repair comparison, the intact resultant torques under each condition (both heads loaded, SH only and LH only) were used to normalize the resultant torque in the subsequent repairs and conditions. The graphs present normalized data in order simplify the comparisons.

4.5 Data Analysis

Due to the anatomical differences between specimens, large variations in the loads at the wrist were expected between the intact arms. The small sample size meant normal distribution of the data could not be assumed and was therefore tested for each parameter in each group using the Shapiro-Wilk test (Appendix F). The Wilcoxon signed-rank test was then used to compare paired nonparametric data while a paired t-test was used to compare parametric data (Appendix F). All statistical analysis was performed on the force and torque data. Paired testing allows for the comparison of intact flexion and supination contributions, treating the LH and SH as paired data points on the same specimen. For the repair comparison the paired testing compares the differences in supination torque within the same specimen. In this way, statistical differences can be detected in the presence of large variance or standard deviations between subjects.

5. Results

The results of **objective a**, the intact contribution of the SH and LH to total flexion force, and **objective b**, the intact SH and LH contribution to total supination torque are presented first in this chapter (Section 5.1). The results of the intact supination testing also serve as a baseline for **objective c**, the anatomic and non-anatomic repair comparison. The repair comparison results are also presented in this chapter (Section 5.2). This chapter presents the aggregated data from all specimens; individual specimen data are provided in Appendix A.

5.1 Intact contributions

The intact flexion force and supination torque generated at the wrist are summarized below for the fixed flexion angle of 90° with the forearm in 45° pronation, at neutral and with the forearm in 45° supination. It should be noted that theoretically the contributions of the individual heads should be cumulative and equal to loading of both heads at the same time. However, as can be seen in the following tables and graphs, this is not the case practically. The SH and LH individual contributions combine to a total contribution greater than that of both heads loaded simultaneously. The elbow complex is not completely rigid and the proximal radius deflects due to loading which reduces the effective moment arm when both heads are loaded. This phenomenon is reduced by loading the flexion-extension stabilizers but is not eliminated. A paired t-test was used unless otherwise noted for groups where the data was not normally distributed;, in such cases, the Wilcoxon signed rank test for non-parametric data was used.

5.1.1 Contribution to Flexion

With the elbow at a fixed 90 degrees of flexion, the flexion force is measured with the forearm in 45 degrees of pronation, at neutral and with the forearm in 45 degrees of supination. The average flexion forces at the level of the wrist as a result of loading the biceps tendons are summarized in Table 5.

Table 5. Mean flexion force (*Wilcoxon signed rank test, +Significant difference).

Orientation	Head	Unconstrained Flexion (N)		p value
		Mean	SD	
45° Pro	Both	12.37	3.64	0.017^{*+}
	SH	8.44	2.35	
	LH	6.75	1.87	
Neutral	Both	12.55	3.56	0.017^{*+}
	SH	8.48	2.28	
	LH	6.95	1.71	
45° Sup	Both	13.34	4.41	0.010^{+}
	SH	8.63	2.74	
	LH	6.77	2.21	

The flexion force from loading either head does not appear to change significantly as a result of forearm rotation. In all three forearm orientations, the SH of the biceps consistently contributes significantly more to elbow flexion than the LH.

The SH and LH individual flexion force data is normalized by the flexion force from loading both heads (Both) in order to assess their contributions to total biceps elbow flexion force. The normalized data is presented in Table 6 and Figure 34.

Table 6. Normalized contribution to flexion.

Orientation	Head	Normalized Flexion	
		Mean	SD
45° Pro	Both	1.00	
	SH	0.69	0.07
	LH	0.55	0.07
Neutral	Both	1.00	
	SH	0.69	0.12
	LH	0.56	0.07
45° Sup	Both	1.00	
	SH	0.66	0.07
	LH	0.51	0.09

On average the SH contributes 14% more to total biceps flexion force than the LH for the same muscle load.

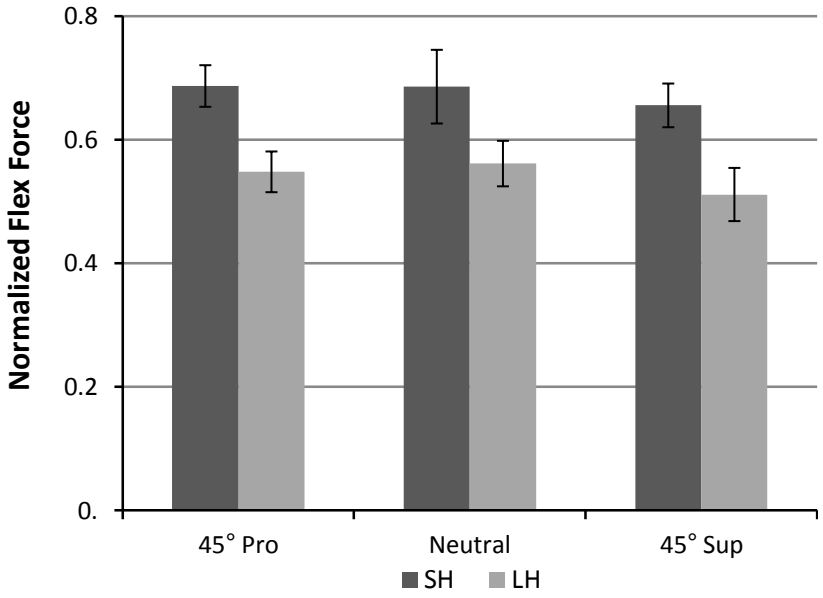

Figure 34. Normalized flexion contribution of the LH and SH (error bars = 1 SD).

5.1.2 Contribution to Supination

The average forearm supination torques generated at the wrist as a result of loading the intact SH and LH in the three fixed forearm orientations are presented in Table 7.

Table 7. Mean supination torque (*Wilcoxon signed rank test, +Significant difference).

Orientation	Head	Unconstrained Torque (Nm)		p value
		Mean	SD	
45° Pro	Both	0.95	0.26	0.079
	SH	0.56	0.17	
	LH	0.49	0.18	
Neutral	Both	1.06	0.28	0.093*
	SH	0.64	0.15	
	LH	0.56	0.15	
45° Sup	Both	0.89	0.22	0.092
	SH	0.49	0.16	
	LH	0.49	0.11	

Biceps supination torque generally diminishes once the arm is in supination as can be seen from the reduced torque with the SH or the LH loaded in supination.

The SH and LH torques are normalized by the torque generated by both heads loaded simultaneously in order to assess their individual contributions to total biceps supination torque. This data is summarized in Table 8 and Figure 35 below.

Table 8. Normalized contribution to supination.

Orientation	Head	Normalized Torque	
		Mean	SD
45° Pro	Both	1.00	
	SH	0.61	0.11
	LH	0.52	0.09
Neutral	Both	1.00	
	SH	0.61	0.06
	LH	0.52	0.05
45° Sup	Both	1.00	
	SH	0.54	0.12
	LH	0.56	0.07

The SH is a stronger elbow supinator with the arm in 45° of pronation and at neutral. The SH generates 9% more torque at the wrist than the LH. The trend changes at 45° of supination as the LH contributes slightly more than the SH, the shift is consistent across all specimens but the difference is not as pronounced.

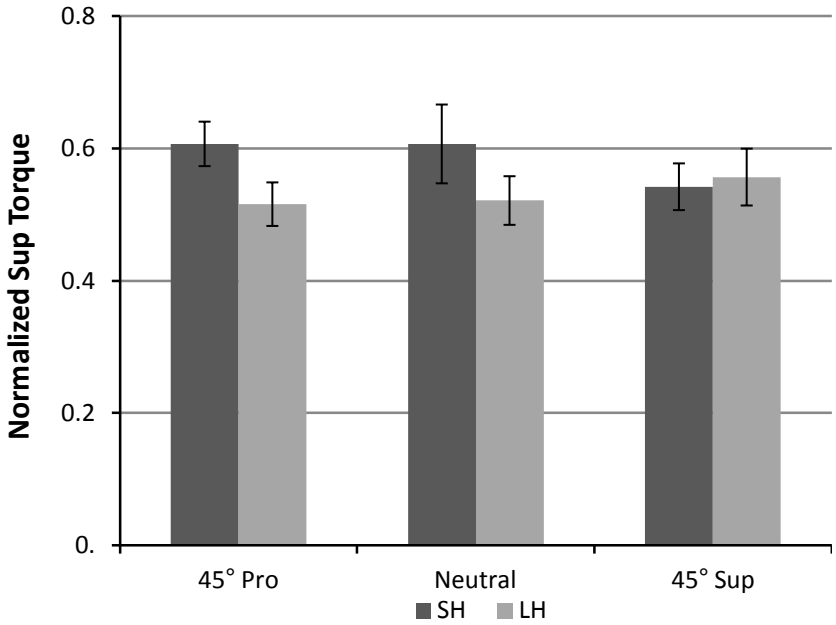

Figure 35. Normalized supination contribution of the LH and SH (error bars = 1 SD).

5.2 Repair Evaluation

For the repair evaluation portion of the study, only forearm supination torque was measured. This was done due to testing time constraints. Clinically, the positioning of both heads distally and increasing the flexion moment arm is understood as favourable and in fact, the deliberate repair of the DBT distal to the original insertion is done in the case of very weak elbow flexion.[3] Additionally, supination torque is the more important clinical measure following repair since other elbow flexors, the brachialis in particular, have been shown to contribute and compensate for flexion deficiency while supination torque is more significantly diminished.[3]

One specimen failed during loading of the SH after non-anatomic repair. This is probably a result of low bone density as the suture anchor avulsed out of the bone. This is not completely

unexpected when considering the age of some of the donors in the study. The type of failure made it impossible for re-repair and as a result no data is available for non-anatomic repair of the SH in neutral rotation and no data is available for all non-anatomically repaired heads in pronation in this specimen.

As in the intact muscle contributions, it is noted that in some specimens the resulting supination torque at the wrist from individual LH and SH loading sums up to a higher torque than when both heads a simultaneously loaded at the same time. As aforementioned, this is primarily a result of the load vector causing the deflection of the radial tuberosity towards to the forearm long axis when both heads are loaded which diminishes the supination moment arm and results in a lower torque for the same total muscle force.

Table 9. Mean repair supination torque ([*]Wilcoxon signed rank test, [+]Significant difference).

Orientation	Head	Anatomic		Non-Anatomic		p value
		Mean (Nm)	SD	Mean (Nm)	SD	
45° Pro	Both	1.07	0.37	0.99	0.35	0.113
	SH	0.62	0.22	0.58	0.56	0.310[*]
	LH	0.59	0.18	0.55	0.15	0.388
Neutral	Both	1.12	0.34	0.94	0.40	0.034[+]
	SH	0.65	0.25	0.58	0.27	0.123[*]
	LH	0.62	0.14	0.58	0.23	0.361
45° Sup	Both	0.95	0.24	0.59	0.48	0.008[+]
	SH	0.52	0.15	0.35	0.29	0.012[+]
	LH	0.54	0.08	0.33	0.22	0.009[+]

The actual supination moment means and standard deviations for both repairs are summarized in Table 9. This repair supination torque data was normalized in each of the cases to its initial intact supination torque in Table 10, and is presented in the repair charts that follow. The normalized comparison is more clinically relevant than an absolute torque measure since repair strength is generally patient specific and is better compared to the pre-rupture or the unaffected intact contralateral limb in in-vivo studies. In each case the repair is normalized to the corresponding intact scenario (e.g. anatomic repair LH supination torque with the forearm in pronation is normalized to the intact LH supination torque in pronation etc…).

Table 10. Normalized repair supination torque.

Orientation	Head	Anatomic		Non-Anatomic	
		Mean (Nm)	SD	Mean (Nm)	SD
45° Pro	Both	1.14	0.03	1.06	0.08
	SH	1.11	0.08	1.11	0.14
	LH	1.15	0.05	1.11	0.10
Neutral	Both	1.01	0.02	0.85	0.11
	SH	0.99	0.06	0.90	0.15
	LH	0.99	0.07	0.88	0.09
45° Sup	Both	1.03	0.06	0.60	0.19
	SH	0.99	0.13	0.63	0.23
	LH	0.96	0.07	0.59	0.18

The above data is visualized for direct comparison in Figure 36, Figure 37 and Figure 38 in the following pages.

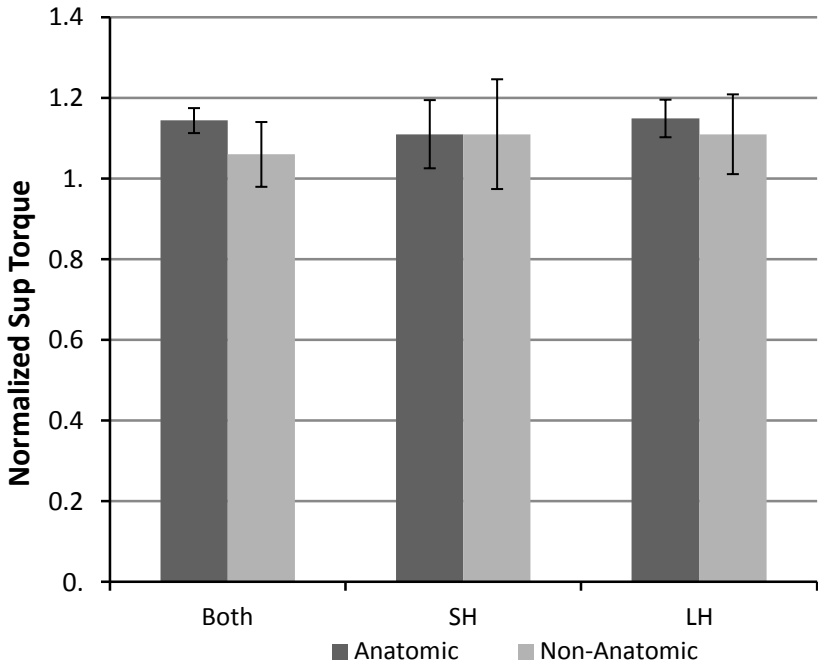

Figure 36. Normalized supination torque @ 45° pronation (error bars = 1 SD).

There was no difference in supination force between anatomic and non-anatomic repairs when the forearm was in 45° of pronation.

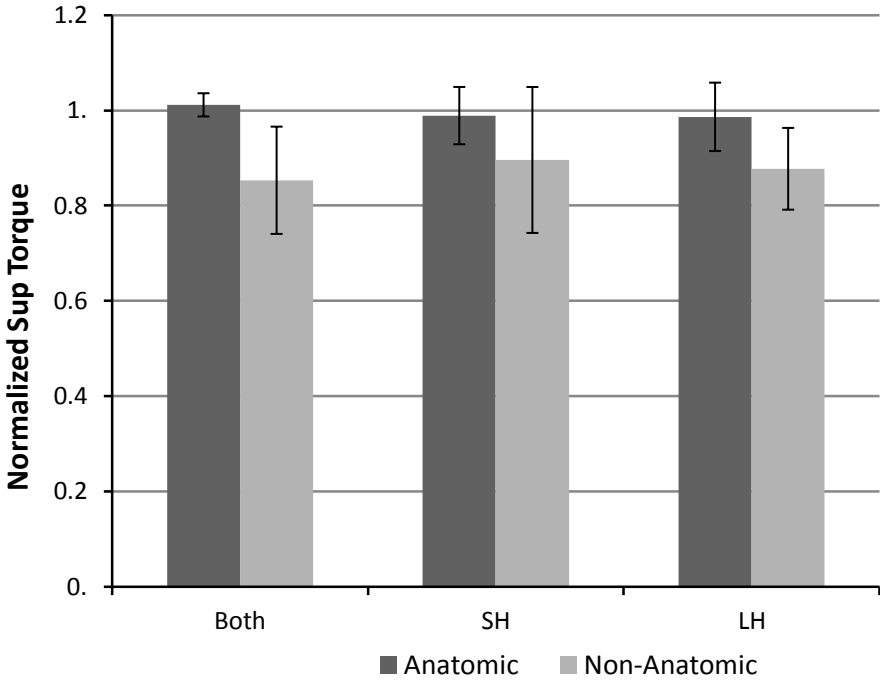

Figure 37. Normalized supination torque @ neutral (error bars = 1 SD).

However, with the forearm in neutral rotation, there was a 15% difference in supination force when comparing anatomic and non-anatomic repairs. The anatomic repairs generated more supination force.

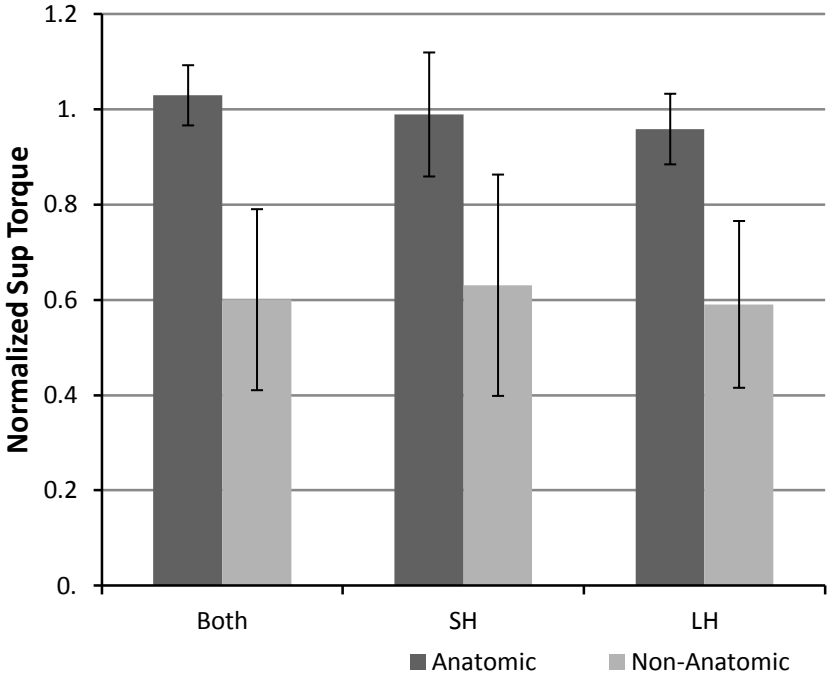

Figure 38. Normalized supination torque @ 45° supination (error bars = 1 SD).

With the forearm in a position of 45° of supination, the anatomic repairs generated 40% more supination force than the non-anatomic repairs. All anatomic repairs showed no difference when compared with intact tendon measurements.

When the SH and LH were repaired in a non-anatomic position, there was a significant loss of supination torque generated, most notably when the forearm was positioned in 45º of supination. In this position, the SH and LH generated 36% and 38% less supination torque respectively

6. Discussion

The results of the intact tendon contribution testing as well as the anatomic and non-anatomic repair findings will be discussed in this chapter. The study limitations as well as those of the simulator are explored and followed by recommendations for future work and improvement in the design.

6.1 Intact Biceps contribution

The SH of the biceps is consistently a greater flexor of the elbow at 90° of elbow flexion. This supports the hypothesis and assumption based on the recent anatomic studies in which the SH insertion is the more distal of the two heads and as such has a larger flexion moment arm about the elbow flexion axis than that of the LH.[5,6]

The results of the supination torque testing at first appear to detract from the expectations of the anatomic studies which place the LH of the biceps more ulnar at the insertion into the radial tuberosity than the SH. In this study it was found that the SH was the greater contributor to supination torque with the forearm in pronation and at neutral at an average of 10% difference in torque consistent across the tested specimens. A possible explanation for this difference is that in pronation, the distal biceps tendon wraps around the tuberosity as it rotates posteriorly; this effectively negates the "cam" effect advantage of the LH insertion, whereas the more radial location of the SH places it at a mechanical advantage and away from long axis of the radius. Unwrapping of the tendon as the forearm rotates towards neutral and supination gradually places

the LH insertion, with its more ulnar insertion, at a more mechanically advantageous angle. This shifts the torque contribution to the LH as noted in the results.[5]

Given the eccentric vector of pull of the biceps brachii relative to the long axis of the radius, partial distal biceps ruptures likely originate from the leading edge, i.e. the SH, and propagate to the posteriorly situated LH in a complete rupture. Supporting this theory is the recent observation of partial ruptures involving only the SH as seen on MRI.[40] In light of this study findings, partial ruptures repair should be treated surgically as they affect the SH which has a dominant role not only in elbow flexion but also in supination of the arm from a pronated position.

This study would have been the first to approach the distal biceps tendon as the bifurcated complex that it increasingly appears to be. However, during the data collection phase of the project, Jarrett et al. published an anatomic and biomechanical study assessing the contributions of the biceps LH and SH to elbow flexion and supination by applying constant load ramps and calculating the muscle moment arms.[21] The Jarrett study closely matches the methodology of this project with some differences. Flexion and supination efficiency are reported in the form of moment arms. The nature of the study lends itself to this kind of analysis since the comparison is done with the same loads on both muscles and therefore any differences in resultant force or torque are attributable to the anatomic differences in the moment arms. Comparison of the outcome measures is however still possible, since in both studies the relative contributions of the LH and SH to forearm flexion and supination force and torque are assessed. In fact our findings mirror those found in the Jarrett study for both flexion force and supination torque. Jarrett et al. report that the SH is consistently the greater contributor to flexion, contributing 15% more to flexion than the LH. They also found the SH to be a greater contributor to biceps supination with

the forearm in pronation and at neutral. They report that the SH has an 8% and 13% advantage over the LH with the elbow in pronation and at neutral rotation, with the LH becoming the greater contributor to supination when the forearm in in 60° of supination. This study tested pronation supination at 45° and a similar shift towards to the LH is noted, though the advantage is not as great at 2% in this study versus 8% in the Jarrett study. Furthermore this study benefits from having a larger sample size of eights versus the six used in the Jarrett investigation.

Our findings indicate that the resultant force at the wrist is not only a function of the anatomic moment arms, but is also affected by elbow stability and motion of the proximal radius. The fact that the forces and moments generated by loading the LH and SH individually are not commutative to the loading of both heads simultaneously supports this idea. The individual loads were closer to the combined loading results once the proximal radius was better stabilized. Jarrett et al. only loaded the biceps tendons and therefore did not incorporated muscular stabilization of the joint. In our study, tracking of the non-stabilized joint has shown that the LH and SH insertions can move by up to 3 mm due to loading. These displacements could have a significant effect when the reported moment arms are in the range of 6-10 mm.

An argument can be made that analysis of the contributions of the LH and SH and their position on the radial tuberosity can be simplified to a mathematical study of the moment arm at the level of the tuberosity "cam". However, the variability in tuberosity morphology and the differences observed in this study with regards to the rotation of the insertion obfuscate simple vector analysis and highlight the importance of experimental testing.[41]

6.2 Repair Evaluation

Distal biceps tendon ruptures lead to loss of flexion and supination. The goal of a distal biceps tendon rupture repair is to restore normal function.[42–44] It is thought that an anatomic repair will give the most successful result in restoring normal function. This study showed that repairing the tendon to its anatomical footprint, restored biceps supination force to that of the "intact" specimen, with the arm in 45° of supinated, in neutral rotation and in 45° of pronation.

However, this was not the case for the non-anatomic repair. When the biceps was repaired in a non-anatomic position the supination force decreased slightly with the forearm in neutral rotation and significantly with the forearm in 45° of supination.

The lack of significant differences in a pronated position is not surprising. Since the radial tuberosity moves posteriorly and the apex is hidden around the back of the radius in this position, it no longer contributes to extending the attachment site away from the long axis of the radius and increasing the moment arm of the biceps tendon. In this position the tendon lies on the radial shaft and has equal moment arms irrespective of repair placement on the tuberosity.

Two previous biomechanical studies have looked at the effect of repair site of the distal biceps tendon. Henry et al. studied eleven matched pairs and concluded that there was no significant difference in repair to anatomic or non-anatomic with the forearm in neutral rotation. In both repairs compared in the Henry et al. study, the tuberosity was burred to create a trough prior to tendon repair. The repair employed a bone tunnel technique compared to the anchor repair technique used in this study. The repair as done by Henry et al. for the anatomic repair is shown in Figure 39 below. It is reasonable to construe that creating a trough at the insertion diminishes the tuberosity cam effect and negates the mechanical advantage afforded by anatomic repair to

supination force. This may explain the significant differences in this study between repairs when compared to Henry et al.

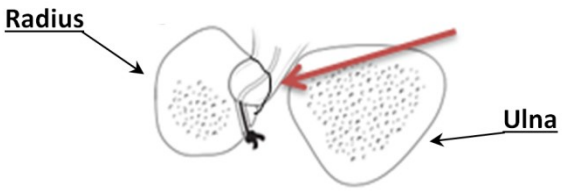

Figure 39. Axial view of the forearm at the level of the tuberosity showing anatomic repair technique as done by Henry et al. The black continuity curve and red arrow indicate the bone loss associated with the repair.

Schmidt et al. examined 6 cadaveric specimens with four repair sites in three forearm rotations (60° pronation, Neutral and 60° supination).[45] Although no distinction was made between the two heads, they found that non-anatomic repair significantly decreased the supination force generated in neutral and supinated positions, supporting our findings in this study.

Recent clinical studies reported on biceps strength after surgical repair and reported excellent results with restoration of supination strength from 92- 96%. In many of these papers, supination torque is only tested in a neutral rotation.[44,46–49] Based on the present study, patients would have to be tested in some degree of supination to detect any significant differences that exist between the repair techniques. Niemeyer et al. recently found significant differences in comparing two surgical techniques with a reported loss of 33% when testing in different forearm positions.[44] These findings are in agreement with the results of the present study.

6.3 Study Limitations

This study model loaded the biceps, brachialis and triceps brachii with physiologic loads but did not account for many other muscles that contribute to supination of the forearm and stability of the elbow. While joint stability was simulated by loading the major elbow flexors and extensors, the assessed stability remains somewhat removed from the in-vivo conditions as a result of lack of muscle tone which provides constant support and stability in a live patient. Another limitation is due to the variation of muscle force generated in-vivo, compared to the constant loads applied in this experiment. The LH of the distal biceps tendon has a smaller cross section than the SH and as such it is possible that a lower muscle force is generated and transmitted through the LH. However, muscle force and function is variable and using the same force for both muscles allowed for analysis of the mechanical function. Due to the severe time constraints of testing a fresh-frozen cadaver, this study did not assess the effect of varying the elbow flexion angle and various muscle loads, though the noted trends are expected to be consistent. Furthermore, this study is limited to testing isometric force and torque and cannot reproduce a patient's ability to heal, remodel and more importantly perhaps, the ability to adapt. The sample size (N=8) while small was sufficient to detect significant differences. It should be noted that type 2 statistical error is possible in the cases where differences were noted but not found to be statistically significant. Due to the scarcity of cadavers and the large variances across specimens experimental biomechanics studies commonly suffer from being under powered.

6.4 Simulator limitations and recommendations

6.4.1 Automated Loading

A major limitation of the simulator is due to the currently static loading modality. The application of discreet loads combined with the required set up time limited the tested elbow orientations in this study to only one flexion angle, three forearm angles and only one load level for this experiment. This highlights the need to automate the loading process with servomotors. To increase efficiency during data collection, servomotors may be added to each muscle to allow for continuous and quick loading. The addition of servomotors would significantly decrease the time required for one loading cycle from 20 minutes to 2 minutes. With servomotors more orientations and repeated measures can be completed with one fresh frozen cadaver.

6.4.2 Alignment Eyelets

The current simulator design employs a combination of an adjustable eyelet and alignment pulleys to direct the muscle force cable. Fillets were welded to the eyelets to reduce the potential for the cable catching and ensure a smooth sliding surface between the cable and eyelet guides. With higher loads and in the more extreme positions of the alignment rod, where the cable angle is lower than 90 degrees, the friction losses in routing can become substantial. A post study load verification experiment indicated that there are significant system routing and friction losses of 15-20% (Figure 40 and Table 11). This was determined by attaching the muscle cables directly to the load cell after routing through the cable alignment system.

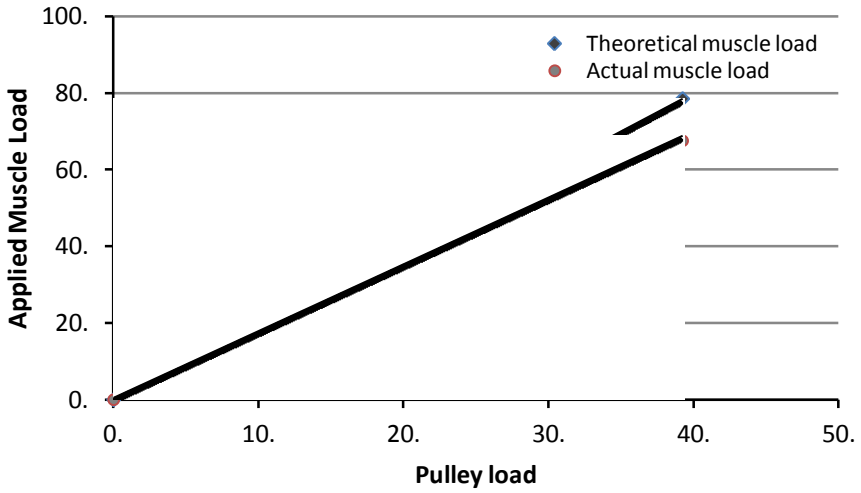

Figure 40. Applied muscle load verification.

The actual load applied through the muscles was not critical for this study as it investigated relative contributions with the same load applied under the various conditions. That is, the diminished muscle loads due to friction were applied on both heads and in both anatomic and non-anatomic scenarios. Therefore the relative contributions measured are not expected to change. However, to increase the versatility of the simulator and allow for reliable, absolute, muscle force application and measurement, it is recommended that the eyelet design be replaced with second alignment pulley at the end of the adjustable rod. This would change the sliding contact to a rolling contact and minimize routing and friction forces.

Table 11. Actual muscle load and friction losses.

Applied Static Load	Theoretical muscle load	Actual muscle load	% Error
0	0	0	0
4.91	9.81	7.78	21
9.81	19.62	15.60	20
14.72	29.43	28.38	4
19.62	39.24	38.68	1
24.53	49.05	43.46	11
29.43	58.86	50.22	15
34.34	68.67	60.44	12
39.24	78.48	67.52	14
44.15	88.29	74.88	15

7. Conclusions

7.1 Conclusion

The SH of the biceps is an especially important flexor, contributing 14% more to elbow flexion force when compared to the LH. The SH is also an important supinator with the forearm between pronation and neutral. The LH of the distal biceps plays a bigger role and contributes more than the SH to supination strength when the arm is in supination. Given that the SH is most often implicated in partial tendon ruptures and that it is a significant contributor to flexion and supination, this study supports the notion that partial ruptures should be treated and repaired surgically.

The repair evaluation in this study supports the anatomic repair of the biceps tendon. Making sure to reattach the tendon posterior to the apex radial tuberosity is important. In this repair position, the biceps can generate supination torque similar to an intact tendon throughout the full range of motion by utilizing the tuberosity "cam". If the biceps is repaired too radially, the biceps will not be able to generate full supination force from neutral to full supination. This study also highlights the importance of supination strength testing at multiple positions throughout the forearm range of motion to properly evaluate the effectiveness of distal biceps tendon repair.

7.2 Summary of Contributions

- The biceps study adds clinically important information regarding the more nuanced anatomy of the distal insertion of the biceps, providing mechanical evidence in support of the distinct consideration and roles of the LH and SH. The findings have direct implications in the treatment of distal biceps tendon ruptures, partial tears and the decision making process regarding the course of surgical intervention. The study stresses the importance of anatomic repair of distal biceps ruptures and the need to test elbow supination strength in various forearm rotations in order to properly evaluate the functional success of repair.

- An elbow joint load simulator was designed, commissioned and used to simulate load of the major elbow flexors and extensors in an unconstrained model. The simulator has been shown to reliably load the elbow muscles. The simulator has an interchangeable and modular design, and will subsequently be upgraded with servomotors to increase its versatility and use for other projects as the Orthopaedic Biomechanics Laboratory.

- A tracking algorithm and an elbow coordinate system were also developed to assess elbow kinematics using the Polaris optical tracking system. The system was used to track the motion of the radius specifically in this study, and allowed for measuring the initial joint laxity as well as evaluating the improved kinematic stability afforded by loading the primary elbow extensor and flexor.

8. References

1. Safran MR, Graham SM. Distal biceps tendon ruptures: incidence, demographics, and the effect of smoking. *Clin Orthop Relat Res*. 2002;(404):275-83. Available at: http://www.ncbi.nlm.nih.gov/pubmed/12439270. Accessed August 9, 2014.
2. Sarda P, Qaddori A, Nauschutz F, Boulton L, Nanda R, Bayliss N. Distal biceps tendon rupture: Current concepts. *Injury*. 2013;44:417-420. doi:10.1016/j.injury.2012.10.029.
3. Morrey BF. *The Elbow and Its Disorders*. 4th ed. Philadelphia: Saunders Company; 2009. Available at: http://books.google.com/books?id=G9SdBoI6KjsC&pgis=1. Accessed August 6, 2014.
4. Bain GI, Johnson LJ, Turner PC. Treatment of partial distal biceps tendon tears. *Sports Med Arthrosc*. 2008;16(3):154-61. doi:10.1097/JSA.0b013e318183eb60.
5. Athwal GS, Steinmann SP, Rispoli DM. The distal biceps tendon: footprint and relevant clinical anatomy. *J Hand Surg Am*. 2007;32(8):1225-9. doi:10.1016/j.jhsa.2007.05.027.
6. Cucca YY, McLay SVB, Okamoto T, Ecker J, McMenamin PG. The biceps brachii muscle and its distal insertion: observations of surgical and evolutionary relevance. *Surg Radiol Anat*. 2010;32(4):371-5. doi:10.1007/s00276-009-0575-y.
7. Baker BE, Bierwagen D. Rupture of the distal tendon of the biceps brachii. Operative versus non-operative treatment. *J Bone Joint Surg Am*. 1985;67(3):414-7. Available at: http://www.ncbi.nlm.nih.gov/pubmed/3972865. Accessed August 6, 2014.
8. Bain GI, Prem H, Heptinstall RJ, Verhellen R, Paix D. Repair of distal biceps tendon rupture: a new technique using the Endobutton. *J Shoulder Elbow Surg*. 2000;9(2):120-6. Available at: http://www.ncbi.nlm.nih.gov/pubmed/10810691. Accessed August 6, 2014.
9. Lintner S, Fischer T. Repair of the distal biceps tendon using suture anchors and an anterior approach. *Clin Orthop Relat Res*. 1996;(322):116-9. Available at: http://www.ncbi.nlm.nih.gov/pubmed/8542686. Accessed August 6, 2014.
10. Rantanen J, Orava S. Rupture of the distal biceps tendon. A report of 19 patients treated with anatomic reinsertion, and a meta-analysis of 147 cases found in the literature. *Am J Sports Med*. 1999;27(2):128-32. Available at: http://www.ncbi.nlm.nih.gov/pubmed/10102089. Accessed August 6, 2014.
11. Sotereanos DG, Pierce TD, Varitimidis SE. A simplified method for repair of distal biceps tendon ruptures. *J Shoulder Elbow Surg*. 2000;9(3):227-33. Available at: http://www.ncbi.nlm.nih.gov/pubmed/10888168. Accessed August 6, 2014.
12. Kulshreshtha R, Singh R, Sinha J, Hall S. Anatomy of the distal biceps brachii tendon and its clinical relevance. *Clin Orthop Relat Res*. 2007;456:117-20. doi:10.1097/BLO.0b013e31802f78aa.
13. Sassmannshausen G, Mair SD, Blazar PE. Rupture of a bifurcated distal biceps tendon. A case report. *J Bone Joint Surg Am*. 2004;86-A(12):2737-40. Available at: http://www.ncbi.nlm.nih.gov/pubmed/15590862. Accessed August 6, 2014.

14. Murray WM, Delp SL, Buchanan TS. Variation of muscle moment arms with elbow and forearm position. *J Biomech*. 1995;28(5):513-25. Available at: http://www.ncbi.nlm.nih.gov/pubmed/7775488. Accessed August 6, 2014.

15. Landa J, Bhandari S, Strauss EJ, Walker PS, Meislin RJ. The effect of repair of the lacertus fibrosus on distal biceps tendon repairs: a biomechanical, functional, and anatomic study. *Am J Sports Med*. 2009;37(1):120-3. doi:10.1177/0363546508324694.

16. Krushinski EM, Brown JA, Murthi AM. Distal biceps tendon rupture: biomechanical analysis of repair strength of the Bio-Tenodesis screw versus suture anchors. *J Shoulder Elbow Surg*. 2007;16(2):218-23. doi:10.1016/j.jse.2006.05.006.

17. Idler CS, Montgomery WH, Lindsey DP, Badua PA, Wynne GF, Yerby SA. Distal biceps tendon repair: a biomechanical comparison of intact tendon and 2 repair techniques. *Am J Sports Med*. 2006;34(6):968-74. doi:10.1177/0363546505284185.

18. Henry J, Feinblatt J, Kaeding CC, et al. Biomechanical analysis of distal biceps tendon repair methods. *Am J Sports Med*. 2007;35(11):1950-4. doi:10.1177/0363546507305009.

19. Bremer AK, Sennwald GR, Favre P, Jacob HAC. Moment arms of forearm rotators. *Clin Biomech (Bristol, Avon)*. 2006;21(7):683-91. doi:10.1016/j.clinbiomech.2006.03.002.

20. Berlet GC, Johnson JA, Milne AD, Patterson SD, King GJ. Distal biceps brachii tendon repair. An in vitro biomechanical study of tendon reattachment. *Am J Sports Med*. 1998;26(3):428-32. Available at: http://www.ncbi.nlm.nih.gov/pubmed/9617408. Accessed August 6, 2014.

21. Jarrett CD, Weir DM, Stuffmann ES, Jain S, Miller MC, Schmidt CC. Anatomic and biomechanical analysis of the short and long head components of the distal biceps tendon. *J Shoulder Elbow Surg*. 2012;21(7):942-8. doi:10.1016/j.jse.2011.04.030.

22. Moore KL, Dalley AF, Agur AMR. *Clinically Oriented Anatomy*. 6th ed. Lippincott Williams & Wilkins; 2006:1209.

23. Flloyd RT, Clem W. *Manual of the Structural Kinesiology*. 14th ed. Boston: McGraw-Hill; 2001.

24. Amis AA, Dowson D, Wright V, Miller JH. The derivation of elbow joint forces, and their relation to prosthesis design. *J Med Eng Technol*. 1979;3(5):229-34. Available at: http://www.ncbi.nlm.nih.gov/pubmed/490614. Accessed August 6, 2014.

25. Zimmerman NB. Clinical application of advances in elbow and forearm anatomy and biomechanics. *Hand Clin*. 2002;18(1):1-19. Available at: http://www.ncbi.nlm.nih.gov/pubmed/12143408. Accessed August 6, 2014.

26. Moore DC, Hogan KA, Crisco JJ, Akelman E, Dasilva MF, Weiss A-PC. Three-dimensional in vivo kinematics of the distal radioulnar joint in malunited distal radius fractures. *J Hand Surg Am*. 2002;27(2):233-42. Available at: http://www.ncbi.nlm.nih.gov/pubmed/11901382. Accessed August 6, 2014.

27. Grégory T, Roure P, Fontès D. Repair of distal biceps tendon rupture using a suture anchor: description of a new endoscopic procedure. *Am J Sports Med*. 2009;37(3):506-11. doi:10.1177/0363546508326985.

28. Hallam P, Bain GI. Repair of chronic distal biceps tendon ruptures using autologous hamstring graft and the Endobutton. *J Shoulder Elbow Surg*. 2004;13(6):648-51. doi:10.1016/S1058274604000771.

29. Hartman MW, Merten SM, Steinmann SP. Mini-open 2-incision technique for repair of distal biceps tendon ruptures. *J Shoulder Elbow Surg*. 2007;16(5):616-20. doi:10.1016/j.jse.2006.10.021.

30. Shukla DR, Morrey BF, Thoreson AR, An K-N, O'Driscoll SW. Distal biceps tendon rupture: an in vitro study. *Clin Biomech (Bristol, Avon)*. 2012;27(3):263-7. doi:10.1016/j.clinbiomech.2011.09.010.

31. Ferreira LM. Development of an active elbow motion simulator and coordinate systems to evaluate kinematics in multiple positions. 2011.

32. Kuxhaus L. Development Of A Feedback-Controlled Elbow Simulator: Design Validation And Clinical Application. 2008.

33. Wuelker N, Wirth CJ, Plitz W, Roetman B. A dynamic shoulder model: reliability testing and muscle force study. *J Biomech*. 1995;28(5):489-99. Available at: http://www.ncbi.nlm.nih.gov/pubmed/7775486. Accessed August 6, 2014.

34. Poitras P, Kingwell SP, Ramadan O, Russell DL, Uhthoff HK, Lapner P. The effect of posterior capsular tightening on peak subacromial contact pressure during simulated active abduction in the scapular plane. *J Shoulder Elbow Surg*. 2010;19(3):406-13. doi:10.1016/j.jse.2009.09.009.

35. Magnusen J. Design and fabrication of an elbow motion simulator. 2004.

36. Amis AA, Dowson D, Wright V. Elbow joint force predictions for some strenuous isometric actions. *J Biomech*. 1980;13(9):765-75. Available at: http://www.ncbi.nlm.nih.gov/pubmed/7440591. Accessed August 6, 2014.

37. Haugstvedt JR, Berger RA, Berglund LJ. A mechanical study of the moment-forces of the supinators and pronators of the forearm. *Acta Orthop Scand*. 2001;72(6):629-34. doi:10.1080/000164701317269076.

38. Wu G, van der Helm FCT, Veeger HEJD, et al. ISB recommendation on definitions of joint coordinate systems of various joints for the reporting of human joint motion--Part II: shoulder, elbow, wrist and hand. *J Biomech*. 2005;38(5):981-992. Available at: http://www.ncbi.nlm.nih.gov/pubmed/15844264. Accessed July 21, 2014.

39. Brownhill JR, Furukawa K, Faber KJ, Johnson JA, King GJW. Surgeon accuracy in the selection of the flexion-extension axis of the elbow: an in vitro study. *J Shoulder Elbow Surg*. 2006;15(4):451-6. doi:10.1016/j.jse.2005.09.011.

40. Koulouris G, Malone W, Omar IM, Gopez AG, Wright W, Kavanagh EC. Bifid insertion of the distal biceps brachii tendon with isolated rupture: magnetic resonance findings. *J Shoulder Elbow Surg*. 2009;18(6):e22-5. doi:10.1016/j.jse.2009.03.018.

41. Mazzocca AD, Cohen M, Berkson E, et al. The anatomy of the bicipital tuberosity and distal biceps tendon. *J Shoulder Elbow Surg*. 2007;16(1):122-7. doi:10.1016/j.jse.2006.04.012.

42. Morrey BF, Askew LJ, An KN, Dobyns JH. Rupture of the distal tendon of the biceps brachii. A biomechanical study. *J Bone Joint Surg Am*. 1985;67(3):418-21. Available at: http://www.ncbi.nlm.nih.gov/pubmed/3972866. Accessed August 6, 2014.

43. Nesterenko S, Domire ZJ, Morrey BF, Sanchez-Sotelo J. Elbow strength and endurance in patients with a ruptured distal biceps tendon. *J Shoulder Elbow Surg*. 2010;19(2):184-9. doi:10.1016/j.jse.2009.06.001.

44. Niemeyer P, Köstler W, Bley T, et al. Anatomical refixation for acute ruptures of the distal biceps tendon using a novel transcortical refixation system. *Arch Orthop Trauma Surg*. 2008;128(6):573-81. doi:10.1007/s00402-007-0400-1.

45. Schmidt CC, Weir DM, Wong AS, Howard M, Miller MC. The effect of biceps reattachment site. *J Shoulder Elbow Surg*. 2010;19(8):1157-65. doi:10.1016/j.jse.2010.05.027.

46. Cheung E V, Lazarus M, Taranta M. Immediate range of motion after distal biceps tendon repair. *J Shoulder Elbow Surg*. 2005;14(5):516-8. doi:10.1016/j.jse.2004.12.003.

47. Cil A, Merten S, Steinmann SP. Immediate active range of motion after modified 2-incision repair in acute distal biceps tendon rupture. *Am J Sports Med*. 2009;37(1):130-5. doi:10.1177/0363546508323749.

48. Sutton KM, Dodds SD, Ahmad CS, Sethi PM. Surgical treatment of distal biceps rupture. *J Am Acad Orthop Surg*. 2010;18(3):139-48. Available at: http://www.ncbi.nlm.nih.gov/pubmed/20190104. Accessed August 6, 2014.

49. McKee MD, Hirji R, Schemitsch EH, Wild LM, Waddell JP. Patient-oriented functional outcome after repair of distal biceps tendon ruptures using a single-incision technique. *J Shoulder Elbow Surg*. 2005;14(3):302-6. doi:10.1016/j.jse.2004.09.007.

50. Pearl ML. Proximal humeral anatomy in shoulder arthroplasty: Implications for prosthetic design and surgical technique. *J Shoulder Elb Surg*. 2004;14(1 Suppl S):99S-104S. doi:10.1016/j.jse.2004.09.025.

51. Pratt V. Least-Squares Fitting of Algebraic Surfaces. *Sun microsystems Inc Stanford Univerity*. 1987.

52. Ferreira LM, King GJW, Johnson JA. Motion-derived coordinate systems reduce inter-subject variability of elbow flexion kinematics. *J Orthop Res*. 2011;29(4):596-601. doi:10.1002/jor.21278.

Appendix A: Intact and Repair individual specimen data

			S1						S2					
			Intact		Anatomic Repair		Non-Anatomic Repair		Intact		Anatomic Repair		Non-Anatomic Repair	
			Mean	Stdev	Mean	Stdev	Mean	Stdev	Mean	Stdev	Mean	Stdev	Mean	Stdev
Flex Froce (N)	Pro	Both	10.63	0.85	NA				20.51	1.23	NA			
		SH	7.43	1.08					13.61	1.46				
		LH	5.45	0.89					10.20	0.54				
	Neut	Both	12.99	2.83					20.90	0.39				
		SH	7.12	0.80					13.76	1.68				
		LH	5.75	0.75					10.92	2.13				
	Sup	Both	12.85	2.63					22.56	0.50				
		SH	7.37	1.29					14.76	2.16				
		LH	4.60	0.73					9.93	2.13				
Tor (Nm)	Pro	Both	0.92	0.06	0.97	0.03	0.95	0.05	1.37	0.02	1.68	0.02	1.57	0.08
		SH	0.59	0.03	0.57	0.01	0.54	0.04	0.80	0.04	1.03	0.05	0.96	0.02
		LH	0.52	0.06	0.56	0.01	0.47	0.01	0.62	0.03	0.81	0.02	0.76	0.04
	Neut	Both	1.02	0.05	1.00	0.02	0.53	0.01	1.73	0.05	1.77	0.02	1.74	0.07
		SH	0.65	0.05	0.51	0.01	0.26	0.02	1.00	0.02	1.17	0.01	1.13	0.06
		LH	0.53	0.02	0.57	0.03	0.34	0.01	0.88	0.04	0.89	0.04	0.99	0.05
	Sup	Both	0.95	0.04	0.72	0.00	0.09	0.00	1.33	0.02	1.43	0.02	1.40	0.07
		SH	0.49	0.09	0.31	0.02	0.04	0.03	0.66	0.01	0.81	0.02	0.78	0.11
		LH	0.62	0.02	0.40	0.01	0.07	0.03	0.61	0.01	0.64	0.04	0.68	0.01

			S3						S4					
			Intact		Anatomic Repair		Non-Anatomic Repair		Intact		Anatomic Repair		Non-Anatomic Repair	
			Mean	Stdev	Mean	Stdev	Mean	Stdev	Mean	Stdev	Mean	Stdev	Mean	Stdev
Flex Force (N)	Pro	Both	8.63	0.43					10.49	0.36				
		SH	6.58	0.38					7.44	0.36				
		LH	4.40	0.45					7.47	0.55				
	Neut	Both	8.82	0.34					13.05	0.33				
		SH	6.60	1.10			NA		9.40	0.37			NA	
		LH	4.60	0.36					8.77	0.54				
	Sup	Both	10.87	0.35					13.47	0.35				
		SH	8.50	0.23					8.76	0.24				
		LH	6.60	0.28					9.19	0.62				
Tor (Nm)	Pro	Both	0.98	0.00	1.09	0.08	* failure	* failure	0.84	0.00	1.00	0.02	1.03	0.03
		SH	0.67	0.04	0.64	0.07	* failure	* failure	0.44	0.02	0.58	0.02	0.58	0.01
		LH	0.45	0.01	0.53	0.02	* failure	* failure	0.52	0.01	0.58	0.01	0.66	0.00
	Neut	Both	1.20	0.03	1.29	0.01	1.08	*failure	1.19	0.03	1.14	0.01	0.69	0.19
		SH	0.79	0.05	0.74	0.03	0.61	* failure	0.66	0.01	0.62	0.02	0.62	0.08
		LH	0.63	0.02	0.63	0.04	* failure	* failure	0.83	0.05	0.69	0.00	0.65	0.24
	Sup	Both	0.99	0.01	1.09	0.03	0.60	0.10	0.82	0.02	0.94	0.04	0.11	0.06
		SH	0.61	0.08	0.57	0.03	0.25	0.03	0.55	0.01	0.44	0.02	0.08	0.05
		LH	0.59	0.08	0.57	0.02	0.38	0.07	0.60	0.02	0.56	0.04	0.11	0.05

			S5						S6					
			Intact		Anatomic Repair		Non-Anatomic Repair		Intact		Anatomic Repair		Non-Anatomic Repair	
			Mean	Stdev	Mean	Stdev	Mean	Stdev	Mean	Stdev	Mean	Stdev	Mean	Stdev
Flex Force (N)	Pro	Both	11.08	0.88	NA				20.38	0.56	NA			
		SH	6.96	0.74					14.33	0.47				
		LH	6.68	1.12					10.82	0.25				
	Neut	Both	13.70	0.09					21.87	0.36				
		SH	9.04	0.32					15.05	0.51				
		LH	8.90	0.86					13.57	0.19				
	Sup	Both	12.41	1.15					21.21	0.53				
		SH	7.35	0.21					13.35	0.49				
		LH	8.00	0.66					12.52	0.31				
Tor (Nm)	Pro	Both	1.12	0.03	1.25	0.01	1.11	0.08	1.26	0.02	1.36	0.02	1.06	0.01
		SH	0.59	0.03	0.66	0.00	0.58	0.04	0.85	0.09	0.73	0.02	0.56	0.02
		LH	0.63	0.03	0.74	0.03	0.63	0.01	0.68	0.05	0.71	0.05	0.61	0.03
	Neut	Both	1.21	0.02	1.13	0.03	0.88	0.03	1.22	0.01	1.26	0.04	1.15	0.05
		SH	0.62	0.05	0.57	0.06	0.45	0.04	0.72	0.09	0.71	0.02	0.59	0.10
		LH	0.69	0.04	0.61	0.01	0.49	0.00	0.76	0.05	0.61	0.05	0.73	0.03
	Sup	Both	0.86	0.02	0.86	0.04	0.26	0.01	1.13	0.02	1.10	0.02	0.91	0.01
		SH	0.43	0.03	0.47	0.02	0.13	0.00	0.71	0.03	0.56	0.03	0.56	0.05
		LH	0.50	0.01	0.55	0.01	0.18	0.01	0.74	0.07	0.64	0.06	0.50	0.01

			S7						S8					
			Intact		Anatomic Repair		Non-Anatomic Repair		Intact		Anatomic Repair		Non-Anatomic Repair	
			Mean	Stdev	Mean	Stdev	Mean	Stdev	Mean	Stdev	Mean	Stdev	Mean	Stdev
Flex Force (N)	Pro	Both	5.54	0.17	NA				8.13	0.29	NA			
		SH	3.54	0.21					6.74	0.23				
		LH	3.12	0.25					5.36	0.47				
	Neut	Both	6.81	0.21					7.21	0.23				
		SH	4.60	0.14					5.70	0.10				
		LH	4.12	0.29					4.78	0.25				
	Sup	Both	6.35	0.07					8.09	0.32				
		SH	4.87	0.13					5.80	0.34				
		LH	4.12	0.10					5.06	0.58				
Tor (Nm)	Pro	Both	0.56	0.03	0.63	0.05	0.71	0.02	0.52	0.00	0.63	0.00	0.46	0.22
		SH	0.30	0.01	0.34	0.03	0.38	0.02	0.35	0.03	0.44	0.02	0.50	0.06
		LH	0.32	0.02	0.33	0.02	0.45	0.01	0.31	0.01	0.38	0.01	0.33	0.10
	Neut	Both	0.77	0.03	0.81	0.01	0.74	0.01	0.70	0.00	0.72	0.03	0.83	0.02
		SH	0.46	0.02	0.47	0.02	0.42	0.01	0.41	0.02	0.45	0.02	0.59	0.03
		LH	0.43	0.01	0.54	0.01	0.43	0.02	0.44	0.00	0.45	0.02	0.41	0.02
	Sup	Both	0.84	0.02	0.87	0.01	0.67	0.04	0.66	0.00	0.75	0.08	0.67	0.00
		SH	0.48	0.00	0.49	0.02	0.39	0.05	0.38	0.02	0.54	0.10	0.49	0.01
		LH	0.52	0.01	0.55	0.01	0.40	0.02	0.43	0.00	0.45	0.04	0.37	0.04

Appendix B: Biceps Loading Schedule

			Intact			Anatomic Repair			Non-Anatomic Repair		
Method	Forearm Orientation	Load	Head			Head			Head		
Unconstrained Flexion	45 Pro	80	□ B	□ S	□ L						
			□ S	□ L	□ S						
			□ L	□ B	□ B						
	Neut	80	□ B	□ S	□ L						
			□ S	□ L	□ S						
			□ L	□ B	□ B						
	45 Sup	80	□ B	□ S	□ L						
			□ S	□ L	□ S						
			□ L	□ B	□ B						
Unconstrained Torque	45 Pro	80	□ B	□ S	□ L	□ B	□ S	□ L	□ B	□ S	□ L
			□ S	□ L	□ S	□ S	□ L	□ S	□ S	□ L	□ S
			□ L	□ B	□ B	□ L	□ B	□ B	□ L	□ B	□ B
	Neut	80	□ B	□ S	□ L	□ B	□ S	□ L	□ B	□ S	□ L
			□ S	□ L	□ S	□ S	□ L	□ S	□ S	□ L	□ S
			□ L	□ B	□ B	□ L	□ B	□ B	□ L	□ B	□ B
	45 Sup	80	□ B	□ S	□ L	□ B	□ S	□ L	□ B	□ S	□ L
			□ S	□ L	□ S	□ S	□ L	□ S	□ S	□ L	□ S
			□ L	□ B	□ B	□ L	□ B	□ B	□ L	□ B	□ B

Appendix C: Load Transfer Analysis and Modification

The initial design for transferring the load at the wrist to the load cell was done with the assumption of negligible channel cross-talk. As shown in Figure 41, the experiment design included fixing a radial transverse torque pin directly to the load adapter with compression screws, to measure elbow flexion and supination simultaneously. This initial design would reduce testing time. However, during the first pilot, two major deficiencies of this design were identified.

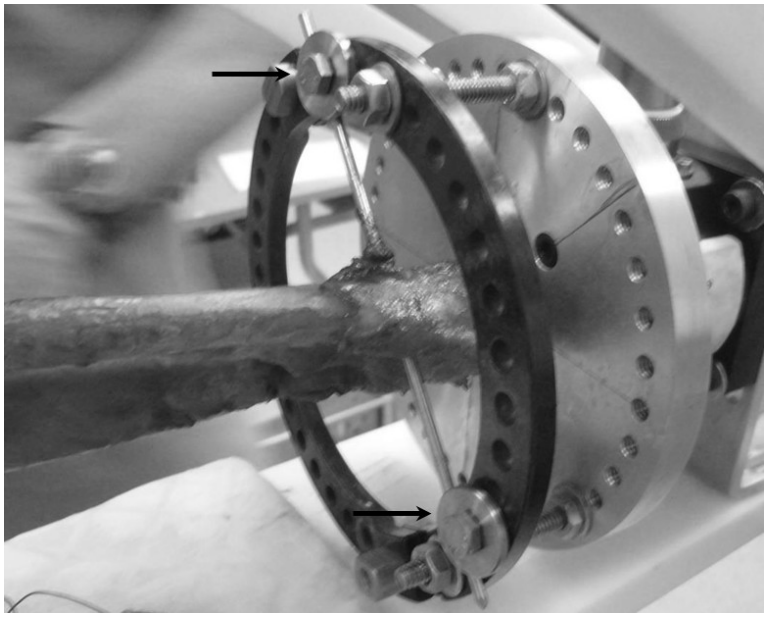

Figure 41. Rigid fixation of the radius to the fixator (initial wrist load to load cell transfer design).

First, rigid fixation of the distal radius to the adapter resulted in reaction forces that would otherwise not be observed in the unconstrained in-vivo scenario. As the radius is rotated about the ulna, the initially transversely inserted fixation pin diverges and is no longer parallel to the

fixator and load cell and the load transfer was no longer aligned with the long axis of the arm. This change in orientation is a result of the bone geometry and axial translation of the radius through its rotation range as discussed in Section 2.

Second, the AMTI load cell is specifically designed to mitigate cross-talk across the measured channels when subjected to off-axis loads, practically. Cross-talk is the mechanical coupling between mutually perpendicular axes which affects the signal output in multi-axis load cells. In this case, by rigidly fixing the distal radius to the load cell, the non-physiological reaction loads along the x-axis and z-axis (corresponding to medial-lateral and axial loads) affected the output of the y-axis (flexion force).

Using the inverse of manufacturer supplied sensitivity matrix (Table 13**)** for this load cell and conversion equation for each of the 6 load cell channels below to resolve the force readings to voltage output signal**,** the channels were decoupled and the true loads in each channel determined and compared to the initial load cell output.

$$\boldsymbol{F \text{ or } M = \frac{V_{out}}{V_{exc}.S.G.10^{-6}}}$$

Where

$\boldsymbol{F}$ – The applied load on the load

$\boldsymbol{M}$ – The applied moment on the load cell

$\boldsymbol{V_{out}}$ – The output voltage for an applied F or M

$\boldsymbol{V_{exc}}$ – The excitation voltage for the given channel

$\boldsymbol{S}$ – The sensitivity of F or M

G – The channel gain

Table 12 highlights the large cross talk effects associated with the rigid radius fixation design.

Table 12. Effect of multi-axis load cell channel cross-talk.

Channel	Direct Measure	Decoupled Measure	% Difference
Fx	1.43	0.28	413.2
Fy	26.96	29.61	8.9
Fz	16.89	19.88	15.0
Mx	4.12	4.10	0.5
My	0.79	0.80	0.9
Mz	1.10	1.09	1.0

In order to ensure closer approximation of the unconstrained in-vivo wrist load condition and to reduce the significant cross talk and off-axis torques and forces observed during the initial pilot, the distal attachment of the wrist to the load cell adapter was modified.

Adopting a technique similar to that used by Henry et al. the flexion force and supination torque measurements were decoupled. That is, rather than having fixed attachment points to the load cell, the ulna and radius were connected to the load cell separately depending on which load was to be measured.

Table 13. Load cell sensitivity matrix

0.197056	-0.001945602	-0.001085145	0.00208299	-0.00307	-0.00111
0.000177	0.195548818	-0.003736639	0.00270409	0.000897	-0.00045
-0.0023	0.002335071	0.771244842	-0.0040688	0.005875	-0.00103
1.2E-05	-2.21253E-05	0.000300071	0.00387033	-4.3E-05	-1.3E-05
-2.5E-05	-7.80718E-05	0.000144654	2.5505E-05	0.00386	-3.4E-05
5.19E-05	-3.97348E-05	-2.39692E-05	-5.095E-06	8.6E-07	0.005525

Appendix D: Kinematic tracking definition and Matlab scripts

D.1 Description of the tracking system

The Polaris passive marker optical tracking system has a volume RMS distance error of 0.35 mm. At its most basic level, this system relies on the principal of triangulation, whereby resolving the distance of an object from at least two different reference locations, and knowing the offset angles and distances between the reference points, the object of interest can be tracked and located within the field of interest. This concept has been applied successfully to track large rigid body motion in applications such as motion capture for animation. The Polaris system was designed, and is used extensively to study human body kinematics such as gait analysis and joint range of motion both in-vivo and in-vitro and has also been used in computer-navigated orthopaedic surgical protocols. The system employs a pair of infrared cameras with a fixed offset. Reflective location markers are arranged in unique geometries forming "tools". The location markers are tracked according to their centroid, and represent a single point in space. Therefore, object needs at least three of them to be tracked as a rigid body experiencing translations as well as rotations in space. The tools are distinguished by their unique patterns. Pattern recognition algorithms identify the marker clusters as tools and track their position and orientation. The pattern origin can be defined arbitrarily; in this case one of the markers in each tool is defined as the tool origin. The tools are positioned on the rigid bodies to be tracked. The cameras emit an infrared signal at fixed intervals, the tools reflect the attenuated signals back to the cameras and the location of the tools and hence the rigid bodies are resolved.

D.2 Tool tracking and transformation

The process of registration defines the spatial relation between the landmarks on each bone to the tracked tool in that bone. It therefore becomes only necessary to track the single tool in the bone after the initial registration due to the reasonable assumption that the bones are rigid bodies particularly under physiologic loads.

Each tool is tracked by the Polaris camera system and the rotation and translation of the tools in the camera's global reference system are recorded as a seven cell array with the first four cells representing tool rotation in quaternion form and the last three cells representing the tool translation as follows:

$$\boldsymbol{Q} = [q_w\ , q_x\ , q_y\ , q_z\ , T_x\ , T_y\ , T_z\ ]$$

Quaternion definition of rotations has advantages over Euler angle rotation matrices, particularly when tracking multiple segments and reference frames since they can be added and multiplied algebraically and rotations are easily invertible. However, we are only interested in tracking two segments at most at a time, the ulna relative to humerus for flexion, and radius relative to ulna for pro/supination. The quaternion tracking data is therefore converted to the more intuitive Euler angle rotation matrix (**R**) for analysis using the qat2mat.m Matlab routine driven by the equation below**.**

$$\boldsymbol{R} = \begin{bmatrix} 1-2q_y^2-2q_z^2 & 2q_xq_y-2q_zq_w & 2q_xq_z-2q_yq_w \\ 2q_xq_y-2q_zq_w & 1-2q_x^2-2q_z^2 & 2q_yq_z-2q_xq_w \\ 2q_xq_z-2q_yq_w & 2q_yq_z-2q_xq_w & 1-2q_x^2-2q_y^2 \end{bmatrix}$$

As was stated previously, the Polaris system tracks the rigid body tools and not the digitized landmarks. Therefore it is necessary to transform the localized landmark data from the registration phase to the global coordinate system. The landmarks are then used to construct bone segment coordinate systems. The segment axes are then transformed into the reference joint coordinate system (JCS) and the resulting rotation matrix is resolved for the Euler angles that define the joint orientation.

The following transformation equation and notation is used to transform from one coordinate frame to another, in this case, from a local coordinate system to a global one:

$$^{G}\boldsymbol{P}_{L} = {}^{G}\boldsymbol{R}_{L}\ \boldsymbol{P}_{L} + \boldsymbol{T}_{G}$$

Where

$\boldsymbol{P}_{G}$ – Final point in global coordinate system

$\boldsymbol{R}_{L}^{G}$ – 3x3 rotation matrix from local to global coordinate system

$\boldsymbol{P}_{L}$ – Initial point in local coordinate system

$\boldsymbol{T}_{G}$ – Translation vector from local to global coordinate system

D.3 Elbow Joint Coordinate System

In order to track the elbow kinematics, three bone segment coordinate systems (for the humerus, ulna and radius) are created using International Society of Biomechanics recommendation for bone segment and joint coordinate systems.[38] Two JCS's relating the bone segment coordinate systems defined above are used as per ISB recommendation. The humeroulnar joint coordinate

system is used to relate the motion of the ulna to the humerus and primarily track the elbow flexion angle and follows ZXY angle order. The radioulnar joint coordinate system is used to relate the motion of the radius to the ulna and specifically track forearm pro/supination and follows XZY angle order. The definitions of the bone segments and the corresponding rotation matrices used to relate the orientation of the segments are described here. The humeral bone segment coordinate system was defined as follows (Figure 42):

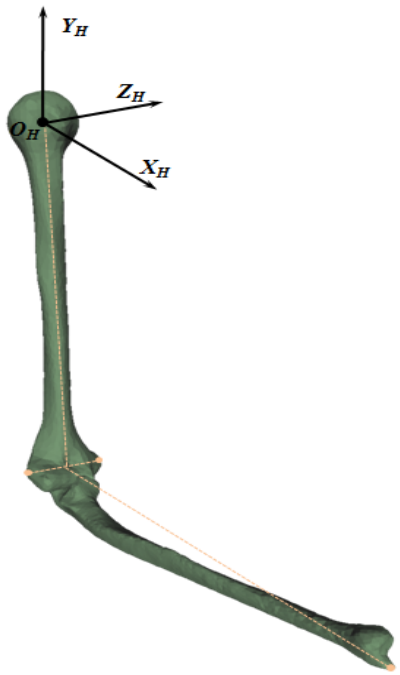

Figure 42. Humerus bone segment coordinate system.

Where

$\boldsymbol{O_H}$ – The origin, coincident to the humeral head center of rotation

$\boldsymbol{Y_H}$ – The long axis of the humerus, defined by the line extending from the midpoint between the medial (ME) and lateral (LE) epicondyles and directed towards the humeral head center of rotation

$\boldsymbol{Z_H}$ –The elbow flexion axis, defined by the line extending from ME and LE

$\boldsymbol{X_H}$ – Defined as the line mutually perpendicular to ZH and YH and pointing forward

Described in vector form as adopted for kinematic tracking, the rotation matrix for the transformation from the humeral coordinate system to the global coordinate system is given by:

$$^{G}\boldsymbol{R}_H = \left[{}^{G}\boldsymbol{I}_H \;\; {}^{G}\boldsymbol{J}_H \;\; {}^{G}\boldsymbol{K}_H \right]$$

Where

$$^{G}\boldsymbol{K}_H = \boldsymbol{Z}_H : \frac{\boldsymbol{ME}_H - \boldsymbol{LE}_H}{\left\| \boldsymbol{ME}_H - \boldsymbol{LE}_H \right\|}$$

$$^{G}\boldsymbol{J}_H = \boldsymbol{Y}_H : \frac{\boldsymbol{O}_H - \left(\frac{\boldsymbol{ME}_H + \boldsymbol{LE}_H}{2} \right)}{\left\| \boldsymbol{O}_H - \left(\frac{\boldsymbol{ME}_H + \boldsymbol{LE}_H}{2} \right) \right\|}$$

$$^{H}\boldsymbol{I}_U : {}^{H}\boldsymbol{J}_U \times {}^{H}\boldsymbol{K}_U$$

The rotation center of the humeral head is required to define the long axis of the Humerus. Since it is not possible to directly digitize the center with the probe, the humeral head articular surface, which can be approximated by a sphere, was instead digitized with multiple points creating a point cloud.[50] A Matlab routine, SphereFit.m, was used to fit a sphere to the point cloud and the coordinates of the best fit sphere was used as the humeral head center of rotation. The code, as

published by Alan Jennings[4], is an adaptation of the general least-squares fitting of algebraic surfaces method described by Pratt and minimizes the following error function for a sphere[51]:

$$\sum_{i=1}^{n}(x_i - x_c)^2 + (y_i - y_c)^2 + (z_i - z_c)^2 - r^2)^2$$

Where

(x_i, y_i, z_i) is a data point from the traced surface point cloud

(x_c, y_c, z_c) is the center of the best fit sphere

r is the radius of the sphere

Next, the ulnar bone segment coordinate system is defined as follows (Figure 43):

[4] http://www.mathworks.com/matlabcentral/fileexchange/34129-sphere-fit--least-squared-

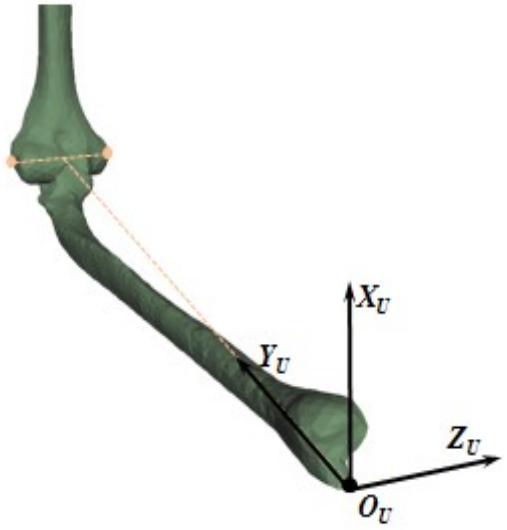

Figure 43. Ulna bone segment coordinate system.

Where

O_U – The origin, coincident to ulnar styloid US

Y_U – The long axis of the ulna, defined by the line extending from the US and directed towards the midpoint between the ME and LE

X_U – The norm to the plane formed by the US, ME and LE and directed forward.

Z_U – Defined as the line mutually perpendicular to YU and XU and pointing to the right

The corresponding rotation matrix transforming the ulna coordinate system to the humeral coordinate system given by:

$$^{H}\boldsymbol{R}_{U} = \left[{}^{H}\boldsymbol{I}_{U} \;\; {}^{H}\boldsymbol{J}_{U} \;\; {}^{H}\boldsymbol{K}_{U} \right]$$

Where

$$^{H}\boldsymbol{J}_{U} = \boldsymbol{Y}_{U} : \frac{\boldsymbol{US}_{U} - \left(\frac{\boldsymbol{ME}_{H} + \boldsymbol{LE}_{H}}{2} \right)}{\left\| \boldsymbol{US}_{U} - \left(\frac{\boldsymbol{ME}_{H} + \boldsymbol{LE}_{H}}{2} \right) \right\|}$$

$$^{H}\boldsymbol{K}_{U} = \boldsymbol{Z}_{U} : \left[\frac{\boldsymbol{US}_{U} - \boldsymbol{ME}_{H}}{\left\|\boldsymbol{US}_{U} - \boldsymbol{ME}_{H}\right\|}\right] \times \left[\frac{\boldsymbol{US}_{U} - \boldsymbol{LE}_{H}}{\left\|\boldsymbol{US}_{U} - \boldsymbol{LE}_{H}\right\|}\right]$$

$$^{H}\boldsymbol{I}_{U} = \boldsymbol{X}_{U} : {}^{H}\boldsymbol{J}_{U} \times {}^{H}\boldsymbol{K}_{U}$$

Finally, the radial bone segment coordinate system is defined as follows (Figure 44):

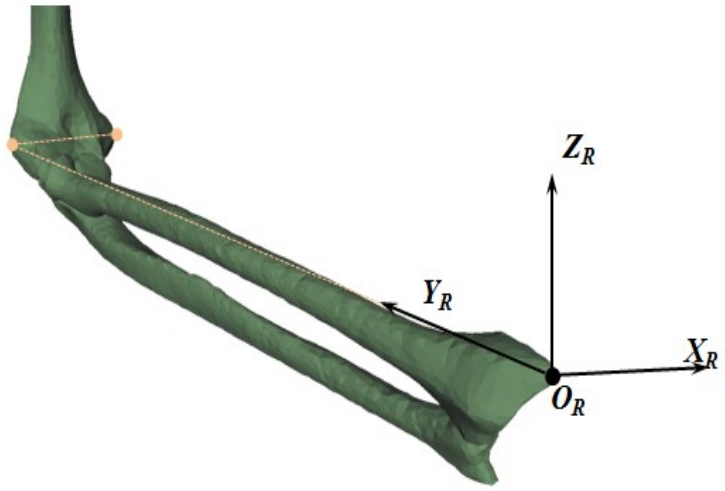

Figure 44. Radius bone segment coordinate system.

Where

O_R - The origin, coincident to the most caudal point on the radial styloid (RS)

Y_R - The long axis of the radius, defined as the line extending from the RS and directed towards the LE.

X_R - The norm to the plane formed by RS, US and LE, directed forward

Z_R - The line mutually perpendicular to XR and YR and directed to the right

The corresponding rotation matrix transforming the radius coordinate system to the ulnar coordinate system given by:

$$^{U}\boldsymbol{R}_{R} = \left[{}^{U}\boldsymbol{I}_{R} \;\; {}^{U}\boldsymbol{J}_{R} \;\; {}^{U}\boldsymbol{K}_{R} \right]$$

Where

$$^{U}\boldsymbol{J}_{R} = \boldsymbol{Y}_{R} : \frac{\boldsymbol{RS}_{R} - \boldsymbol{LE}_{H}}{\left\| \boldsymbol{RS}_{R} - \boldsymbol{LE}_{H} \right\|}$$

$$^{U}\boldsymbol{I}_{R} = \boldsymbol{X}_{R} : \left[\frac{\boldsymbol{RS}_{R} - \boldsymbol{ME}_{H}}{\left\| \boldsymbol{RS}_{R} - \boldsymbol{ME}_{H} \right\|} \right] \times \left[\frac{\boldsymbol{RS}_{R} - \boldsymbol{LE}_{H}}{\left\| \boldsymbol{RS}_{R} - \boldsymbol{LE}_{H} \right\|} \right]$$

$$^{U}\boldsymbol{Z}_{R} : {}^{U}\boldsymbol{I}_{R} \times {}^{U}\boldsymbol{J}_{R}$$

Once $\left[{}^{H}\boldsymbol{R}_{U} \right]$ is defined and transformed to the humeral frame of reference, the three rotation angles of the humeroulnar joint, following the ISB recommended ZXY order, are as resolved as follows:

$$^{H}R_{U} = \begin{bmatrix} i_{11} & j_{21} & k_{31} \\ i_{12} & j_{22} & k_{32} \\ i_{13} & j_{23} & k_{33} \end{bmatrix} = \begin{bmatrix} cos\beta cos\gamma & -cos\alpha sin\gamma & cos\gamma sin\beta + cos\beta sin\alpha sin\gamma \\ cos\gamma sin\alpha sin\beta & cos\alpha cos\gamma & -cos\beta cos\gamma sin\alpha + sin\beta sin\gamma \\ -cos\alpha sin\beta & sin\alpha & cos\alpha cos\beta \end{bmatrix}$$

Solving for α

$$\alpha = \text{asin}\left({}^{H}R_{U\,23} \right)$$

Where

$\boldsymbol{\alpha}$ - the elbow flexion angle

$\boldsymbol{\beta}$ - the elbow carrying angle

$\boldsymbol{\gamma}$ - the ulnar axial rotation angle (negligible)

Similarly $\left[{}^{U}\boldsymbol{R}_{R}\right]$ is used to solve for the three radioulnar rotation angles following the ISB recommended XZY order is as follows:

$$
{}^{U}R_{R} = \begin{bmatrix} i_{11} & j_{21} & k_{31} \\ i_{12} & j_{22} & k_{32} \\ i_{13} & j_{23} & k_{33} \end{bmatrix}
$$

$$
= \begin{bmatrix} cos\beta cos\gamma & -sin\gamma & cos\gamma sin\beta \\ sin\alpha sin\beta & cos\alpha cos\gamma & -cos\beta sin\alpha + cos\alpha sin\beta sin\gamma \\ -cos\alpha sin\beta + cos\beta sin\alpha sin\gamma & cos\gamma sin\alpha & cos\alpha cos\beta + sin\alpha sin\beta sin\gamma \end{bmatrix}
$$

Solving for $\boldsymbol{\beta}$

$$\beta = \text{atan2}\left({}^{U}R_{R\ 13}, {}^{U}R_{R\ 11}\right)$$

Where

$\boldsymbol{\beta}$ – the pro/supination angle of the radius relative to the ulna

$\boldsymbol{\alpha}$ – the angle formed by the pro/supination axis relative to the ulna

$\boldsymbol{\gamma}$ – the radius adduction/abduction angle (negligible)

D.4 Limitations of kinematic current model

As previously noted several assumptions were made when implementing the ISB anatomic coordinate systems used for this study. These assumptions may reflect the relatively large variations in tracked angles as seen in Section 3.4. While precise joint angular tracking was not crucial for this biceps study due to static loading and the discrete joint angles employed, accurate tracking of the elbow joint motion is of great importance in the study of joint kinematics and

stability following injury, repair and prosthesis implantation in general. Recent studies have shown that while ISB coordinate system for the elbow is adequate for gross in-vivo motion analysis, where direct palpation and access to the joint articulations is not possible, it does not accurately describe the joint motion.[52]

Additionally, the ISB defined coordinate systems are anatomy driven. More recent work by Louis et al. has shown a motion derived coordinate system for the elbow to be more accurate and reliable in tracking elbow joint kinematics.[52] By recording the joint motions, the flexion and forearm rotation axes can be calculated as helical or screw displacement axes. The intersection of these axes is used to create a function based joint coordinate system that is not reliant on approximation of bony landmarks and geometric approximation. Such a system should adopt in future iterations of the elbow simulator.

D.5 Matlab Code

```
function average_load()

%{
    Function scans Biceps LH vs SH MTS specimen.dat file and returns average
    forces and moments for each trial to loads.txt file.
%}

%Initialize variables
trials=20;

%open work files
%data file from MTS
f_spec=fopen('specimen.DAT','rt');
%open output file
f_loads=fopen('loads.txt','wt');

for trial=1:trials
    %read specimen file
    tmp=textscan(f_spec,'%f %f %f %f %f %f','HeaderLines',6,'delimiter',
'\t');
    %construst load matrix from temporary array
    Load=[tmp{1},tmp{2},tmp{3},tmp{4},tmp{5},tmp{6}];
    %convert to N and Nm
    Mean_Load=1000000*mean(Load);
    fprintf(f_loads,'%f, %f, %f, %f, %f, %f\n',Mean_Load);
end

fclose('all');



function Porixmal_radius()

%{
    Function scans all polaris trial files in directory and returns mean
coordinate and
    transformation data of the proximal head for each trial to Tracking.csv
file.
%}



%Setup work directory path and filename prefix
data_dir = 'E:\Data\Current Studies\Biceps - LH vs SH\Pilot Study\Pilot
3\Polaris';
filename_pfx = 'OLDPRO90_';
total_files = 254;

RadialHeadR=zeros(1,3);
LongHeadR=zeros(1,3);
ShortHeadR=zeros(1,3);
```

```
RadialHeadG=zeros(1,3);
LongHeadG=zeros(1,3);
ShortHeadG=zeros(1,3);


%open output file
f_AvP=fopen('AveragePolaris.txt','wt');
f_Track=fopen('Tracking.txt','wt');

%initialize tool matricies
for file_i=1:total_files


    if file_i<10
        file_num = strcat('00',int2str(file_i));
    elseif file_i<100
        file_num = strcat('0',int2str(file_i));
    else
        file_num = int2str(file_i);
    end;

    filename = fullfile(data_dir,strcat(filename_pfx,file_num,'.csv'));
    f_trial=fopen(filename,'rt');
    if f_trial < 0
        error('Could not open trial file')
    end;

    tmp=textscan(f_trial,'%*s %*s %s %*s %s %*s %*s %*s %*s %s %s
%s',1,'delimiter', ',');
    %Probe=[tmp{1},tmp{2},tmp{3},tmp{4},tmp{5}]

    tmp=textscan(f_trial,'%*s %*s %s %*s %s %s %s %s %s %s %s
%s',1,'delimiter', ',');
    %Humerus=[tmp{1},tmp{2},tmp{3},tmp{4},tmp{5},tmp{6},tmp{7},tmp{8},tmp{9}]

    tmp=textscan(f_trial,'%*s %*s %s %*s %s %s %s %s %s %s %s
%s',1,'delimiter', ',');
    %Radius=[tmp{1},tmp{2},tmp{3},tmp{4},tmp{5},tmp{6},tmp{7},tmp{8},tmp{9}]

    tmp=textscan(f_trial,'%*s %*s %s %*s %s %s %s %s %s %s %s %s
%*s',1,'delimiter', ',');
    %Frame=[tmp{1},tmp{2},tmp{3},tmp{4},tmp{5},tmp{6},tmp{7},tmp{8},tmp{9}]

    for frames=1:49
        tempp=cell2mat(textscan(f_trial,'%*d %*d %*d %*d %*s %*f %*f %*f %*f
%f %f %f %*f',1,'delimiter', ','));
        %make sure tempp ok
        if ~any(isnan(tempp))
            ProbeG(frames,:)=tempp;
        end

        tempr=cell2mat(textscan(f_trial,'%*d %*d %*d %*s %f %f %f %f %f %f %f
%*f',1,'delimiter', ','));
```

```
        if ~any(isnan(tempr))
            RadiusG(frames,:)=tempr;
        end

        temph=cell2mat(textscan(f_trial,'%*d %*d %*d %*s %f %f %f %f %f %f %f
%*f',1,'delimiter', ','));
        if ~any(isnan(temph))
            HumerusG(frames,:)=temph;
        end

        tempf=cell2mat(textscan(f_trial,'%*d %*d %*d %*s %f %f %f %f %f %f %f
%*f',1,'delimiter', ','));
        if ~any(isnan(tempf))
            FrameG(frames,:)=tempf;
        end


        %Convert radial head location from global reference to radial tool
        %reference
        if file_i==1
            q = tempr(1:4);
            TransR = tempr(5:7)';
            RotR = quat2mat(q);
            PG = tempp';
            RadialHead_i=RotR'*(PG-TransR);
            RadialHeadR(frames,:)=RadialHead_i;

        %Convert Long Head insertion location from global reference to radial
tool
        %reference
        elseif file_i==2
            q = tempr(1:4);
            TransR = tempr(5:7)';
            RotR = quat2mat(q);
            PG = tempp';
            LongHeadR_i= RotR'*(PG-TransR);
            LongHeadR(frames,:)=LongHeadR_i;
        %Convert Short Head insertion location from global reference to
radial tool
        %reference
        elseif file_i==3
            q = tempr(1:4);
            TransR = tempr(5:7)';
            RotR = quat2mat(q);
            PG = tempp';
            ShortHeadR_i = RotR'*(PG-TransR);
            ShortHeadR(frames,:)=ShortHeadR_i;

        %For subsequent frames convert RH. LH, SH from radius tool to
        %global
        else
            q = tempr(1:4);
            TransR = tempr(5:7)';
            RotR = quat2mat(q);
            RadialHeadG(frames,:) = RotR*mean(RadialHeadR)'+TransR;
            LongHeadG(frames,:) = RotR*mean(LongHeadR)'+TransR;
```

```
            ShortHeadG(frames,:) = RotR*mean(ShortHeadR)'+TransR;
        end;
    end;

    RadialHeadGMean = mean(RadialHeadG);
    LongHeadGMean = mean(LongHeadG);
    ShortHeadGMean = mean(ShortHeadG);

    if file_i>3
        fprintf(f_Track,'Trial: ');
        fprintf(f_Track,'%f\n',file_i);
        fprintf(f_Track,'Radial Head: ');
        fprintf(f_Track,'%f, %f, %f\n',RadialHeadGMean');
        fprintf(f_Track,'Long Head Insertion: ');
        fprintf(f_Track,'%f, %f, %f\n',LongHeadGMean');
        fprintf(f_Track,'Short Head Insertion: ');
        fprintf(f_Track,'%f, %f, %f\n\n',ShortHeadGMean');
    end


    fclose(f_trial);
end;
fclose(f_AvP);
fprintf('Done')
```

function Tracking()

```
%{
    Function converts initial landmarks to local tool coordinate system.
    Subsequent tracking files are used to create the humeroulnar and
radioulnar
    system coordinate system and the elbow flexion angle and supination
angles are resolved
%}


%Read registration data points and transform to the relevant tracking tool
%Humeral Head from spherefit optimization
importfile('HHg.csv');
humerusg=[HQ0,HQx,HQy,HQz,HTx,HTy,HTz];
HHg=[PTx,PTy,PTz];
HHG=mean(HHg)';
humerusg(1:4)=humerusg(1:4)/norm(humerusg(1:4));
% Humerus Tool Rotation Matrix
q = [humerusg(1:4)];
rotH = quat2mat(q);
% Transpose Humeral head to Humeral Tool Coordinate System
T = humerusg(5:7)';
HHh = rotH'*(HHG-T);

%Lateral Epicondyle
importfile('LEg.csv');
humerusg=[HQ0,HQx,HQy,HQz,HTx,HTy,HTz];
LEg=[PTx,PTy,PTz];
```

```
LEG=mean(LEg)';
humerusg(1:4)=humerusg(1:4)/norm(humerusg(1:4));
% Humerus Tool Rotation Matrix
q = [humerusg(1:4)];
rotH = quat2mat(q);
% Transpose Lateral Epidondyle to Humeral Tool Coordinate System
T = humerusg(5:7)';
LEh = rotH'*(LEG-T);

%Medial Epicondyle
importfile('MEg.csv');
humerusg=[HQ0,HQx,HQy,HQz,HTx,HTy,HTz];
MEg=[PTx,PTy,PTz];
MEG=mean(MEg)';
humerusg(1:4)=humerusg(1:4)/norm(humerusg(1:4));
% Humerus Tool Rotation Matrix
q = [humerusg(1:4)];
rotH = quat2mat(q);
% Transpose Lateral Epidondyle to Humeral Tool Coordinate System
T = humerusg(5:7)';
MEh = rotH'*(MEG-T);

%Ulnar Styloid
importfile('USg.csv');
ulnag=[UQ0,UQx,UQy,UQz,UTx,UTy,UTz];
USg=[PTx,PTy,PTz];
USG=mean(USg)';
ulnag(1:4)=ulnag(1:4)/norm(ulnag(1:4));
% Ulna Tool Rotation Matrix
q = [ulnag(1:4)];
rotU = quat2mat(q);
% Transpose Ulnar styliod to Ulna Tool Coordinate System
T = ulnag(5:7)';
USu = rotU'*(USG-T);

%Radial Styloid
importfile('RSg.csv');
radiusg=[RQ0,RQx,RQy,RQz,RTx,RTy,RTz];
RSg=[PTx,PTy,PTz];
RSG=mean(RSg)';
radiusg(1:4)=radiusg(1:4)/norm(radiusg(1:4));
% Radius Tool Rotation Matrix
q = [radiusg(1:4)];
rotR = quat2mat(q);
% Transpose Ulnar styliod to Ulna Tool Coordinate System
T = radiusg(5:7)';
RSr = rotR'*(USG-T);


% Read F90-S45 file - Elbow at 90 degrees of flexion/45 degrees sup
importfile('F90-S453.csv');
humerusT=[HQ0,HQx,HQy,HQz,HTx,HTy,HTz];
humerusT(1:4)=humerusT(1:4)/norm(humerusT(1:4));
ulnaT=[UQ0,UQx,UQy,UQz,UTx,UTy,UTz];
ulnaT(1:4)=ulnaT(1:4)/norm(ulnaT(1:4));
radiusT=[RQ0,RQx,RQy,RQz,RTx,RTy,RTz];
```

```
radiusT(1:4)=radiusT(1:4)/norm(radiusT(1:4));

% Rotation Matrices for humerus, ulna and radial tools
q = [humerusT(1:4)];
rotH = quat2mat(q);
q = [ulnaT(1:4)];
rotU = quat2mat(q);
q = [radiusT(1:4)];
rotR = quat2mat(q);

% Landmarks to new Global Coordinate System
HHg = rotH*HHh+humerusT(5:7)';
LEg = rotH*LEh+humerusT(5:7)';
MEg = rotH*MEh+humerusT(5:7)';
USg = rotU*USu+ulnaT(5:7)';
RSg = rotR*RSr+radiusT(5:7)';

% Humerus Coordinate System
mid=(MEg+LEg)/2;
j=(HHg-mid)/(norm(HHg-mid));
k=(LEg-MEg)/(norm(LEg-MEg));
i=cross(j,k);
rotHcs=[i j k];

% hum_laxis=j;
% hum_raxis=k;

% Ulnar Coordinate System
mid=(MEg+LEg)/2;
j=(USg-mid)/(norm(USg-mid));
k1=(USg-MEg)/(norm(USg-MEg));
k2=(USg-LEg)/(norm(USg-LEg));
k=cross(k1,k2);
i=cross(j,k);
rotUcs=[i j k]

ulna_laxis=j

ulna_laxis_h=rotHcs'*ulna_laxis

%Flexion angle
Flexion=(asin((-1)*ulna_laxis_h(3)))*180/pi()


% Radial Coordinate System
j=(RSg-LEg)/(norm(RSg-LEg));
i1=(RSg-MEg)/(norm(RSg-MEg));
i2=(RSg-LEg)/(norm(RSg-LEg));
k=cross(i,k);
rotRcs=[i j k]

radius_saxis=i

radius_saxis_u=rotUcs'*radius_saxis
```

```
%Supination angle
Supination=atan2(radius_saxis_u(3),radius_saxis_u(1))*180/pi()
end
```

Appendix E: Stress Analysis Calculations

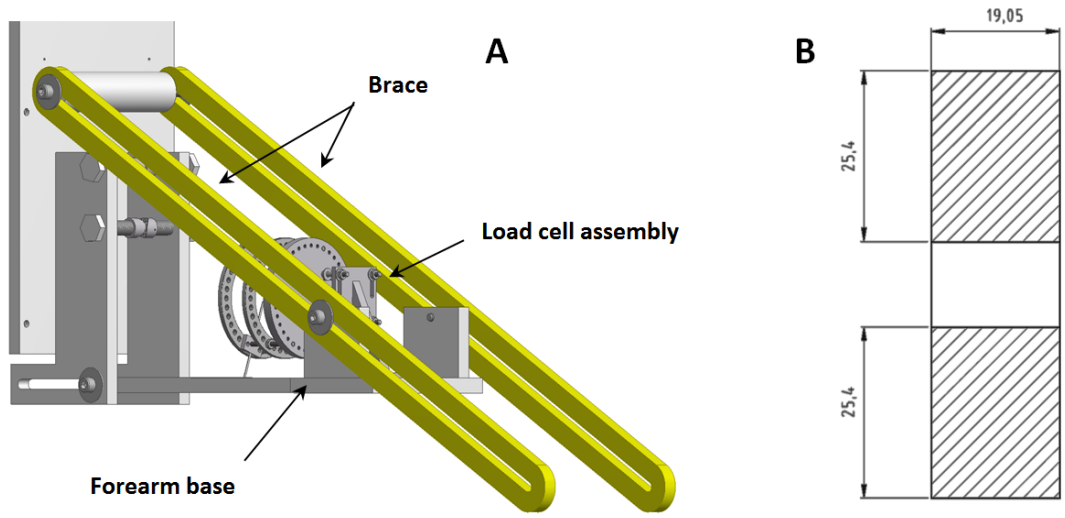

Figure 45. A – Delrin braces loaded by the weight of the load cell adapter and the forearm base. B – Loaded cross-sectional area of braces

Table 14. Total mass of the components supported by the braces

Compoment	kg
Forearm base	2.42
Load cell	0.91
Load cell bracket	0.34
Load cell adapter	0.60
Extermal fixator	0.12
Total supported mass	**4.39**

$$\sigma_{applied} = \frac{P}{A} = \frac{M_{tot}a}{A_{tot}} = \frac{43N}{0.00194mm^2} = 22.26\ KPa$$

$$\varepsilon_{applied} = \frac{\sigma_{applied}}{E} = \frac{0.02226\ MPa}{3000\ MPa} = 7.42 \times 10^{-6}$$

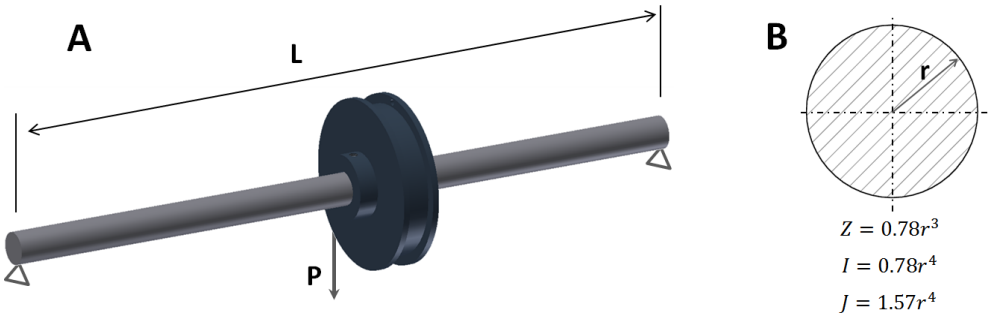

Figure 46. A - Load shaft diagram. B - Shaft cross-section

Table 15. Shaft analysis summary

Mechanical Design Parameters	Value	Unit
Yield stress	1740	MPa
Shear yield stress	1044	MPa
Modulus of elasticity	204	GPa
Shear Modulus	83.9	GPa
P (triceps load shaft)	165.24	N
Torque	3.811	Nm
L (shaft length)	0.3556	m
Radius	0.00794	m
Applied normal stress	37.62	MPa
Applied shear stress	4.85	MPa
Deflection	0.000245	m
Angle of twist	0.149	Degrees
Normal stress safety factor	46	
Shear stress safety factor	>200	

$$\sigma_{normal} = \frac{PL}{4Z} = \frac{19 \times 9.81 \times 0.3556}{4 \times 3.90 \times 10^{-7}} = 37.62\ MPa$$

$$\Delta_{max} = \frac{PL^3}{48EI} = \frac{19 \times 9.81 \times 0.3556^3}{84 \times 204 \times 10^9 \times 3.10 \times 10^{-9}} = 0.000245\ m$$

$$\tau = \frac{Tr}{J} = \frac{3.811 \times 0.00794}{1.57 \times 0.00794^4} = 4.85\ MPa$$

$$\theta = \frac{TL}{GJ} = \frac{3.811 \times 0.3556}{83.9 \times 10^9 \times 1.57 \times 0.00794^4} = 0.\ 149°$$

Appendix F: Statistical Analysis

Intact Data Tests of Normality

	Kolmogorov-Smirnov[a]			Shapiro-Wilk		
	Statistic	df	Sig.	Statistic	df	Sig.
Flex_45P_BH	.289	8	.049	.779	8	.017
Flex_45P_SH	.255	8	.134	.833	8	.064
Flex_45P_LH	.142	8	.200*	.973	8	.918
Flex_N_BH	.327	8	.012	.734	8	.005
Flex_N_SH	.315	8	.019	.765	8	.012
Flex_N_LH	.319	8	.016	.747	8	.008
Flex_45S_BH	.222	8	.200*	.904	8	.315
Flex_45S_SH	.303	8	.029	.825	8	.053
Flex_45S_LH	.127	8	.200*	.974	8	.924
Sup_45P_BH	.123	8	.200*	.991	8	.996
Sup_45P_SH	.173	8	.200*	.942	8	.635
Sup_45P_LH	.181	8	.200*	.948	8	.692
Sup_N_BH	.341	8	.007	.634	8	.000
Sup_N_SH	.363	8	.003	.722	8	.004
Sup_N_LH	.232	8	.200*	.870	8	.150
Sup_45S_BH	.248	8	.160	.930	8	.517
Sup_45S_SH	.257	8	.130	.895	8	.262
Sup_45S_LH	.163	8	.200*	.929	8	.508

a. Lilliefors Significance Correction

*. This is a lower bound of the true significance.

Intact Paired Samples Test

		Paired Differences					t	df	Sig. (2-tailed)
					95% Confidence Interval of the Difference				
		Mean	Std. Deviation	Std. Error Mean	Lower	Upper			
Pair 1	Flex_45P_SH - Flex_45P_LH	1.68661	1.02377	.36196	.83072	2.54251	4.660	7	.002
Pair 2	Flex_N_SH - Flex_N_LH	1.53270	.98429	.34800	.70981	2.35558	4.404	7	.003
Pair 3	Flex_45S_SH - Flex_45S_LH	1.86129	1.51609	.53602	.59381	3.12877	3.472	7	.010
Pair 4	Sup_45P_SH - Sup_45P_LH	.06955	.09392	.03320	-.00896	.14807	2.095	7	.074
Pair 5	Sup_N_SH - Sup_N_LH	.08160	.10808	.03821	-.00876	.17196	2.135	7	.070
Pair 6	Sup_45S_SH - Sup_45S_LH	.00121	.09589	.03390	-.07896	.08138	.036	7	.972

Intact Test Statistics[c]

	Flex_45P_LH - Flex_45P_SH	Flex_N_LH - Flex_N_SH	Flex_45S_LH - Flex_45S_SH	Sup_45P_LH - Sup_45P_SH	Sup_N_LH - Sup_N_SH	Sup_45S_LH - Sup_45S_SH
Z	-2.380[a]	-2.380[a]	-2.521[a]	-1.820[a]	-1.680[a]	.000[b]
Asymp. Sig. (2-tailed)	.017	.017	.012	.069	.093	1.000

a. Based on positive ranks.

b. The sum of negative ranks equals the sum of positive ranks.

c. Wilcoxon Signed Ranks Test

Tests of Normality

	Kolmogorov-Smirnov[a]			Shapiro-Wilk		
	Statistic	df	Sig.	Statistic	df	Sig.
INT_45P_BH	.161	7	.200*	.939	7	.633
INT_45P_SH	.159	7	.200*	.928	7	.531
INT_45P_LH	.229	7	.200*	.869	7	.182
INT_N_BH	.243	7	.200*	.921	7	.477
INT_N_SH	.204	7	.200*	.923	7	.493
INT_N_LH	.180	7	.200*	.895	7	.304
INT_45S_BH	.216	7	.200*	.934	7	.583
INT_45S_SH	.182	7	.200*	.949	7	.721
INT_45S_LH	.189	7	.200*	.961	7	.824
ANA_45P_BH	.160	7	.200*	.942	7	.658
ANA_45P_SH	.163	7	.200*	.949	7	.719
ANA_45P_LH	.175	7	.200*	.930	7	.551
ANA_N_BH	.198	7	.200*	.919	7	.460
ANA_N_SH	.255	7	.187	.769	7	.020
ANA_N_LH	.255	7	.189	.910	7	.397
ANA_45S_BH	.231	7	.200*	.871	7	.190
ANA_45S_SH	.252	7	.198	.913	7	.417
ANA_45S_LH	.233	7	.200*	.906	7	.372
NON_45P_BH	.214	7	.200*	.956	7	.786
NON_45P_SH	.364	7	.006	.796	7	.038
NON_45P_LH	.211	7	.200*	.961	7	.826
NON_N_BH	.267	7	.140	.859	7	.148
NON_N_SH	.296	7	.063	.863	7	.163
NON_N_LH	.212	7	.200*	.910	7	.396
NON_45S_BH	.183	7	.200*	.918	7	.453
NON_45S_SH	.218	7	.200*	.924	7	.499
NON_45S_LH	.179	7	.200*	.945	7	.687

a. Lilliefors Significance Correction

*. This is a lower bound of the true significance.

Repaired Paired Samples Test

		Paired Differences					t	df	Sig. (2-tailed)
					95% Confidence Interval of the Difference				
		Mean	Std. Deviation	Std. Error Mean	Lower	Upper			
Pair 1	INT_45P_BH - ANA_45P_BH	-.13331	.07989	.02825	-.20010	-.06652	-4.720	7	.002
Pair 2	INT_45P_BH - NON_45P_BH	-.04622	.14507	.05483	-.18038	.08795	-.843	6	.432
Pair 3	ANA_45P_BH - NON_45P_BH	.08921	.12745	.04817	-.02866	.20709	1.852	6	.113
Pair 4	INT_45P_SH - ANA_45P_SH	-.04956	.10810	.03822	-.13994	.04081	-1.297	7	.236
Pair 5	INT_45P_SH - NON_45P_SH	-.02576	.16340	.06176	-.17687	.12536	-.417	6	.691
Pair 6	ANA_45P_SH - NON_45P_SH	.03543	.08183	.03093	-.04025	.11111	1.145	6	.296
Pair 7	INT_45P_LH - ANA_45P_LH	-.07594	.05656	.02000	-.12323	-.02866	-3.798	7	.007
Pair 8	INT_45P_LH - NON_45P_LH	-.04382	.09215	.03483	-.12905	.04140	-1.258	6	.255
Pair 9	ANA_45P_LH - NON_45P_LH	.03206	.09125	.03449	-.05233	.11646	.930	6	.388
Pair 10	INT_N_BH - ANA_N_BH	-.01061	.05554	.01964	-.05704	.03583	-.540	7	.606
Pair 11	INT_N_BH - NON_N_BH	.17476	.23490	.08305	-.02162	.37113	2.104	7	.073
Pair 12	ANA_N_BH - NON_N_BH	.18536	.19889	.07032	.01909	.35164	2.636	7	.034
Pair 13	INT_N_SH - ANA_N_SH	.00532	.09035	.03194	-.07022	.08085	.166	7	.873
Pair 14	INT_N_SH - NON_N_SH	.07872	.18103	.06401	-.07263	.23007	1.230	7	.258
Pair 15	ANA_N_SH - NON_N_SH	.07340	.11301	.03995	-.02107	.16788	1.837	7	.109
Pair 16	INT_N_LH - ANA_N_LH	.02366	.09053	.03201	-.05202	.09935	.739	7	.484
Pair 17	INT_N_LH - NON_N_LH	.07446	.11847	.04478	-.03510	.18403	1.663	6	.147
Pair 18	ANA_N_LH - NON_N_LH	.04627	.12382	.04680	-.06824	.16079	.989	6	.361
Pair 19	INT_45S_BH - ANA_45S_BH	-.02312	.11564	.04088	-.11979	.07355	-.565	7	.589
Pair 20	INT_45S_BH - NON_45S_BH	.35898	.33785	.11945	.07653	.64143	3.005	7	.020
Pair 21	ANA_45S_BH - NON_45S_BH	.38210	.29347	.10376	.13675	.62744	3.683	7	.008
Pair 22	INT_45S_SH - ANA_45S_SH	.01553	.13127	.04641	-.09421	.12528	.335	7	.748
Pair 23	INT_45S_SH - NON_45S_SH	.19699	.23517	.08315	.00038	.39360	2.369	7	.050
Pair 24	ANA_45S_SH - NON_45S_SH	.18146	.15240	.05388	.05405	.30887	3.368	7	.012
Pair 25	INT_45S_LH - ANA_45S_LH	.03117	.08989	.03178	-.04398	.10631	.981	7	.359
Pair 26	INT_45S_LH - NON_45S_LH	.23946	.21193	.07493	.06228	.41663	3.196	7	.015
Pair 27	ANA_45S_LH - NON_45S_LH	.20829	.16365	.05786	.07148	.34511	3.600	7	.009

Repaired Test Statistics[b]

	NON_45P_BH - ANA_45P_BH	NON_45P_SH - ANA_45P_SH	NON_45P_LH - ANA_45P_LH	NON_N_BH - ANA_N_BH	NON_N_SH - ANA_N_SH
Z	-1.521[a]	-1.014[a]	-.845[a]	-2.100[a]	-1.540[a]
Asymp. Sig. (2-tailed)	.128	.310	.398	.036	.123

a. Based on positive ranks.

b. Wilcoxon Signed Ranks Test

Repaired Test Statistics[b]

	NON_N_LH - ANA_N_LH	NON_45S_BH - ANA_45S_BH	NON_45S_SH - ANA_45S_SH	NON_45S_LH - ANA_45S_LH
Z	-.845[a]	-2.521[a]	-2.380[a]	-2.380[a]
Asymp. Sig. (2-tailed)	.398	.012	.017	.017

a. Based on positive ranks.

b. Wilcoxon Signed Ranks Test

Appendix G: Elbow Simulator Engineering Drawings

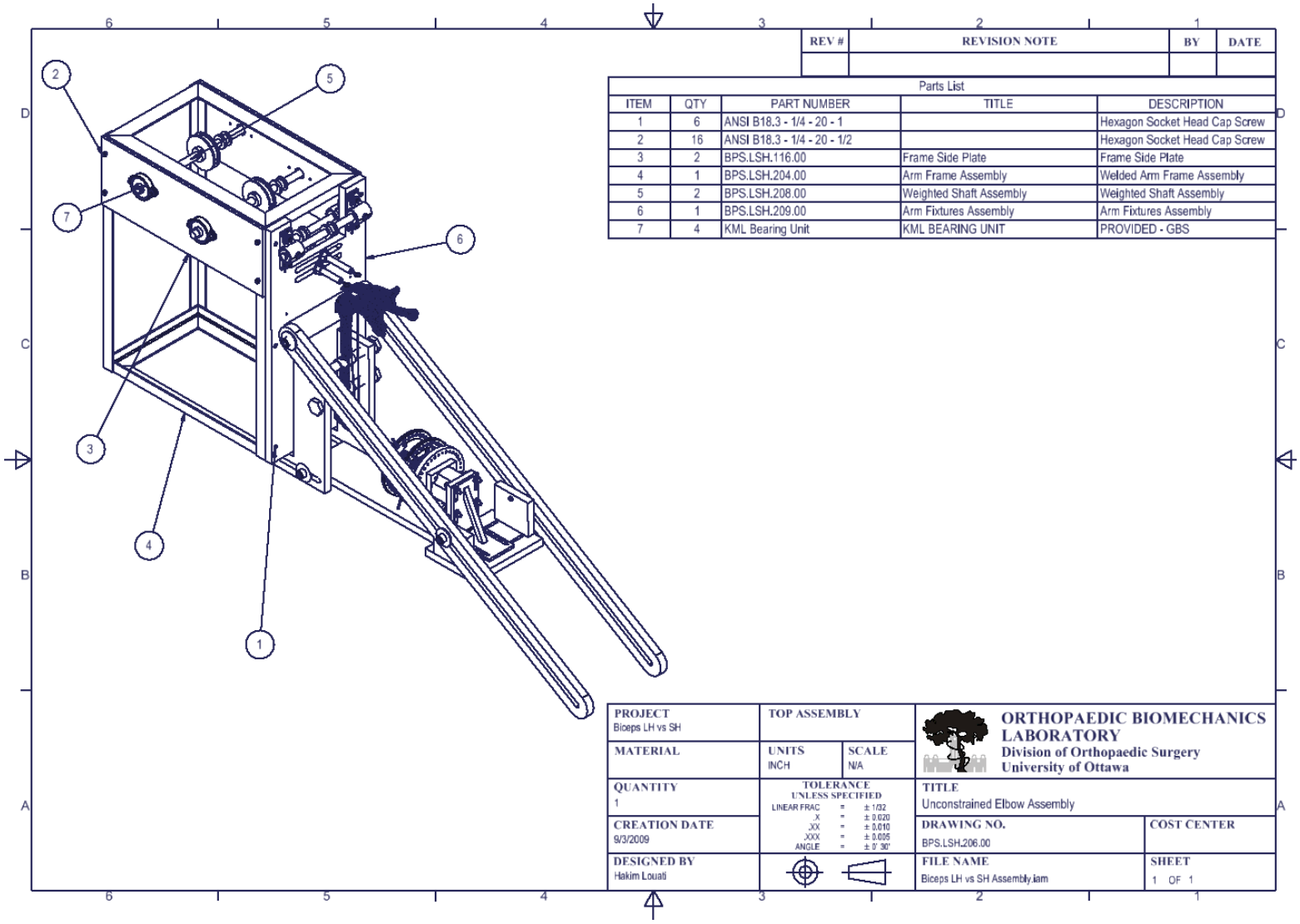

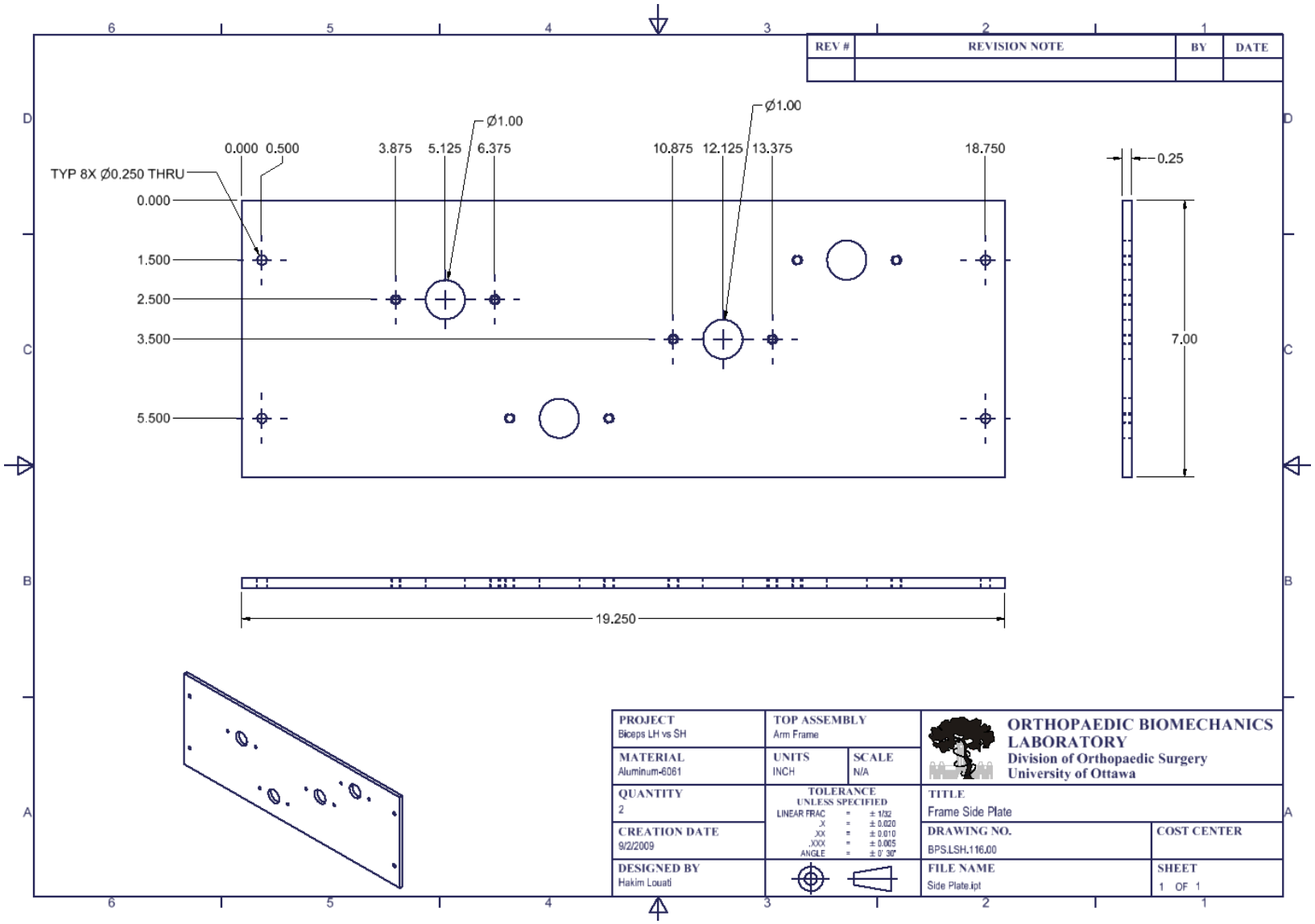
REV #
REVISION NOTE
BY
DATE
TYP 8X Ø0.250 THRU
0.000
0.500
3.875
5.125
6.375
Ø1.00
10.875
12.125
13.375
Ø1.00
18.750
0.000
1.500
2.500
3.500
5.500
0.25
7.00
19.250
PROJECT
Biceps LH vs SH
TOP ASSEMBLY
Arm Frame
MATERIAL
Aluminum-6061
UNITS
INCH
SCALE
N/A
QUANTITY
2
TOLERANCE
UNLESS SPECIFIED
LINEAR FRAC = ± 1/32
.X = ± 0.020
.XX = ± 0.010
.XXX = ± 0.005
ANGLE = ± 0° 30'
CREATION DATE
9/2/2009
DESIGNED BY
Hakim Louati
ORTHOPAEDIC BIOMECHANICS LABORATORY
Division of Orthopaedic Surgery
University of Ottawa
TITLE
Frame Side Plate
DRAWING NO.
BPS.LSH.116.00
COST CENTER
FILE NAME
Side Plate.ipt
SHEET
1 OF 1

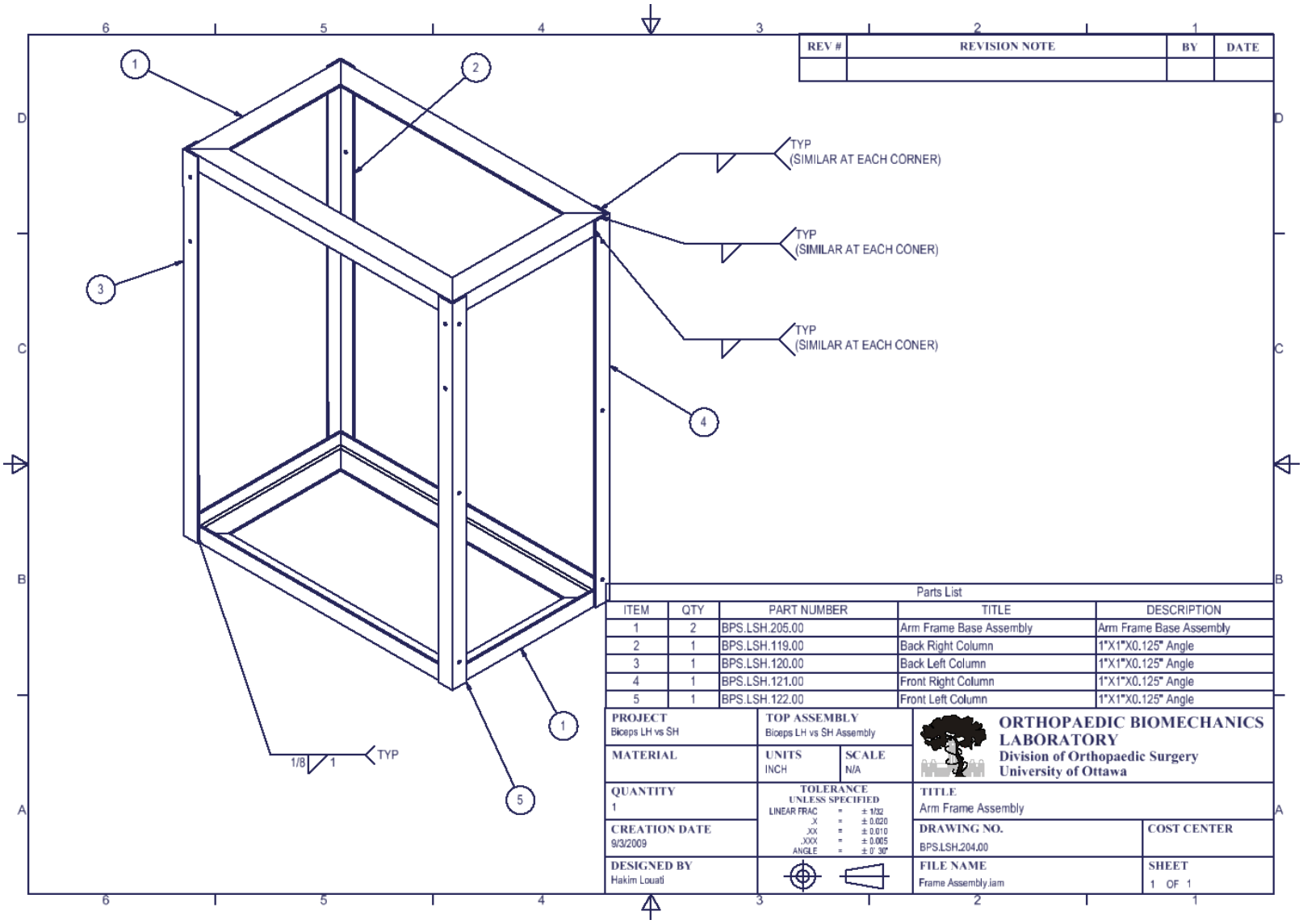
REV #
REVISION NOTE
BY
DATE
TYP
(SIMILAR AT EACH CORNER)
TYP
(SIMILAR AT EACH CONER)
TYP
(SIMILAR AT EACH CONER)
1/8
1
TYP
Parts List
ITEM | QTY | PART NUMBER | TITLE | DESCRIPTION
1 | 2 | BPS.LSH.205.00 | Arm Frame Base Assembly | Arm Frame Base Assembly
2 | 1 | BPS.LSH.119.00 | Back Right Column | 1"X1"X0.125" Angle
3 | 1 | BPS.LSH.120.00 | Back Left Column | 1"X1"X0.125" Angle
4 | 1 | BPS.LSH.121.00 | Front Right Column | 1"X1"X0.125" Angle
5 | 1 | BPS.LSH.122.00 | Front Left Column | 1"X1"X0.125" Angle
PROJECT
Biceps LH vs SH
TOP ASSEMBLY
Biceps LH vs SH Assembly
MATERIAL
UNITS
INCH
SCALE
N/A
QUANTITY
1
TOLERANCE
UNLESS SPECIFIED
LINEAR FRAC = ± 1/32
X = ± 0.020
XX = ± 0.010
XXX = ± 0.005
ANGLE = ± 0° 30'
CREATION DATE
9/3/2009
DESIGNED BY
Hakim Louati
ORTHOPAEDIC BIOMECHANICS LABORATORY
Division of Orthopaedic Surgery
University of Ottawa
TITLE
Arm Frame Assembly
DRAWING NO.
BPS.LSH.204.00
COST CENTER
FILE NAME
Frame Assembly.iam
SHEET
1 OF 1

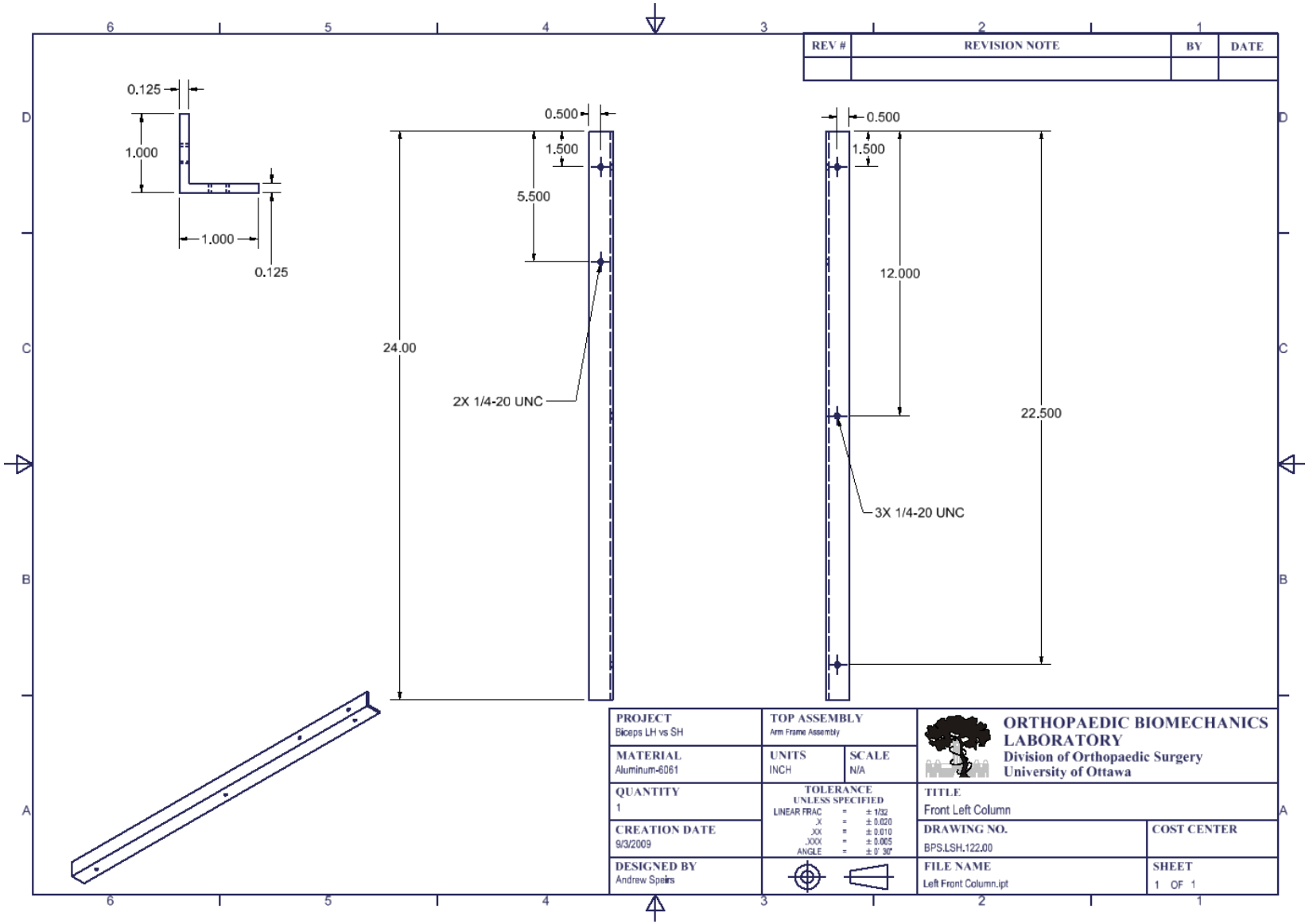
REV #
REVISION NOTE
BY
DATE
0.125
1.000
1.000
0.125
0.500
1.500
5.500
24.00
2X 1/4-20 UNC
0.500
1.500
12.000
22.500
3X 1/4-20 UNC
PROJECT
Biceps LH vs SH
TOP ASSEMBLY
Arm Frame Assembly
MATERIAL
Aluminum-6061
UNITS
INCH
SCALE
N/A
QUANTITY
1
TOLERANCE
UNLESS SPECIFIED
LINEAR FRAC = ± 1/32
.X = ± 0.020
.XX = ± 0.010
.XXX = ± 0.005
ANGLE = ± 0° 30'
ORTHOPAEDIC BIOMECHANICS LABORATORY
Division of Orthopaedic Surgery
University of Ottawa
TITLE
Front Left Column
CREATION DATE
9/3/2009
DRAWING NO.
BPS.LSH.122.00
COST CENTER
DESIGNED BY
Andrew Speirs
FILE NAME
Left Front Column.ipt
SHEET
1 OF 1

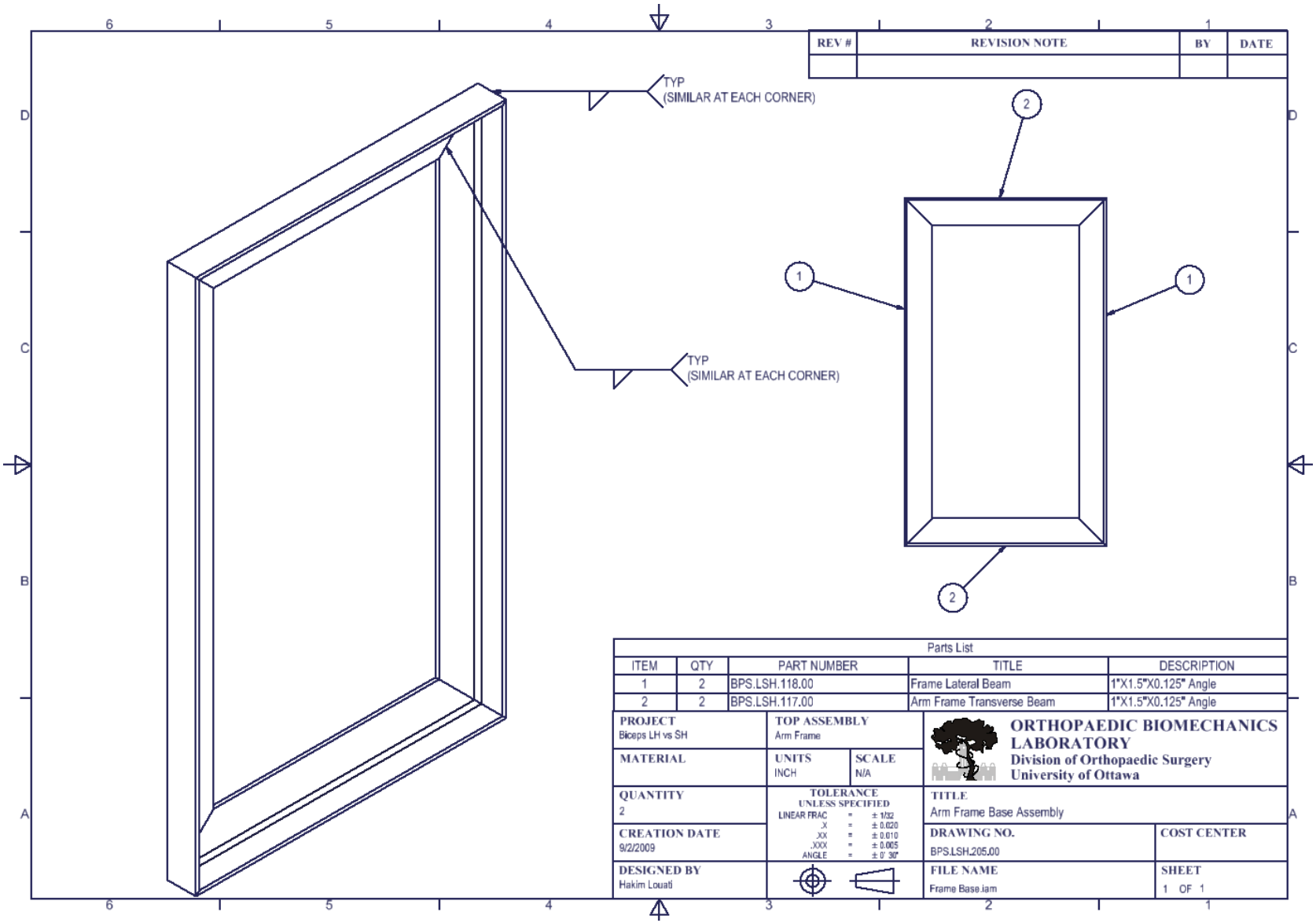
REV #
REVISION NOTE
BY
DATE
TYP
(SIMILAR AT EACH CORNER)
TYP
(SIMILAR AT EACH CORNER)
1
2
Parts List
ITEM | QTY | PART NUMBER | TITLE | DESCRIPTION
1 | 2 | BPS.LSH.118.00 | Frame Lateral Beam | 1"X1.5"X0.125" Angle
2 | 2 | BPS.LSH.117.00 | Arm Frame Transverse Beam | 1"X1.5"X0.125" Angle
PROJECT
Biceps LH vs SH
TOP ASSEMBLY
Arm Frame
MATERIAL
UNITS
INCH
SCALE
N/A
ORTHOPAEDIC BIOMECHANICS LABORATORY
Division of Orthopaedic Surgery
University of Ottawa
QUANTITY
2
TOLERANCE
UNLESS SPECIFIED
LINEAR FRAC = ± 1/32
.X = ± 0.020
.XX = ± 0.010
.XXX = ± 0.005
ANGLE = ± 0° 30'
TITLE
Arm Frame Base Assembly
CREATION DATE
9/2/2009
DRAWING NO.
BPS.LSH.205.00
COST CENTER
DESIGNED BY
Hakim Louati
FILE NAME
Frame Base.iam
SHEET
1 OF 1

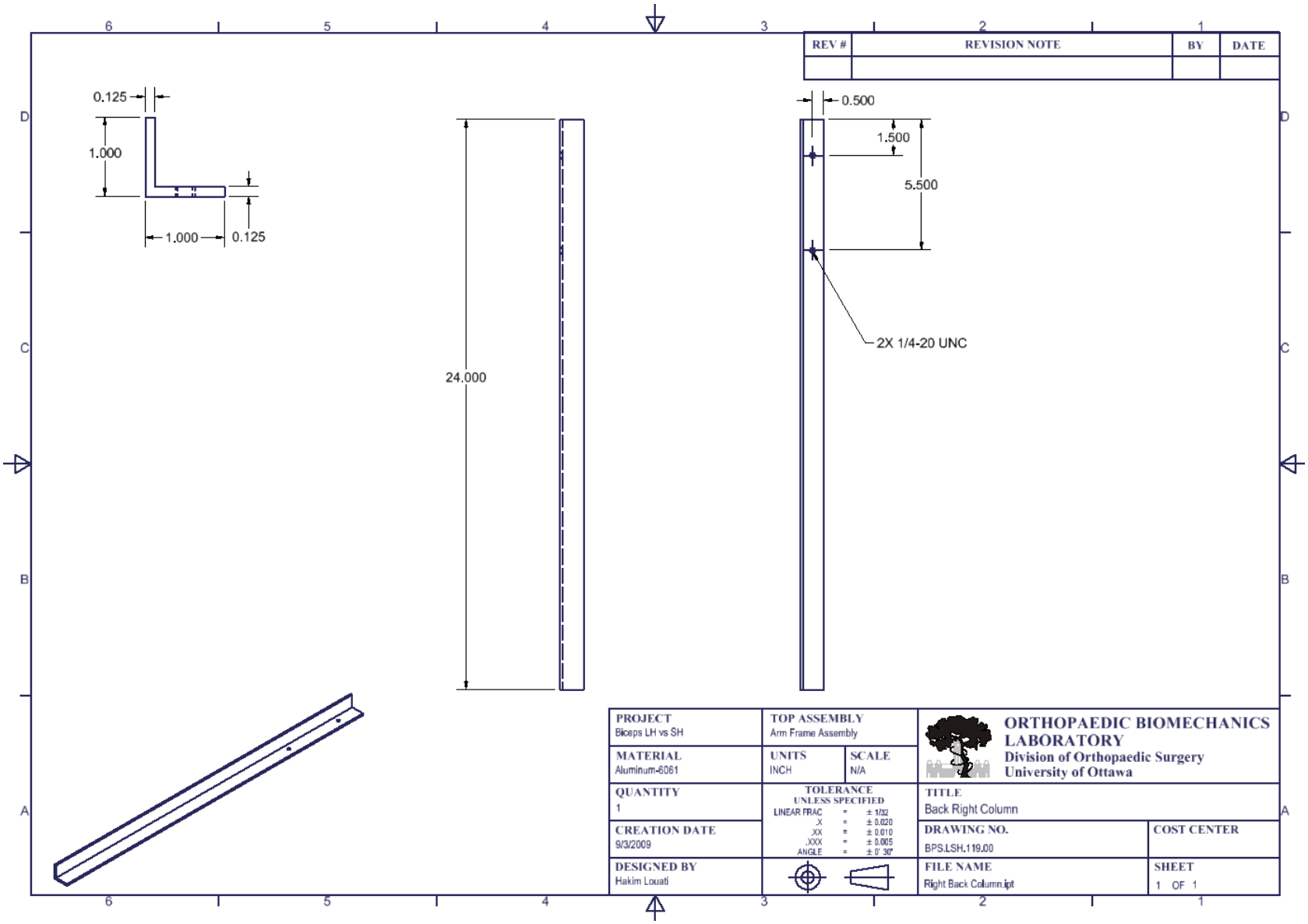
REV #
REVISION NOTE
BY
DATE
0.125
1.000
1.000
0.125
24.000
0.500
1.500
5.500
2X 1/4-20 UNC
PROJECT
Biceps LH vs SH
TOP ASSEMBLY
Arm Frame Assembly
MATERIAL
Aluminum-6061
UNITS
INCH
SCALE
N/A
QUANTITY
1
TOLERANCE
UNLESS SPECIFIED
LINEAR FRAC = ± 1/32
.X = ± 0.020
.XX = ± 0.010
.XXX = ± 0.005
ANGLE = ± 0° 30'
ORTHOPAEDIC BIOMECHANICS LABORATORY
Division of Orthopaedic Surgery
University of Ottawa
TITLE
Back Right Column
CREATION DATE
9/3/2009
DRAWING NO.
BPS.LSH.119.00
COST CENTER
DESIGNED BY
Hakim Louati
FILE NAME
Right Back Column.ipt
SHEET
1 OF 1

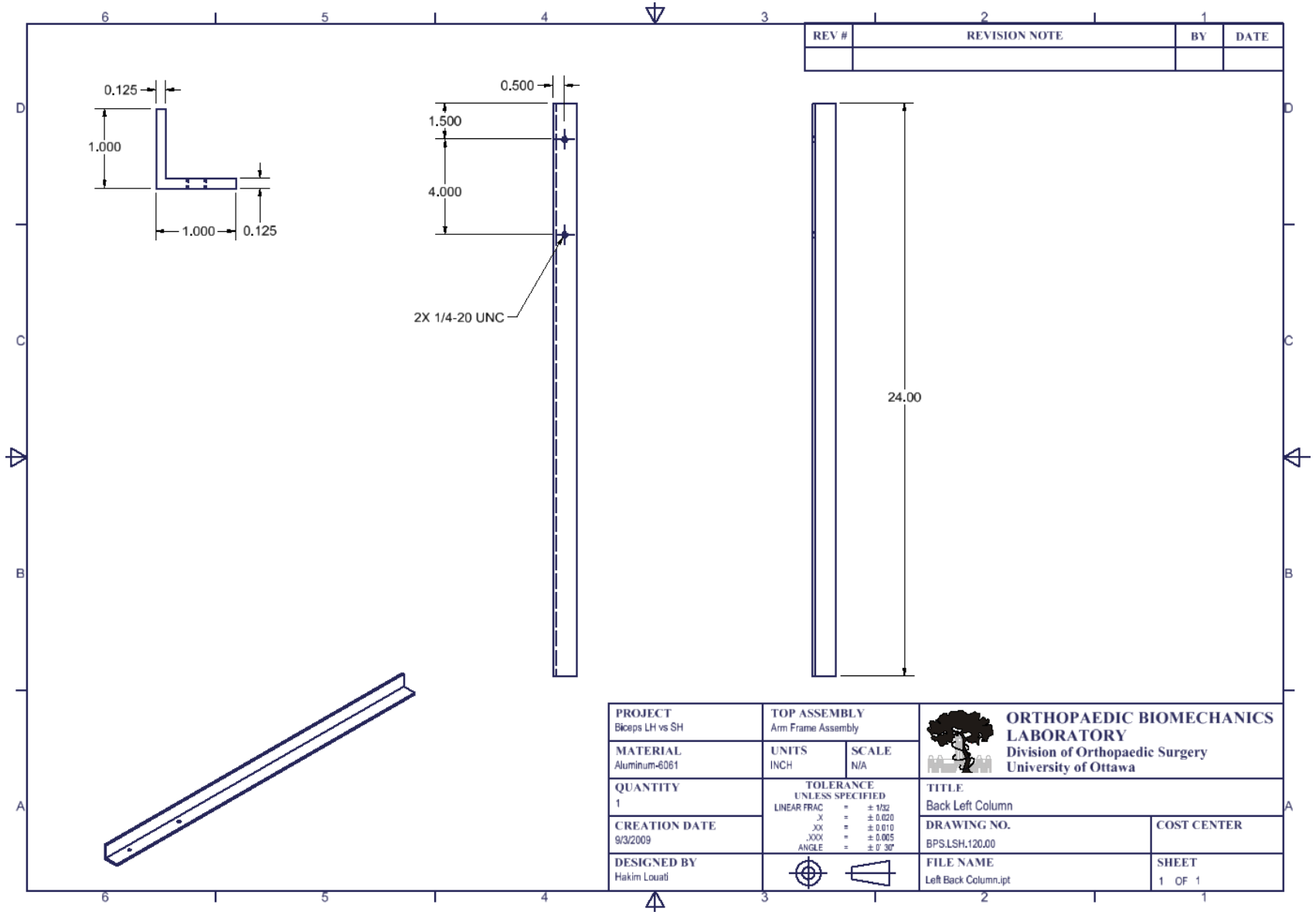
REV #
REVISION NOTE
BY
DATE
0.125
1.000
1.000
0.125
0.500
1.500
4.000
2X 1/4-20 UNC
24.00
PROJECT
Biceps LH vs SH
TOP ASSEMBLY
Arm Frame Assembly
MATERIAL
Aluminum-6061
UNITS
INCH
SCALE
N/A
QUANTITY
1
TOLERANCE
UNLESS SPECIFIED
LINEAR FRAC = ± 1/32
.X = ± 0.020
.XX = ± 0.010
.XXX = ± 0.005
ANGLE = ± 0° 30'
ORTHOPAEDIC BIOMECHANICS LABORATORY
Division of Orthopaedic Surgery
University of Ottawa
TITLE
Back Left Column
CREATION DATE
9/3/2009
DRAWING NO.
BPS.LSH.120.00
COST CENTER
DESIGNED BY
Hakim Louati
FILE NAME
Left Back Column.ipt
SHEET
1 OF 1

REV #	REVISION NOTE	BY	DATE

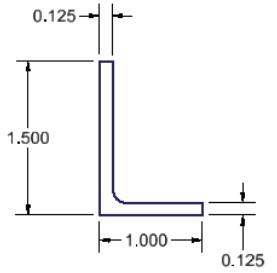

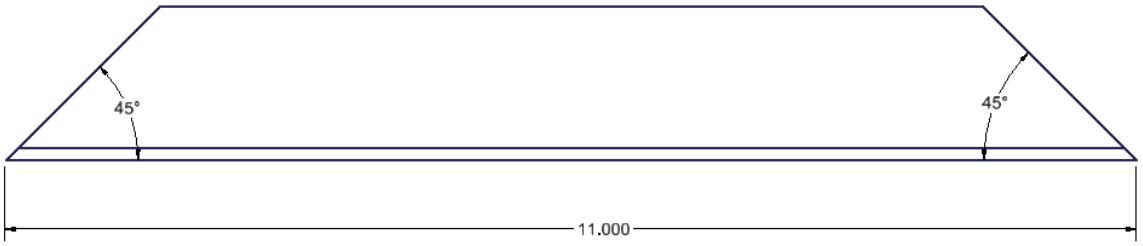

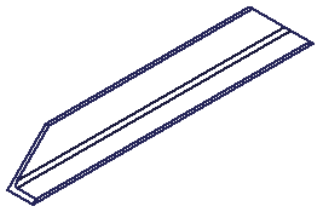

PROJECT: Biceps LH vs SH	TOP ASSEMBLY: Arm Frame		ORTHOPAEDIC BIOMECHANICS LABORATORY Division of Orthopaedic Surgery University of Ottawa
MATERIAL: Aluminum-6061	UNITS: INCH	SCALE: N/A	
QUANTITY: 4	TOLERANCE UNLESS SPECIFIED LINEAR FRAC = ± 1/32 .X = ± 0.020 .XX = ± 0.010 .XXX = ± 0.005 ANGLE = ± 0° 30'		TITLE: Arm Frame Transverse Beam
CREATION DATE: 9/2/2009			DRAWING NO.: BPS.LSH.117.00 / COST CENTER
DESIGNED BY: Hakim Louati			FILE NAME: FrameTransverse Brace.ipt / SHEET: 1 OF 1

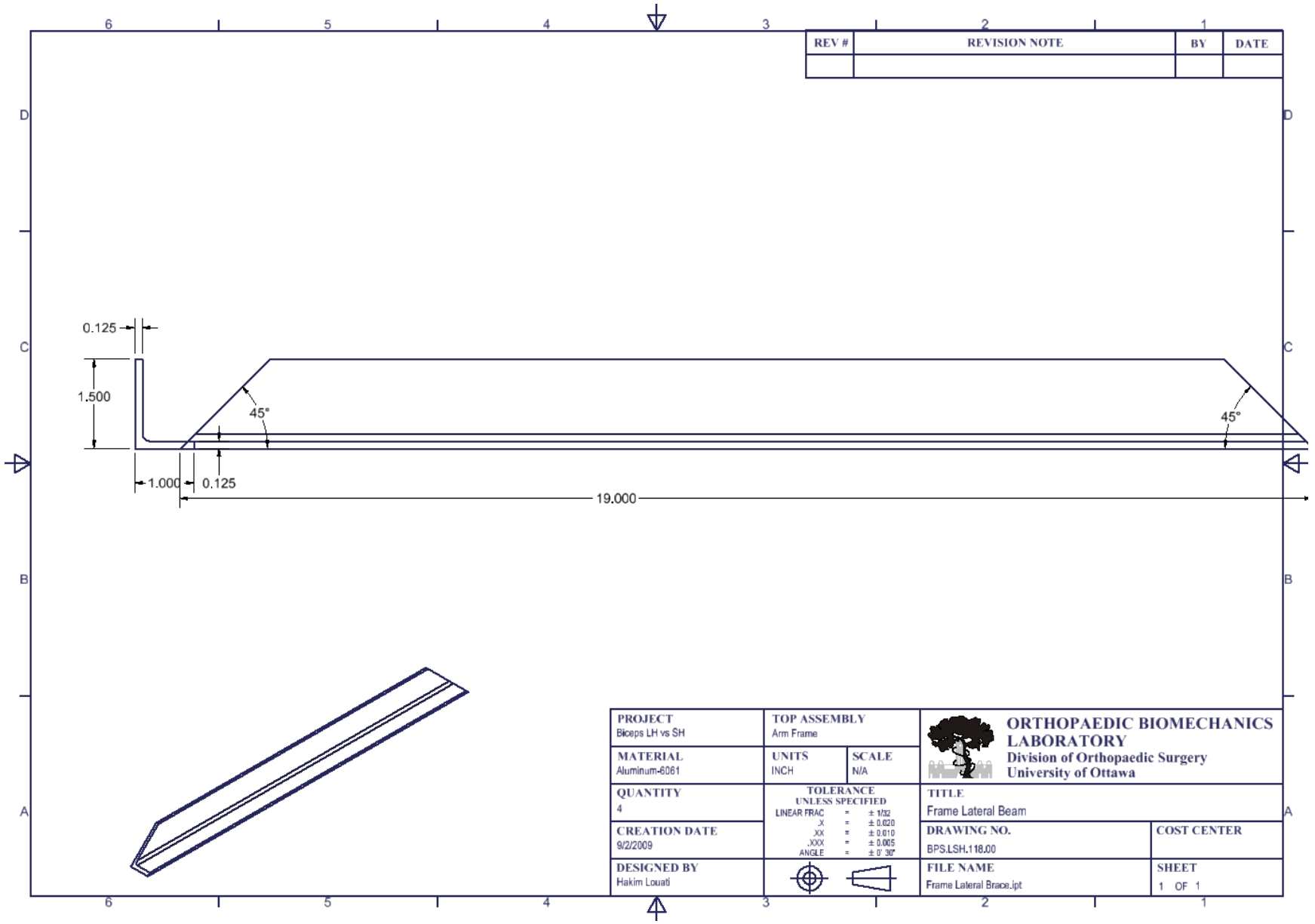
REV #
REVISION NOTE
BY
DATE
0.125
1.500
45°
45°
1.000
0.125
19.000
PROJECT
Biceps LH vs SH
TOP ASSEMBLY
Arm Frame
MATERIAL
Aluminum-6061
UNITS
INCH
SCALE
N/A
QUANTITY
4
TOLERANCE
UNLESS SPECIFIED
LINEAR FRAC = ± 1/32
.X = ± 0.020
.XX = ± 0.010
.XXX = ± 0.005
ANGLE = ± 0° 30"
CREATION DATE
9/2/2009
DESIGNED BY
Hakim Louati
ORTHOPAEDIC BIOMECHANICS LABORATORY
Division of Orthopaedic Surgery
University of Ottawa
TITLE
Frame Lateral Beam
DRAWING NO.
BPS.LSH.118.00
COST CENTER
FILE NAME
Frame Lateral Brace.ipt
SHEET
1 OF 1

REV #	REVISION NOTE	BY	DATE

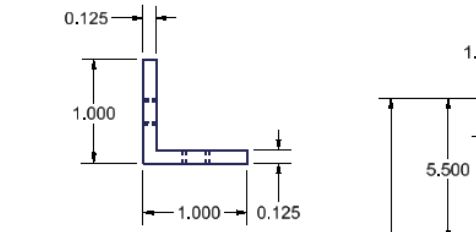

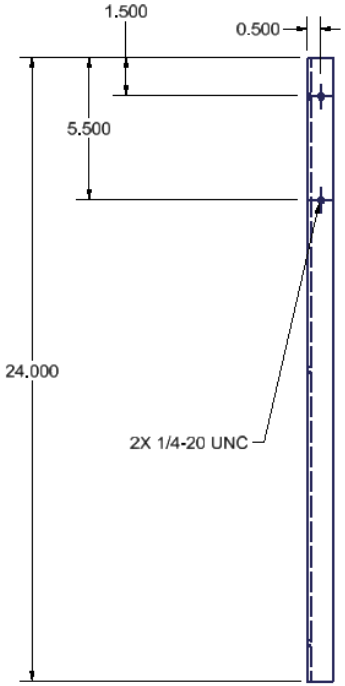

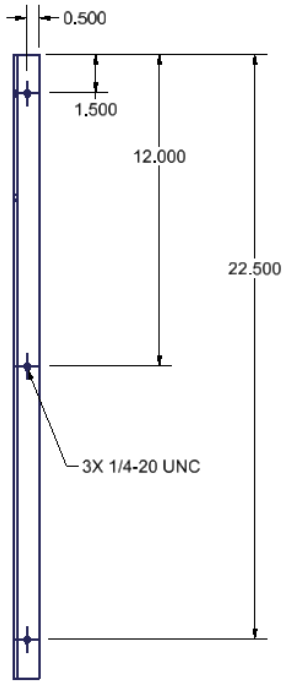

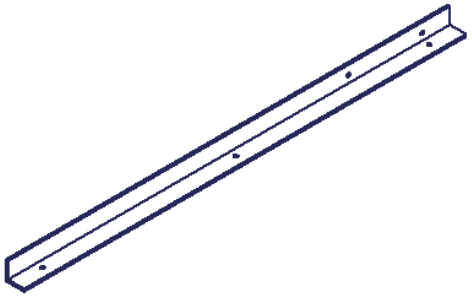

PROJECT: Biceps LH vs SH	TOP ASSEMBLY: Arm Frame Assembly	ORTHOPAEDIC BIOMECHANICS LABORATORY Division of Orthopaedic Surgery University of Ottawa
MATERIAL: Aluminum-6061	UNITS: INCH / SCALE: N/A	
QUANTITY: 1	TOLERANCE UNLESS SPECIFIED: LINEAR FRAC = ± 1/32; .X = ± 0.020; .XX = ± 0.010; .XXX = ± 0.005; ANGLE = ± 0° 30'	TITLE: Front Right Column
CREATION DATE: 9/3/2009		DRAWING NO.: BPS.LSH.121.00 / COST CENTER:
DESIGNED BY: Hakim Louati		FILE NAME: Right Front Column.ipt / SHEET: 1 OF 1

REV #	REVISION NOTE	BY	DATE

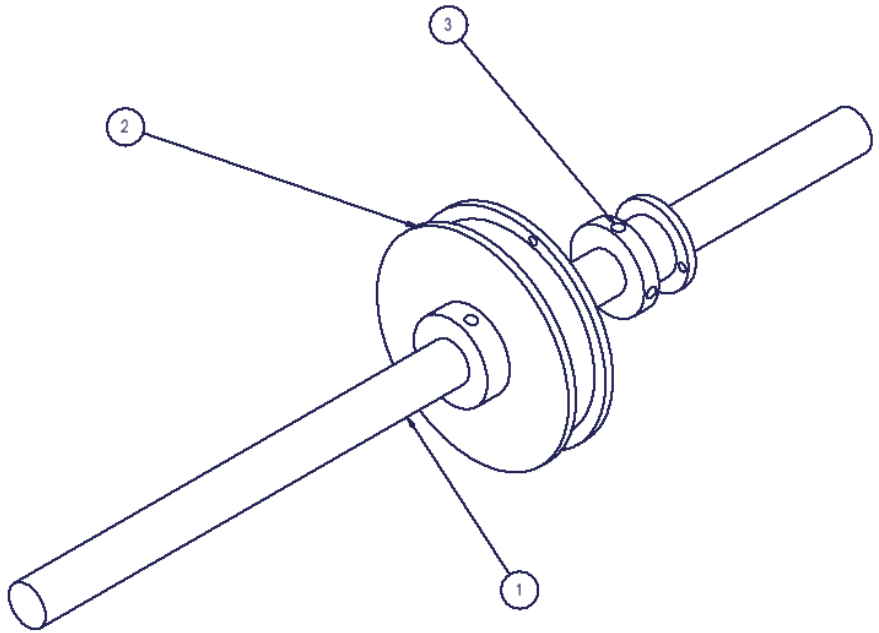

Parts List

ITEM	QTY	PART NUMBER	TITLE	DESCRIPTION
1	1	BPS.LSH.125.00	Weight Shaft	5/8" Dia 14" Shaft
2	1	BPS.LSH.115.00	Load Pulley	Load Attachment Pulley
3	1	BPS.LSH.114.00	Position Pulley	Poistion pulley

PROJECT Biceps LH vs SH	**TOP ASSEMBLY** Biceps LH vs SH	**ORTHOPAEDIC BIOMECHANICS LABORATORY** Division of Orthopaedic Surgery University of Ottawa
MATERIAL	**UNITS** INCH / **SCALE** N/A	
QUANTITY 2	**TOLERANCE** UNLESS SPECIFIED: LINEAR FRAC = ± 1/32; .X = ± 0.020; .XX = ± 0.010; .XXX = ± 0.005; ANGLE = ± 0° 30'	**TITLE** Weighted Shaft Assembly
CREATION DATE 9/3/2009		**DRAWING NO.** BPS.LSH.208.00 / **COST CENTER**
DESIGNED BY Hakim Louati		**FILE NAME** Load Pulley Assembly.iam / **SHEET** 1 OF 1

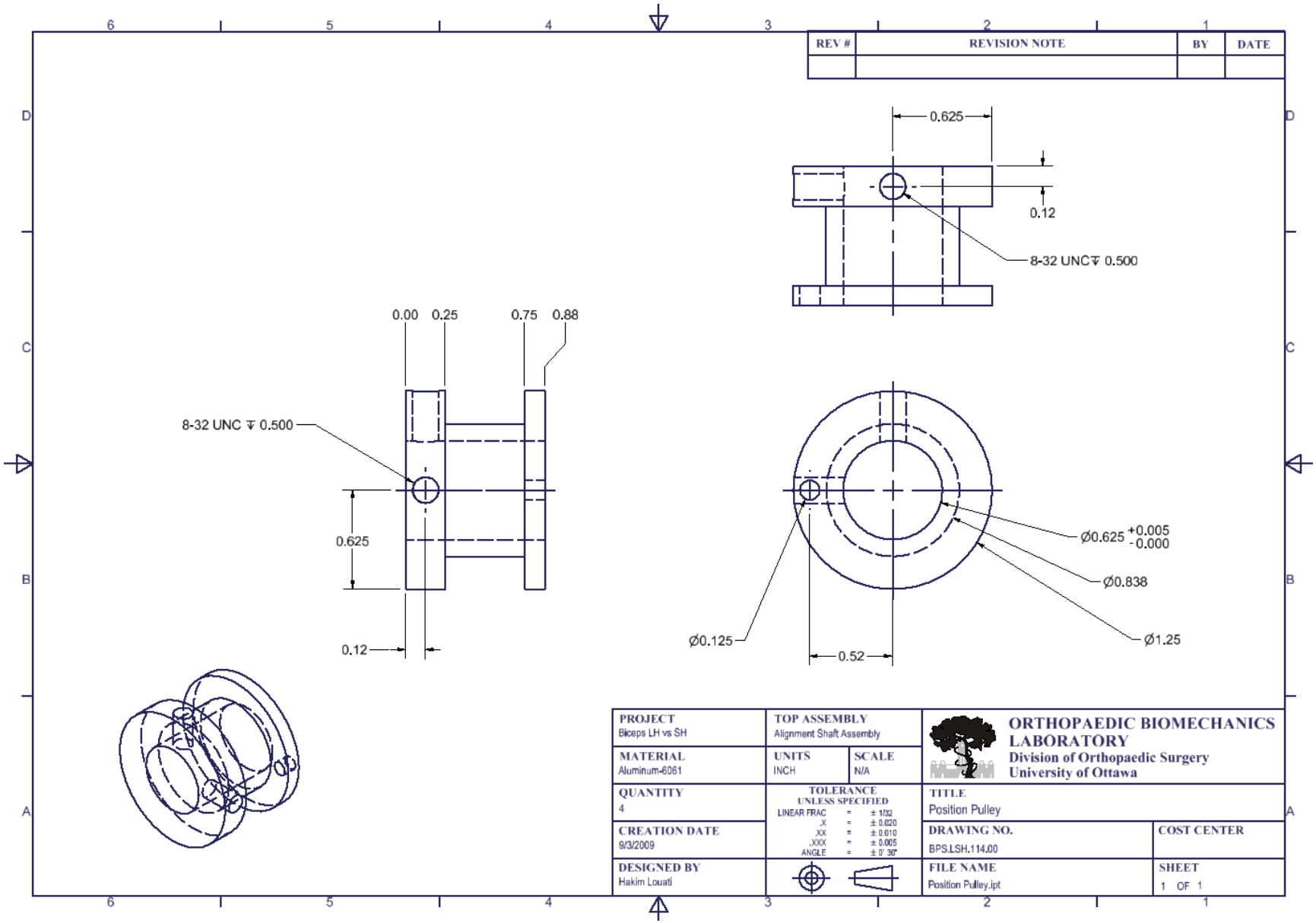
REV #
REVISION NOTE
BY
DATE
0.625
0.12
8-32 UNC↧ 0.500
0.00
0.25
0.75
0.88
8-32 UNC ↧ 0.500
0.625
0.12
Ø0.625 +0.005 -0.000
Ø0.838
Ø1.25
Ø0.125
0.52
PROJECT
Biceps LH vs SH
TOP ASSEMBLY
Alignment Shaft Assembly
MATERIAL
Aluminum-6061
UNITS
INCH
SCALE
N/A
QUANTITY
4
TOLERANCE
UNLESS SPECIFIED
LINEAR FRAC = ± 1/32
.X = ± 0.020
.XX = ± 0.010
.XXX = ± 0.005
ANGLE = ± 0° 30'
CREATION DATE
9/3/2009
DESIGNED BY
Hakim Louati
ORTHOPAEDIC BIOMECHANICS LABORATORY
Division of Orthopaedic Surgery
University of Ottawa
TITLE
Position Pulley
DRAWING NO.
BPS.LSH.114.00
COST CENTER
FILE NAME
Position Pulley.ipt
SHEET
1 OF 1

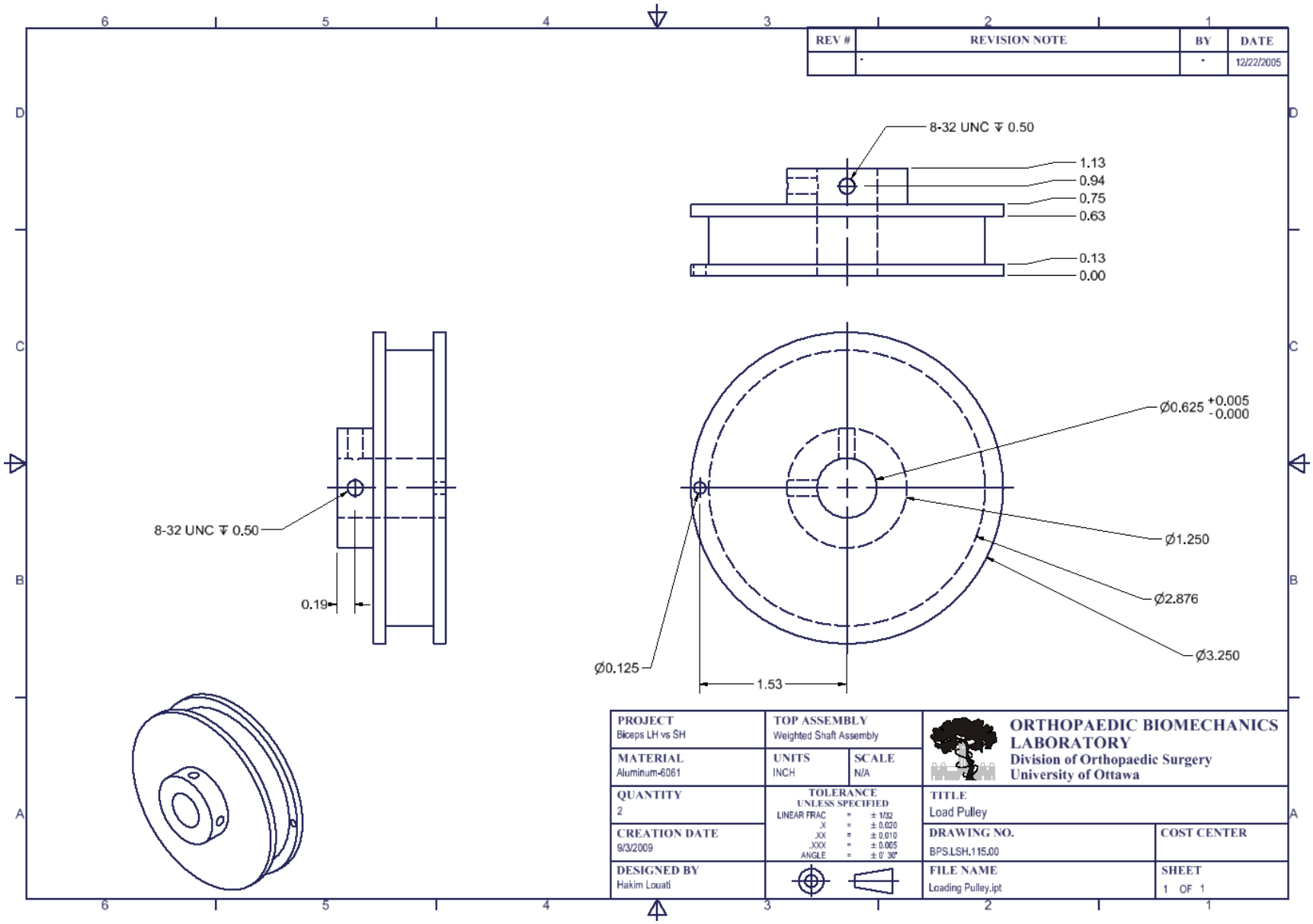
REV # | REVISION NOTE | BY | DATE
- | - | - | 12/22/2005
8-32 UNC ↧ 0.50
1.13
0.94
0.75
0.63
0.13
0.00
8-32 UNC ↧ 0.50
0.19
Ø0.625 +0.005 -0.000
Ø1.250
Ø2.876
Ø3.250
Ø0.125
1.53
PROJECT
Biceps LH vs SH
TOP ASSEMBLY
Weighted Shaft Assembly
MATERIAL
Aluminum-6061
UNITS
INCH
SCALE
N/A
QUANTITY
2
TOLERANCE
UNLESS SPECIFIED
LINEAR FRAC = ± 1/32
.X = ± 0.020
.XX = ± 0.010
.XXX = ± 0.005
ANGLE = ± 0° 30'
CREATION DATE
9/3/2009
DESIGNED BY
Hakim Louati
ORTHOPAEDIC BIOMECHANICS LABORATORY
Division of Orthopaedic Surgery
University of Ottawa
TITLE
Load Pulley
DRAWING NO.
BPS.LSH.115.00
COST CENTER
FILE NAME
Loading Pulley.ipt
SHEET
1 OF 1

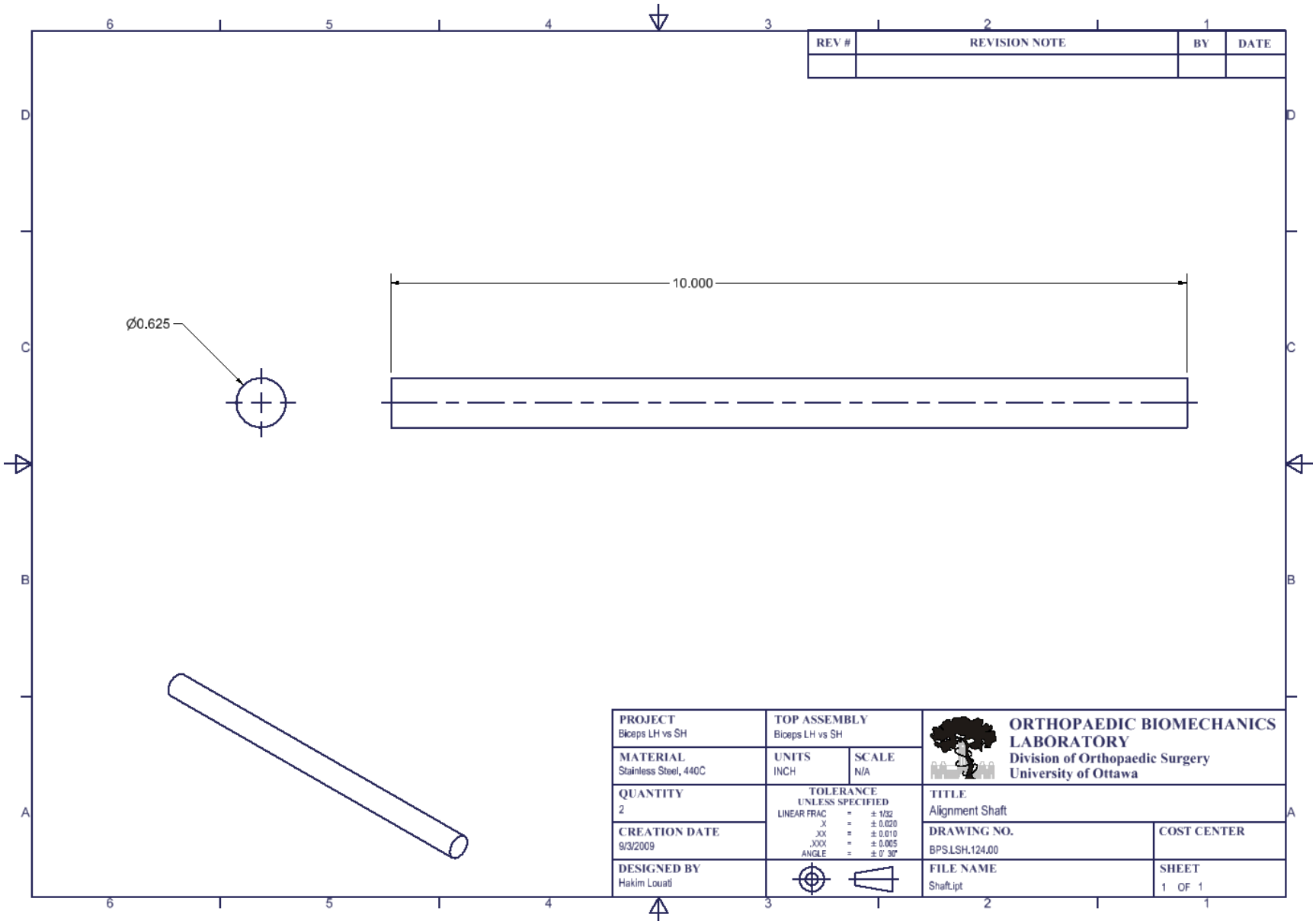
REV #
REVISION NOTE
BY
DATE
10.000
Ø0.625
PROJECT
Biceps LH vs SH
TOP ASSEMBLY
Biceps LH vs SH
MATERIAL
Stainless Steel, 440C
UNITS
INCH
SCALE
N/A
QUANTITY
2
TOLERANCE
UNLESS SPECIFIED
LINEAR FRAC = ± 1/32
.X = ± 0.020
.XX = ± 0.010
.XXX = ± 0.005
ANGLE = ± 0° 30"
CREATION DATE
9/3/2009
DESIGNED BY
Hakim Louati
ORTHOPAEDIC BIOMECHANICS LABORATORY
Division of Orthopaedic Surgery
University of Ottawa
TITLE
Alignment Shaft
DRAWING NO.
BPS.LSH.124.00
COST CENTER
FILE NAME
Shaft.ipt
SHEET
1 OF 1

REV #	REVISION NOTE	BY	DATE

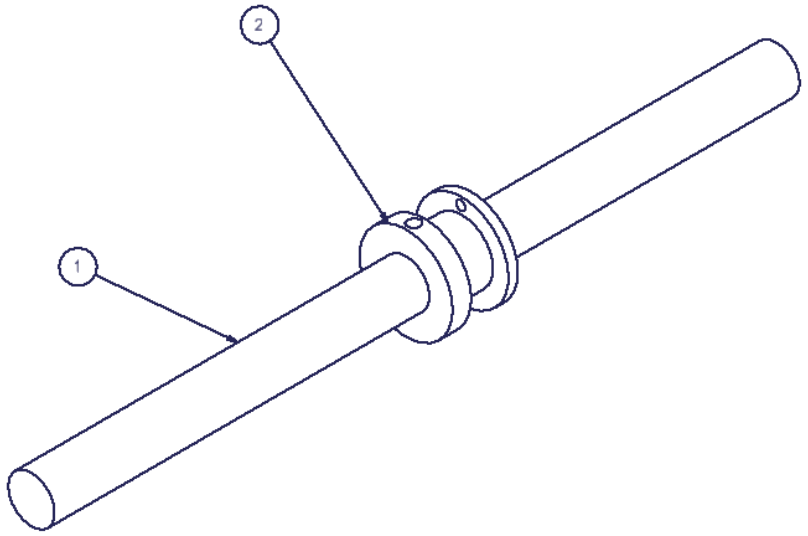

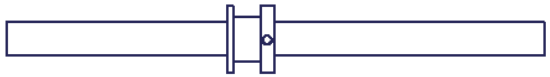

Parts List

ITEM	QTY	PART NUMBER	TITLE	DESCRIPTION
1	1	BPS.LSH.124.00	Alignment Shaft	5/8" Dia 10" Shaft
2	1	BPS.LSH.114.00	Position Pulley	Poistion pulley

PROJECT: Biceps LH vs SH	TOP ASSEMBLY: Arm Fixtures	ORTHOPAEDIC BIOMECHANICS LABORATORY Division of Orthopaedic Surgery University of Ottawa	
MATERIAL	UNITS: INCH / SCALE: N/A		
QUANTITY: 2	TOLERANCE UNLESS SPECIFIED LINEAR FRAC = ± 1/32 .X = ± 0.020 .XX = ± 0.010 .XXX = ± 0.005 ANGLE = ± 0° 30"	TITLE: Alignment Shaft Assembly	
CREATION DATE: 9/3/2009		DRAWING NO.: BPS.LSH.207.00	COST CENTER
DESIGNED BY: Hakim Louati		FILE NAME: Alignment Shaft Assembly.iam	SHEET: 1 OF 1

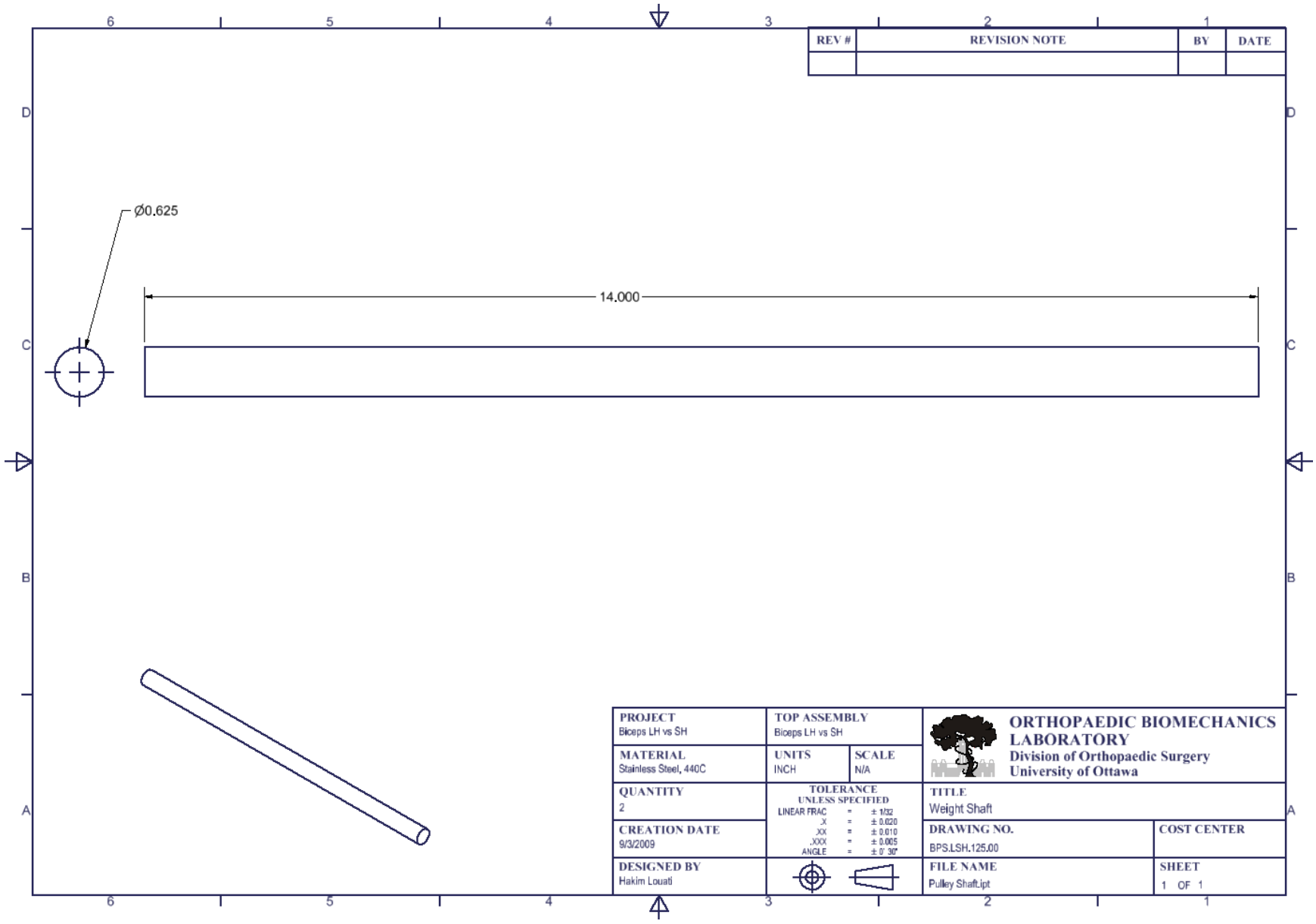
REV #
REVISION NOTE
BY
DATE
Ø0.625
14.000
PROJECT
Biceps LH vs SH
TOP ASSEMBLY
Biceps LH vs SH
MATERIAL
Stainless Steel, 440C
UNITS
INCH
SCALE
N/A
QUANTITY
2
TOLERANCE
UNLESS SPECIFIED
LINEAR FRAC = ± 1/32
.X = ± 0.020
.XX = ± 0.010
.XXX = ± 0.005
ANGLE = ± 0° 30'
ORTHOPAEDIC BIOMECHANICS LABORATORY
Division of Orthopaedic Surgery
University of Ottawa
TITLE
Weight Shaft
CREATION DATE
9/3/2009
DRAWING NO.
BPS.LSH.125.00
COST CENTER
DESIGNED BY
Hakim Louati
FILE NAME
Pulley Shaft.ipt
SHEET
1 OF 1

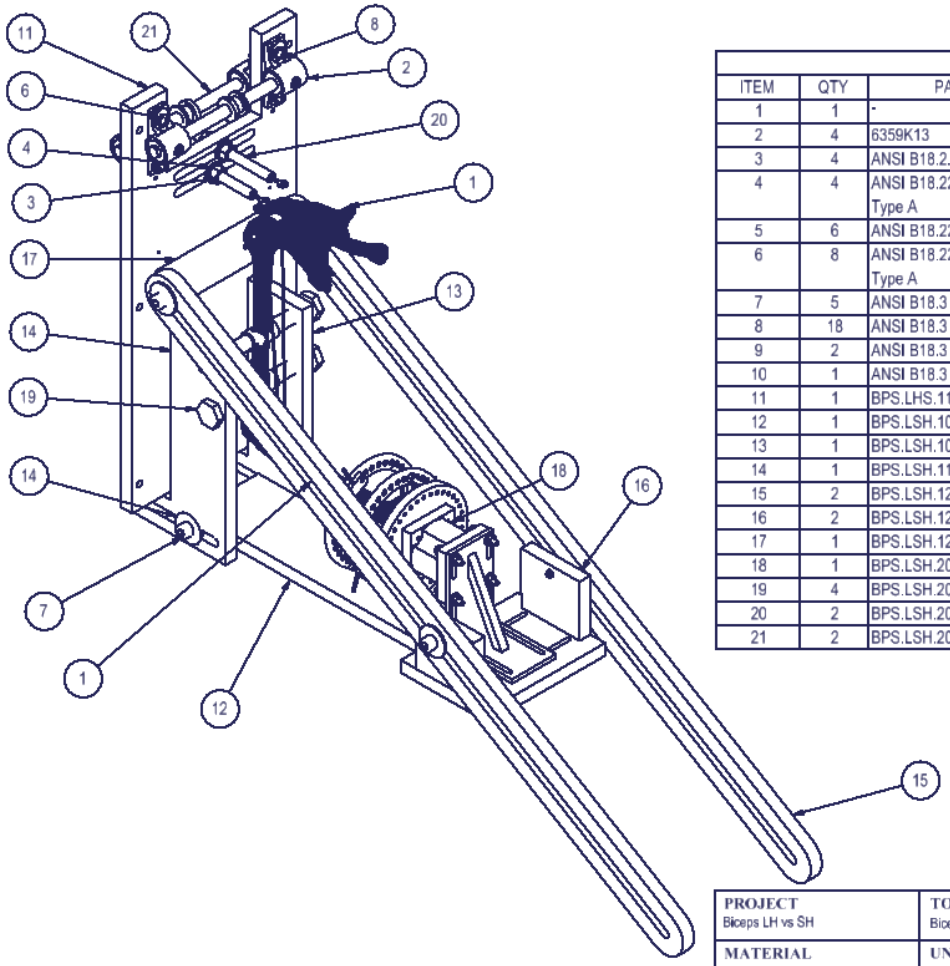

REV #	REVISION NOTE	BY	DATE

Parts List

ITEM	QTY	PART NUMBER	TITLE	DESCRIPTION
1	1	-	Shoulder and Elbow	Shoulder and Elbow
2	4	6359K13	Base Mounted Bearing	PROVIDED - MCMASTER-CARR
3	4	ANSI B18.2.2 - 1/2 - 13		Hex Nut
4	4	ANSI B18.22.1 - 1/2 - narrow - Type A		Washer A
5	6	ANSI B18.22.1 - 1/2 - wide - Type B		Washer B
6	8	ANSI B18.22.1 - 1/4 - narrow - Type A		Washer A
7	5	ANSI B18.3 - 1/2 - 13 - 1 3/4		Hexagon Socket Head Cap Screw
8	18	ANSI B18.3 - 1/4 - 20 - 1		Hexagon Socket Head Cap Screw
9	2	ANSI B18.3 - 3/8 - 16 - 1 1/2		Hexagon Socket Head Cap Screw
10	1	ANSI B18.3 - 3/8 - 16 - 1 3/4		Hexagon Socket Head Cap Screw
11	1	BPS.LHS.113.01	Humerus Back Plate	Humerus Back Plate
12	1	BPS.LSH.106.00	Forearm Base Plate	Forearm Base
13	1	BPS.LSH.109.00	Right Clamp Side Wall	Right Humeral Clamp Side Wall
14	1	BPS.LSH.110.00	Left Clamp Wall	Left Humeral Clamp Side Wall
15	2	BPS.LSH.123.00	Forarm Guide Rail	Forarm Guide Rail
16	2	BPS.LSH.127.00	Forearm Support Block	Forearm Support Block
17	1	BPS.LSH.128.00	Rail Support Block	Rail Support Block
18	1	BPS.LSH.201.00	Load Cell Assembly	Load Cell Assembly
19	4	BPS.LSH.203.00	Humeral Bolt Clamp Assembly	Humerus Clamp Bolt Assembly
20	2	BPS.LSH.206.00	Muscle Alignment Rod	Muscle Alignment Rod
21	2	BPS.LSH.207.00	Alignment Shaft Assembly	Alignment Shaft Assembly

PROJECT: Biceps LH vs SH	TOP ASSEMBLY: Biceps LH vs SH	ORTHOPAEDIC BIOMECHANICS LABORATORY Division of Orthopaedic Surgery University of Ottawa
MATERIAL	UNITS: INCH / SCALE: N/A	
QUANTITY: 1	TOLERANCE UNLESS SPECIFIED LINEAR FRAC = ± 1/32 .X = ± 0.020 .XX = ± 0.010 .XXX = ± 0.005 ANGLE = ± 0° 30'	TITLE: Arm Fixtures Assembly
CREATION DATE: 9/3/2009		DRAWING NO.: BPS.LSH.209.00 / COST CENTER
DESIGNED BY: Hakim Louati		FILE NAME: Arm Fixtures Assembly.iam / SHEET: 1 OF 1

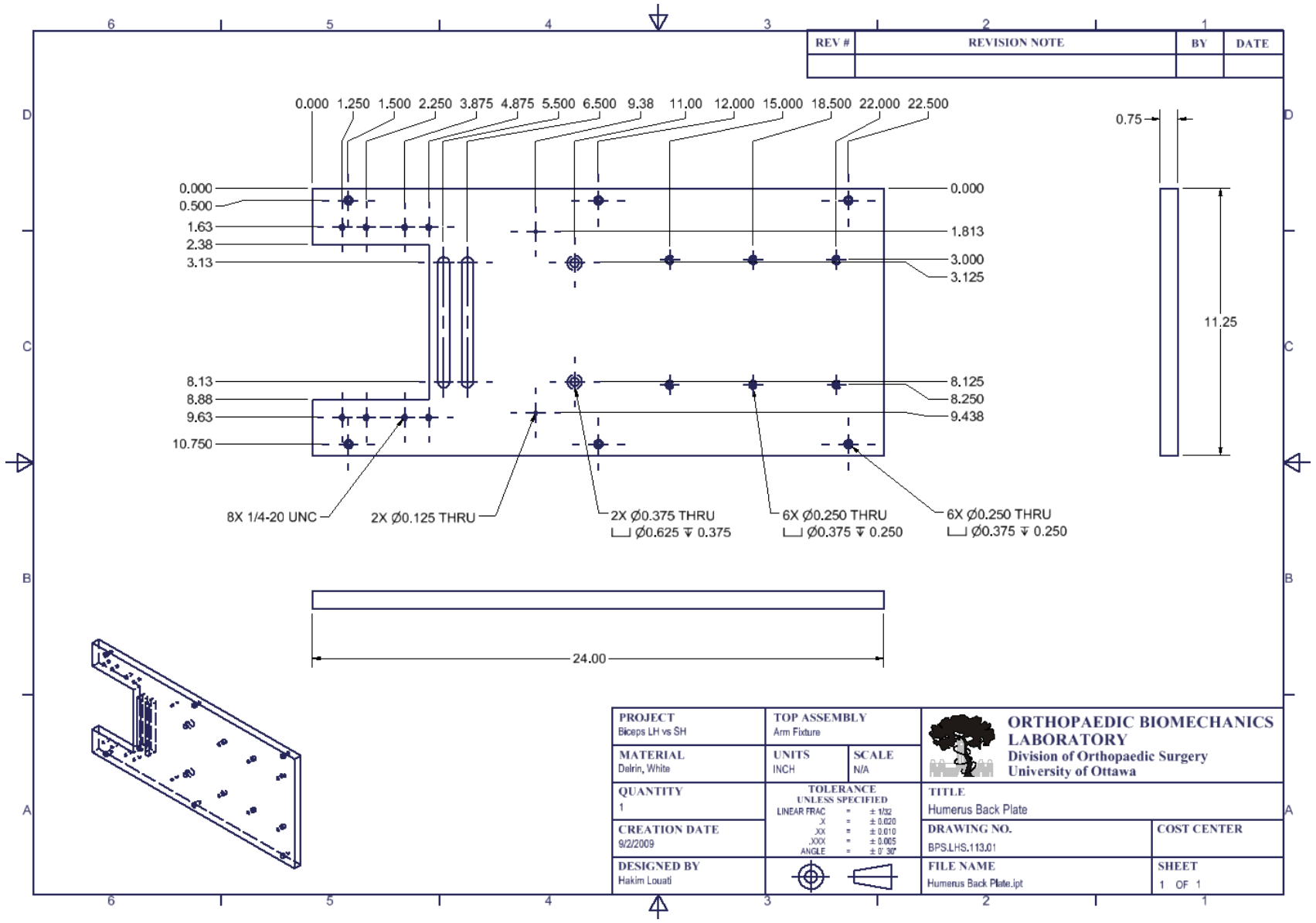
REV # | REVISION NOTE | BY | DATE
0.000 1.250 1.500 2.250 3.875 4.875 5.500 6.500 9.38 11.00 12.000 15.000 18.500 22.000 22.500
0.000
0.500
1.63
2.38
3.13
8.13
8.88
9.63
10.750
0.000
1.813
3.000
3.125
8.125
8.250
9.438
0.75
11.25
8X 1/4-20 UNC
2X Ø0.125 THRU
2X Ø0.375 THRU
⌴ Ø0.625 ↧ 0.375
6X Ø0.250 THRU
⌴ Ø0.375 ↧ 0.250
6X Ø0.250 THRU
⌴ Ø0.375 ↧ 0.250
24.00
PROJECT
Biceps LH vs SH
TOP ASSEMBLY
Arm Fixture
MATERIAL
Delrin, White
UNITS
INCH
SCALE
N/A
QUANTITY
1
TOLERANCE
UNLESS SPECIFIED
LINEAR FRAC = ± 1/32
.X = ± 0.020
.XX = ± 0.010
.XXX = ± 0.005
ANGLE = ± 0° 30'
CREATION DATE
9/2/2009
DESIGNED BY
Hakim Louati
ORTHOPAEDIC BIOMECHANICS LABORATORY
Division of Orthopaedic Surgery
University of Ottawa
TITLE
Humerus Back Plate
DRAWING NO.
BPS.LHS.113.01
COST CENTER
FILE NAME
Humerus Back Plate.ipt
SHEET
1 OF 1

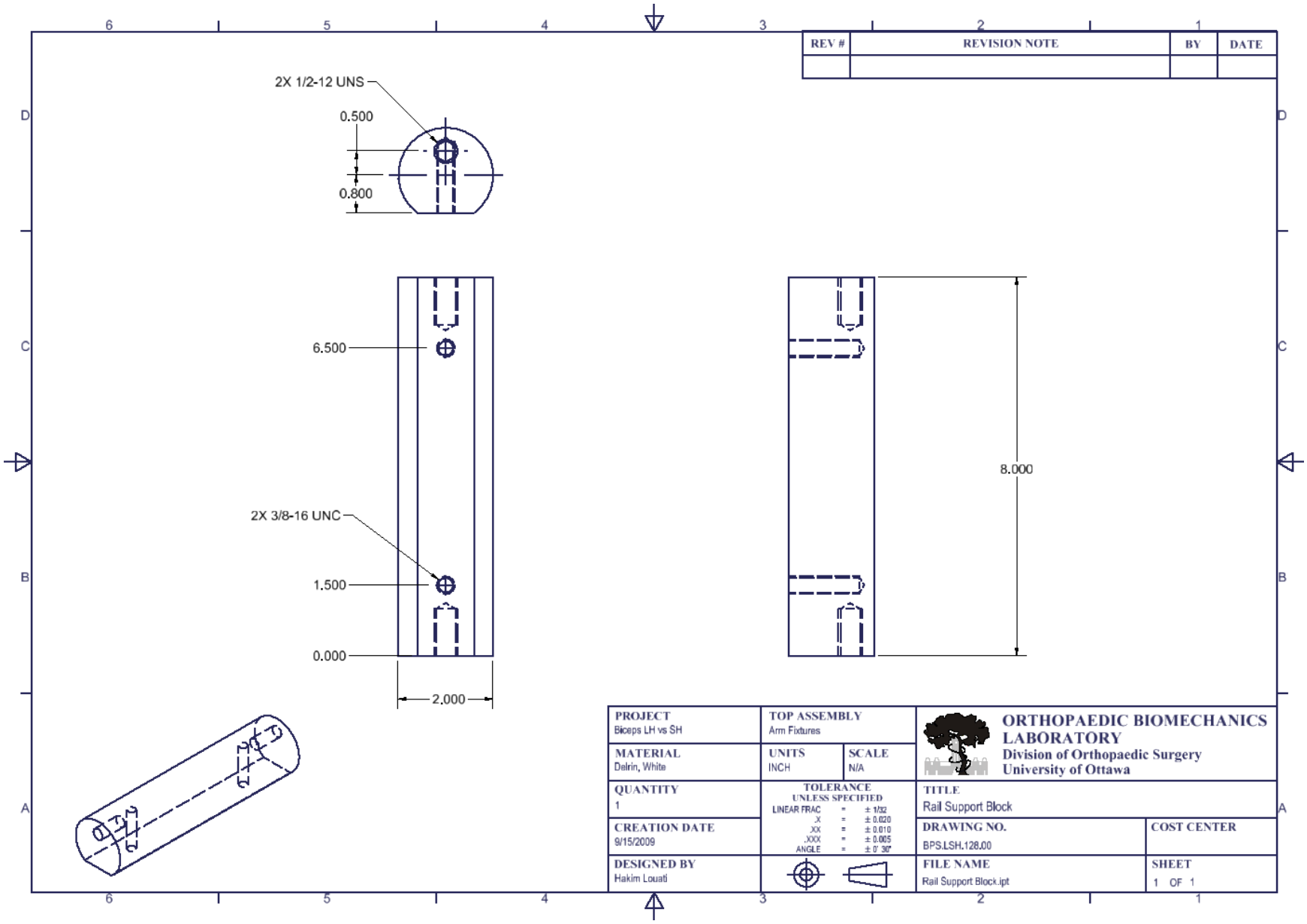
REV #
REVISION NOTE
BY
DATE
2X 1/2-12 UNS
0.500
0.800
6.500
2X 3/8-16 UNC
1.500
0.000
2.000
8.000
PROJECT
Biceps LH vs SH
TOP ASSEMBLY
Arm Fixtures
MATERIAL
Delrin, White
UNITS
INCH
SCALE
N/A
QUANTITY
1
TOLERANCE
UNLESS SPECIFIED
LINEAR FRAC = ± 1/32
.X = ± 0.020
.XX = ± 0.010
.XXX = ± 0.005
ANGLE = ± 0° 30"
CREATION DATE
9/15/2009
DESIGNED BY
Hakim Louati
ORTHOPAEDIC BIOMECHANICS LABORATORY
Division of Orthopaedic Surgery
University of Ottawa
TITLE
Rail Support Block
DRAWING NO.
BPS.LSH.128.00
COST CENTER
FILE NAME
Rail Support Block.ipt
SHEET
1 OF 1

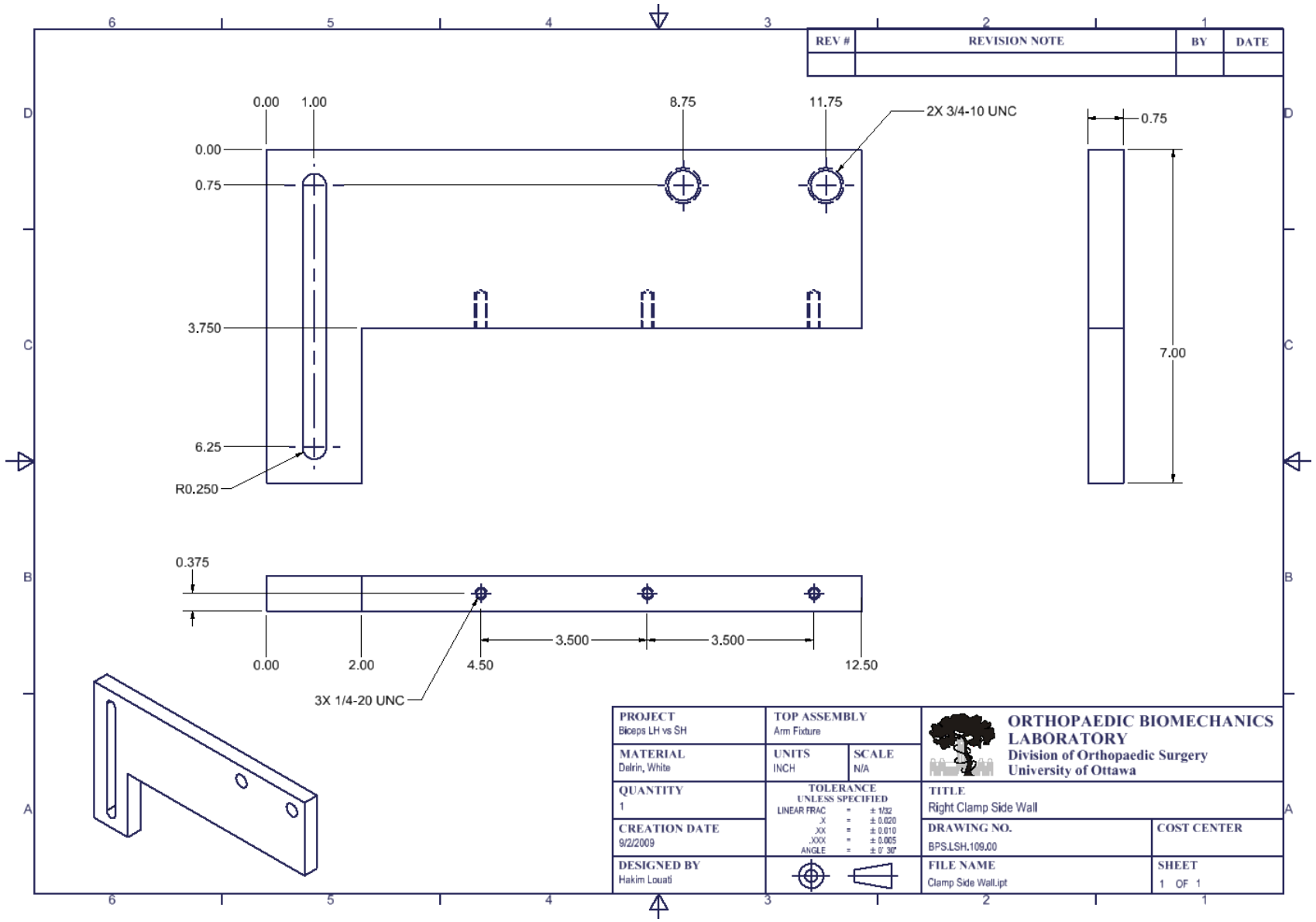
REV #
REVISION NOTE
BY
DATE
0.00
1.00
8.75
11.75
2X 3/4-10 UNC
0.75
0.00
0.75
3.750
6.25
R0.250
7.00
0.375
0.00
2.00
4.50
3.500
3.500
12.50
3X 1/4-20 UNC
PROJECT
Biceps LH vs SH
TOP ASSEMBLY
Arm Fixture
MATERIAL
Delrin, White
UNITS
INCH
SCALE
N/A
QUANTITY
1
TOLERANCE
UNLESS SPECIFIED
LINEAR FRAC = ± 1/32
.X = ± 0.020
.XX = ± 0.010
.XXX = ± 0.005
ANGLE = ± 0° 30'
CREATION DATE
9/2/2009
DESIGNED BY
Hakim Louati
ORTHOPAEDIC BIOMECHANICS LABORATORY
Division of Orthopaedic Surgery
University of Ottawa
TITLE
Right Clamp Side Wall
DRAWING NO.
BPS.LSH.109.00
COST CENTER
FILE NAME
Clamp Side Wall.ipt
SHEET
1 OF 1

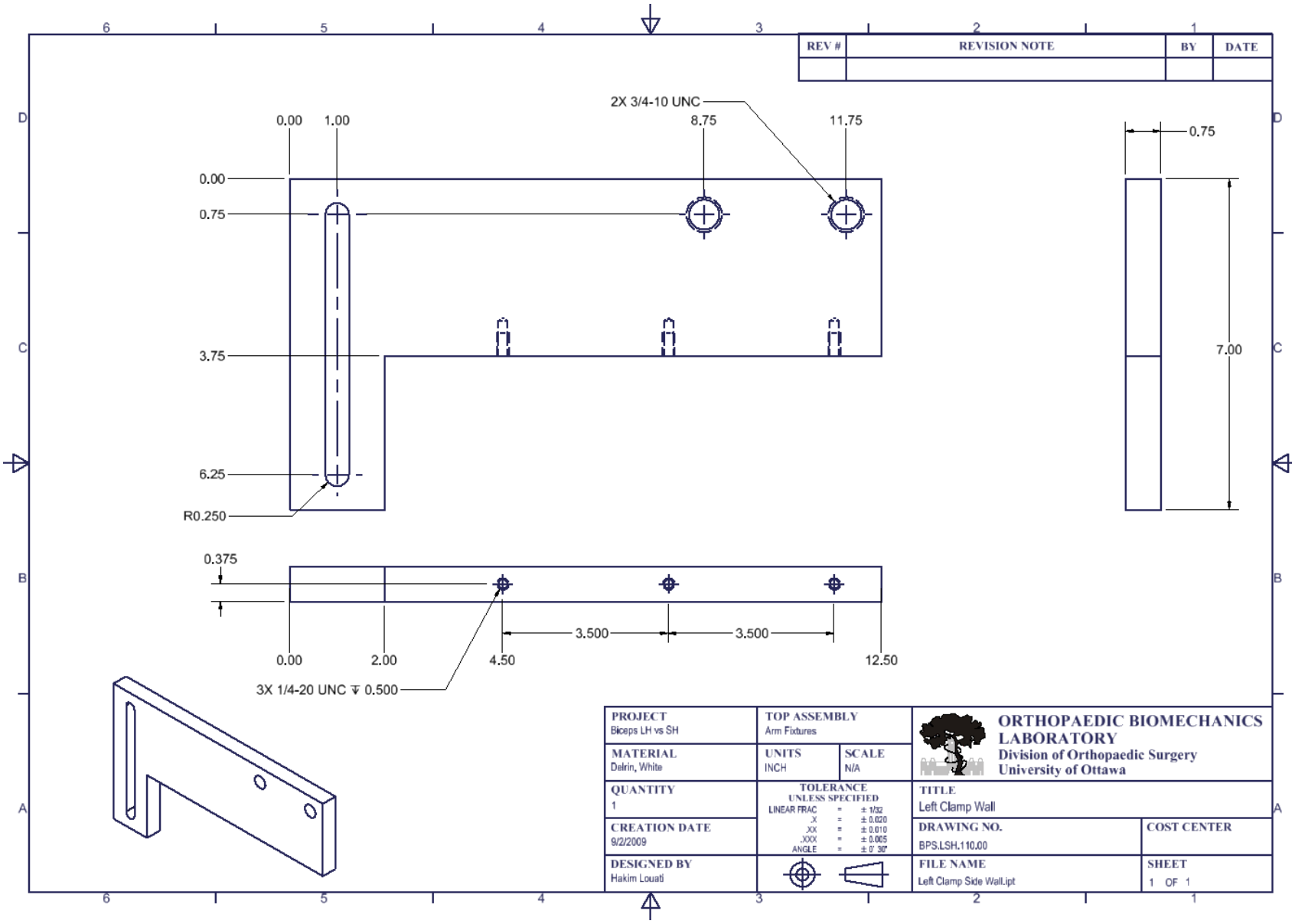
REV #
REVISION NOTE
BY
DATE
2X 3/4-10 UNC
0.00
1.00
8.75
11.75
0.00
0.75
3.75
6.25
R0.250
0.75
7.00
0.375
0.00
2.00
4.50
3.500
3.500
12.50
3X 1/4-20 UNC ↧ 0.500
PROJECT
Biceps LH vs SH
TOP ASSEMBLY
Arm Fixtures
MATERIAL
Delrin, White
UNITS
INCH
SCALE
N/A
QUANTITY
1
TOLERANCE
UNLESS SPECIFIED
LINEAR FRAC = ± 1/32
.X = ± 0.020
.XX = ± 0.010
.XXX = ± 0.005
ANGLE = ± 0° 30'
CREATION DATE
9/2/2009
DESIGNED BY
Hakim Louati
ORTHOPAEDIC BIOMECHANICS LABORATORY
Division of Orthopaedic Surgery
University of Ottawa
TITLE
Left Clamp Wall
DRAWING NO.
BPS.LSH.110.00
COST CENTER
FILE NAME
Left Clamp Side Wall.ipt
SHEET
1 OF 1

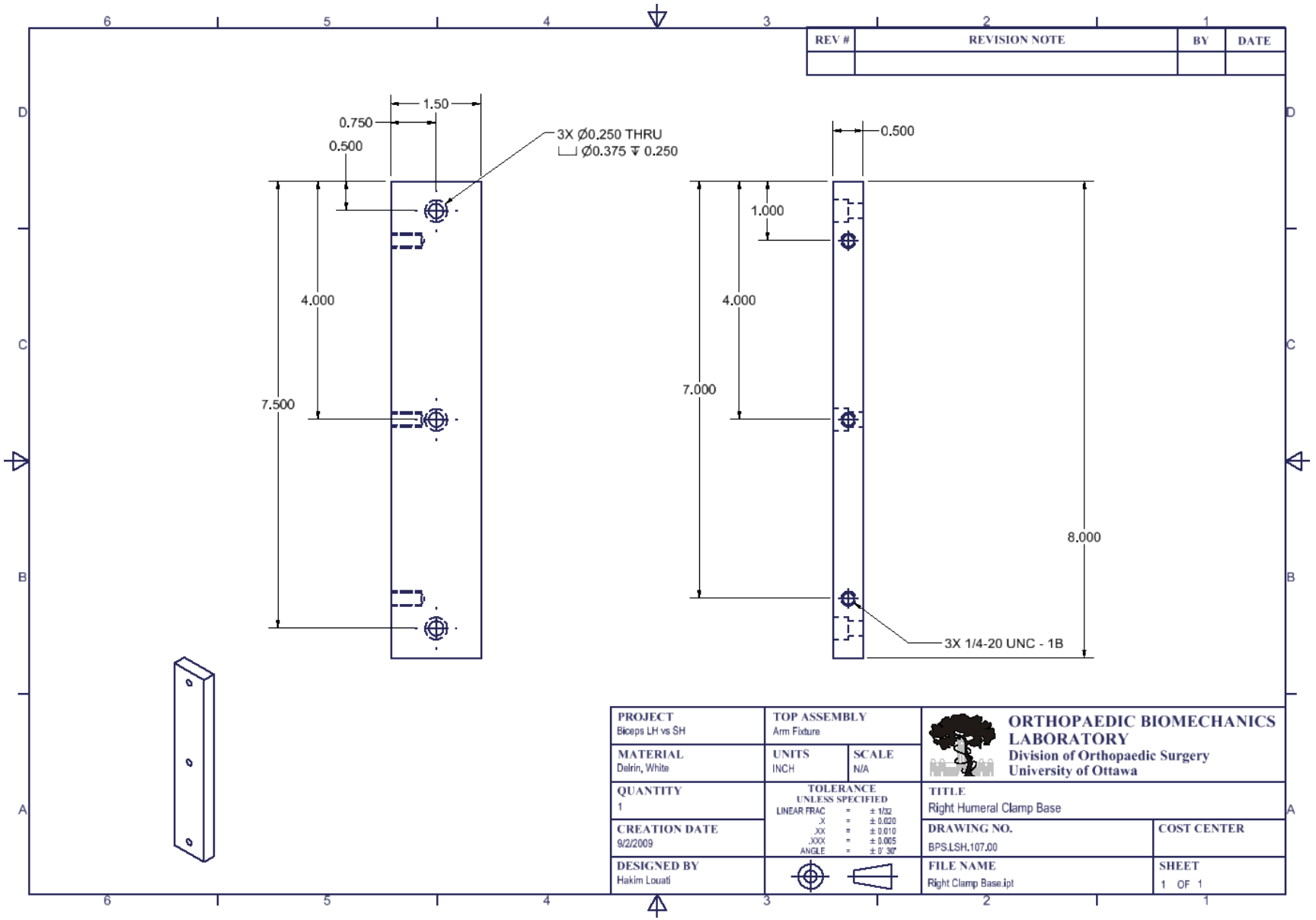
REV #
REVISION NOTE
BY
DATE
1.50
0.750
0.500
3X Ø0.250 THRU
Ø0.375 ↧ 0.250
4.000
7.500
0.500
1.000
4.000
7.000
8.000
3X 1/4-20 UNC - 1B
PROJECT
Biceps LH vs SH
TOP ASSEMBLY
Arm Fixture
MATERIAL
Delrin, White
UNITS
INCH
SCALE
N/A
QUANTITY
1
TOLERANCE
UNLESS SPECIFIED
LINEAR FRAC = ± 1/32
.X = ± 0.020
.XX = ± 0.010
.XXX = ± 0.005
ANGLE = ± 0° 30'
CREATION DATE
9/2/2009
DESIGNED BY
Hakim Louati
ORTHOPAEDIC BIOMECHANICS LABORATORY
Division of Orthopaedic Surgery
University of Ottawa
TITLE
Right Humeral Clamp Base
DRAWING NO.
BPS.LSH.107.00
COST CENTER
FILE NAME
Right Clamp Base.ipt
SHEET
1 OF 1

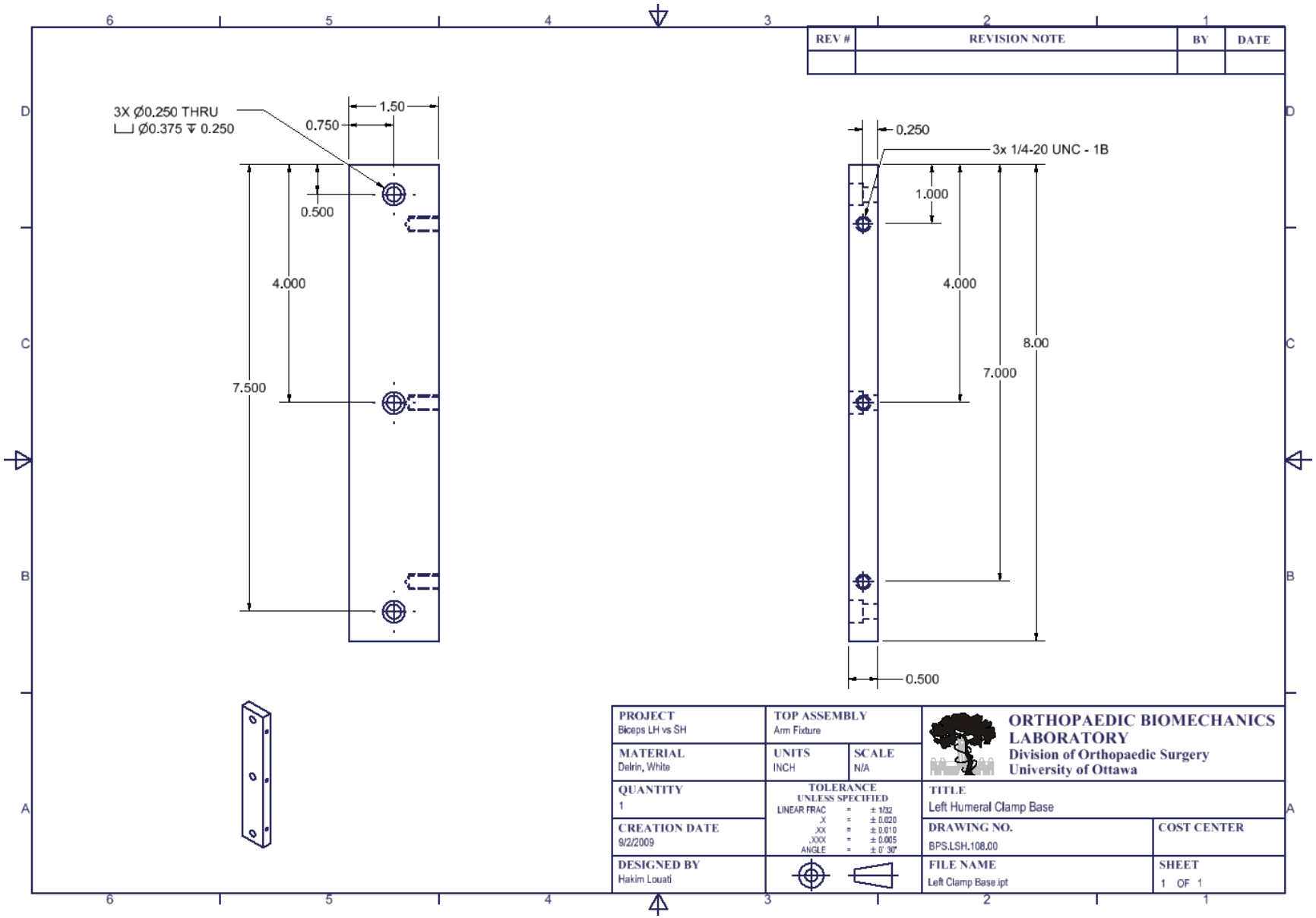
REV #
REVISION NOTE
BY
DATE
3X Ø0.250 THRU
Ø0.375 ↧ 0.250
1.50
0.750
0.500
4.000
7.500
0.250
3x 1/4-20 UNC - 1B
1.000
4.000
8.00
7.000
0.500
PROJECT
Biceps LH vs SH
TOP ASSEMBLY
Arm Fixture
MATERIAL
Delrin, White
UNITS
INCH
SCALE
N/A
QUANTITY
1
TOLERANCE
UNLESS SPECIFIED
LINEAR FRAC = ± 1/32
.X = ± 0.020
.XX = ± 0.010
.XXX = ± 0.005
ANGLE = ± 0° 30'
CREATION DATE
9/2/2009
DESIGNED BY
Hakim Louati
ORTHOPAEDIC BIOMECHANICS LABORATORY
Division of Orthopaedic Surgery
University of Ottawa
TITLE
Left Humeral Clamp Base
DRAWING NO.
BPS.LSH.108.00
COST CENTER
FILE NAME
Left Clamp Base.ipt
SHEET
1 OF 1

REV #	REVISION NOTE	BY	DATE

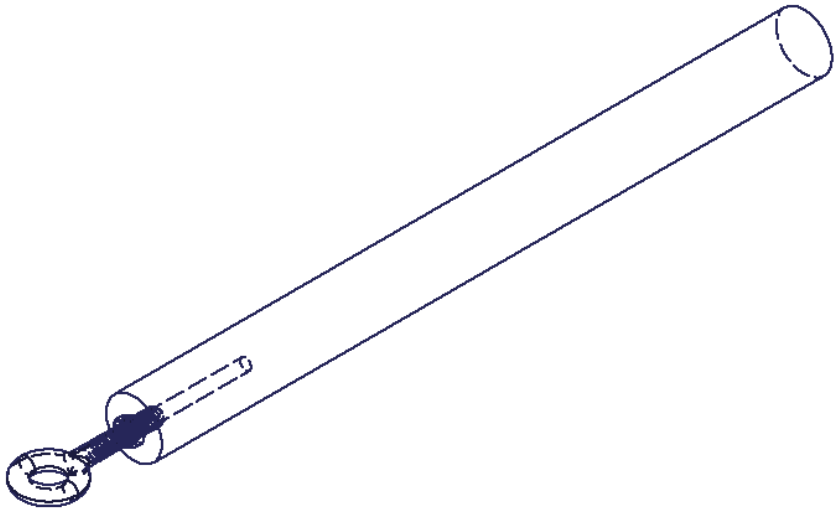

Parts List				
ITEM	QTY	PART NUMBER	TITLE	DESCRIPTION
1	1	BPS.LHS.123.00	1/2" Threaded Rod	1/2" Threaded Rod
2	1	Eyebolt	Eyebolt	6-32 Thread, 3/4" Shank, 5/8" Thread Length

PROJECT: Biceps LH vs SH	TOP ASSEMBLY: Arm Fixture		ORTHOPAEDIC BIOMECHANICS LABORATORY Division of Orthopaedic Surgery University of Ottawa
MATERIAL	UNITS: INCH	SCALE: N/A	
QUANTITY: 2	TOLERANCE UNLESS SPECIFIED LINEAR FRAC = ± 1/32 .X = ± 0.020 .XX = ± 0.010 .XXX = ± 0.005 ANGLE = ± 0° 30"	TITLE: Muscle Alignment Rod	
CREATION DATE: 9/2/2009		DRAWING NO.: BPS.LSH.206.00	COST CENTER
DESIGNED BY: Hakim Louati		FILE NAME: Alignment rod.iam	SHEET: 1 OF 1

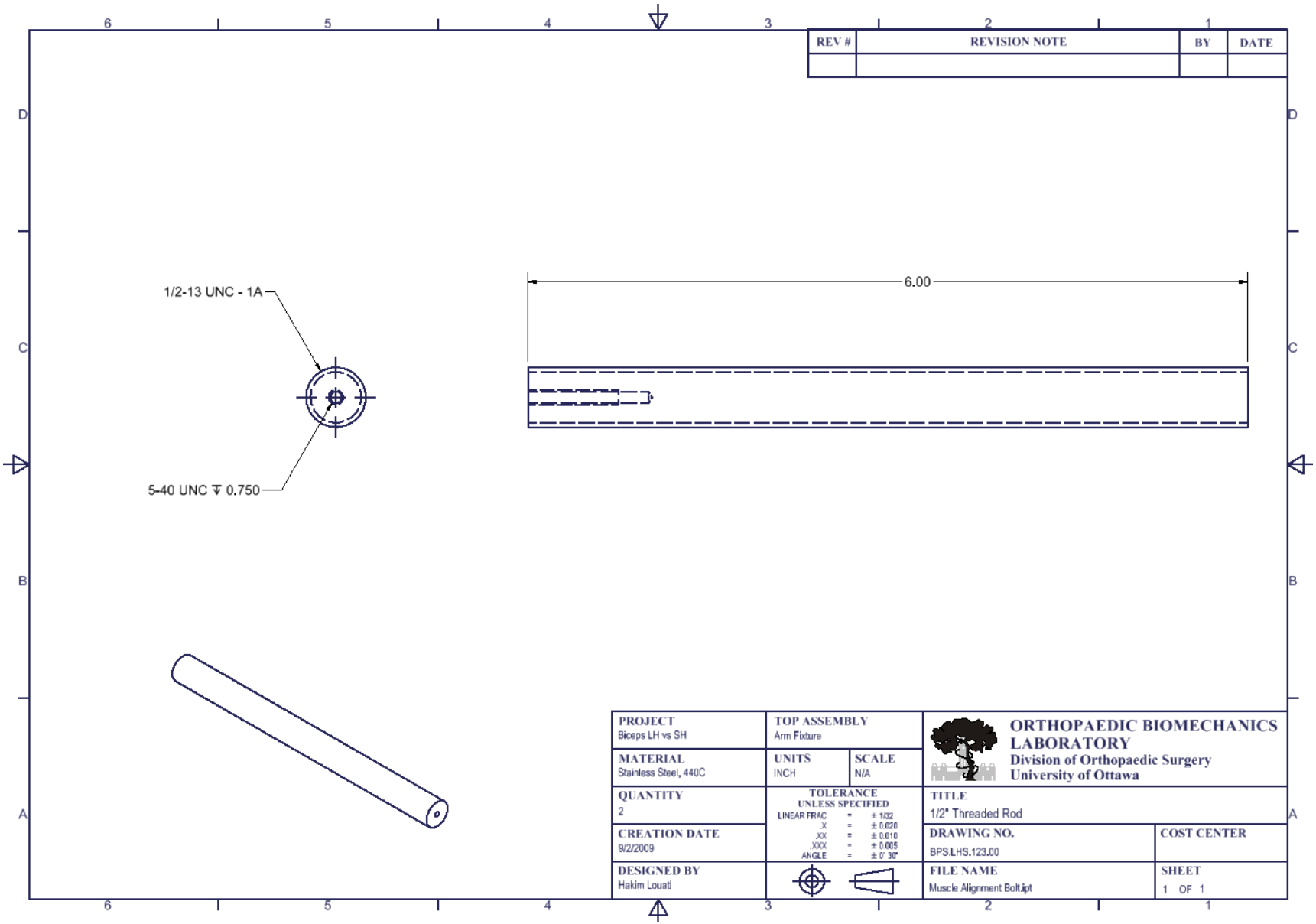
REV #
REVISION NOTE
BY
DATE
1/2-13 UNC - 1A
5-40 UNC ↧ 0.750
6.00
PROJECT
Biceps LH vs SH
TOP ASSEMBLY
Arm Fixture
MATERIAL
Stainless Steel, 440C
UNITS
INCH
SCALE
N/A
QUANTITY
2
TOLERANCE
UNLESS SPECIFIED
LINEAR FRAC = ± 1/32
.X = ± 0.020
.XX = ± 0.010
.XXX = ± 0.005
ANGLE = ± 0° 30'
CREATION DATE
9/2/2009
DESIGNED BY
Hakim Louati
ORTHOPAEDIC BIOMECHANICS LABORATORY
Division of Orthopaedic Surgery
University of Ottawa
TITLE
1/2" Threaded Rod
DRAWING NO.
BPS.LHS.123.00
COST CENTER
FILE NAME
Muscle Alignment Bolt.ipt
SHEET
1 OF 1

REV #	REVISION NOTE	BY	DATE

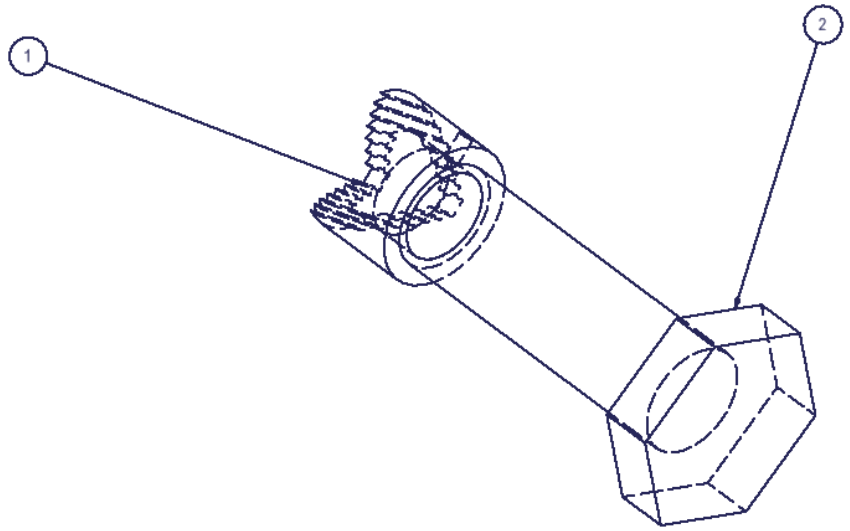

Parts List

ITEM	QTY	PART NUMBER	TITLE	DESCRIPTION
1	1	BPS.LSH.111.00	Humerus Serrated Grip	Humerus Serrated Grip
2	1	BPS.LSH.129.00	Modified Clamp Bolt	Modified Clamp Bolt

PROJECT: Biceps LH vs SH	TOP ASSEMBLY: Arm Fixtures		ORTHOPAEDIC BIOMECHANICS LABORATORY Division of Orthopaedic Surgery University of Ottawa
MATERIAL	UNITS: INCH	SCALE: N/A	
QUANTITY: 4	TOLERANCE UNLESS SPECIFIED LINEAR FRAC = ± 1/32 .X = ± 0.020 .XX = ± 0.010 .XXX = ± 0.005 ANGLE = ± 0° 30"	TITLE: Humeral Bolt Clamp Assembly	
CREATION DATE: 9/3/2009		DRAWING NO.: BPS.LSH.203.00	COST CENTER
DESIGNED BY: Hakim Louati		FILE NAME: Humerus Clamp Bolt Assembly.iam	SHEET: 1 OF 1

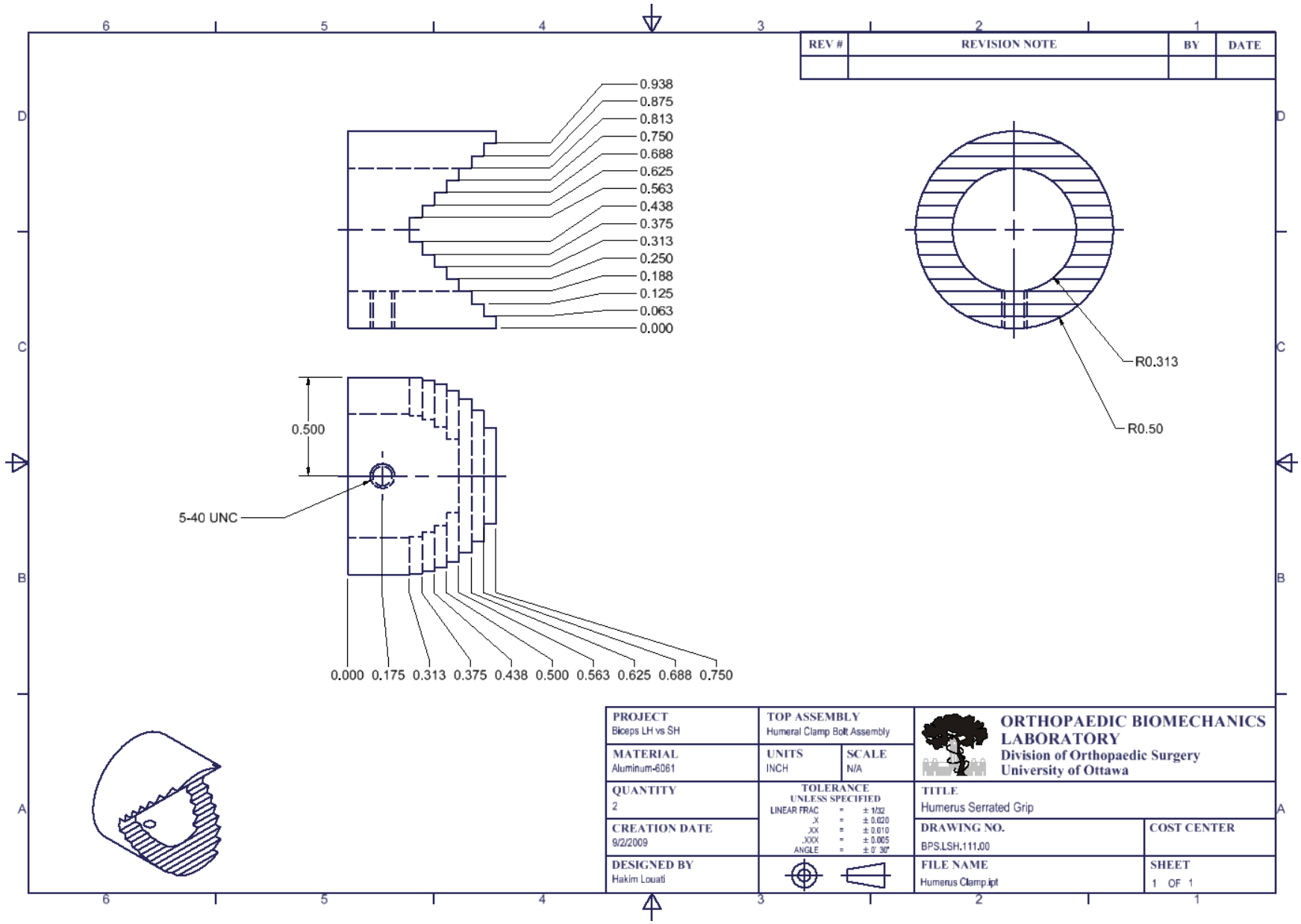
REV #
REVISION NOTE
BY
DATE
0.938
0.875
0.813
0.750
0.688
0.625
0.563
0.438
0.375
0.313
0.250
0.188
0.125
0.063
0.000
R0.313
R0.50
0.500
5-40 UNC
0.000 0.175 0.313 0.375 0.438 0.500 0.563 0.625 0.688 0.750
PROJECT
Biceps LH vs SH
TOP ASSEMBLY
Humeral Clamp Bolt Assembly
MATERIAL
Aluminum-6061
UNITS
INCH
SCALE
N/A
QUANTITY
2
TOLERANCE
UNLESS SPECIFIED
LINEAR FRAC = ± 1/32
.X = ± 0.020
.XX = ± 0.010
.XXX = ± 0.005
ANGLE = ± 0° 30'
CREATION DATE
9/2/2009
DESIGNED BY
Hakim Louati
ORTHOPAEDIC BIOMECHANICS LABORATORY
Division of Orthopaedic Surgery
University of Ottawa
TITLE
Humerus Serrated Grip
DRAWING NO.
BPS.LSH.111.00
COST CENTER
FILE NAME
Humerus Clamp.ipt
SHEET
1 OF 1

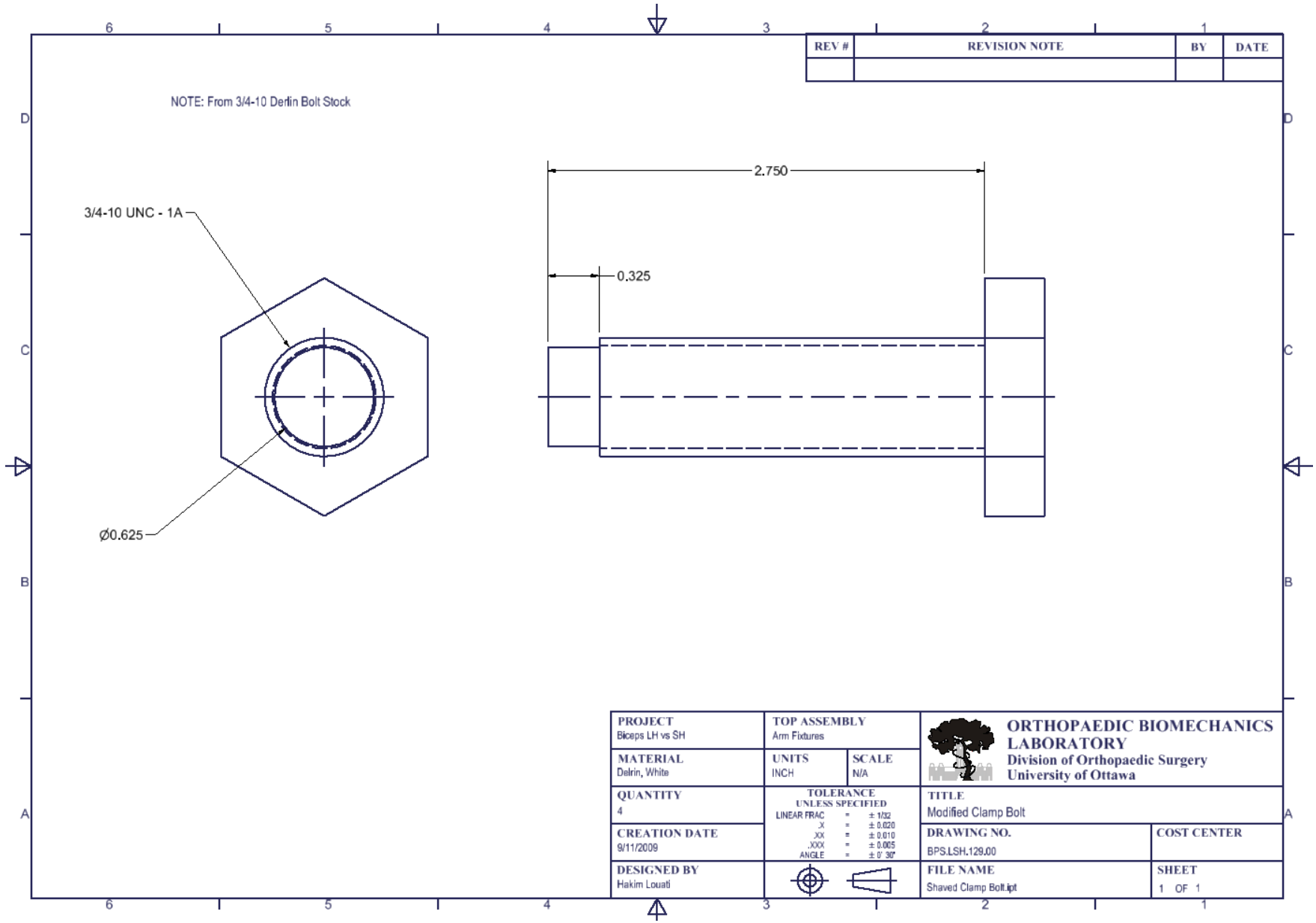
REV #
REVISION NOTE
BY
DATE
NOTE: From 3/4-10 Derlin Bolt Stock
3/4-10 UNC - 1A
Ø0.625
2.750
0.325
PROJECT
Biceps LH vs SH
TOP ASSEMBLY
Arm Fixtures
MATERIAL
Delrin, White
UNITS
INCH
SCALE
N/A
QUANTITY
4
TOLERANCE
UNLESS SPECIFIED
LINEAR FRAC = ± 1/32
.X = ± 0.020
.XX = ± 0.010
.XXX = ± 0.005
ANGLE = ± 0° 30'
CREATION DATE
9/11/2009
DESIGNED BY
Hakim Louati
ORTHOPAEDIC BIOMECHANICS LABORATORY
Division of Orthopaedic Surgery
University of Ottawa
TITLE
Modified Clamp Bolt
DRAWING NO.
BPS.LSH.129.00
COST CENTER
FILE NAME
Shaved Clamp Bolt.ipt
SHEET
1 OF 1

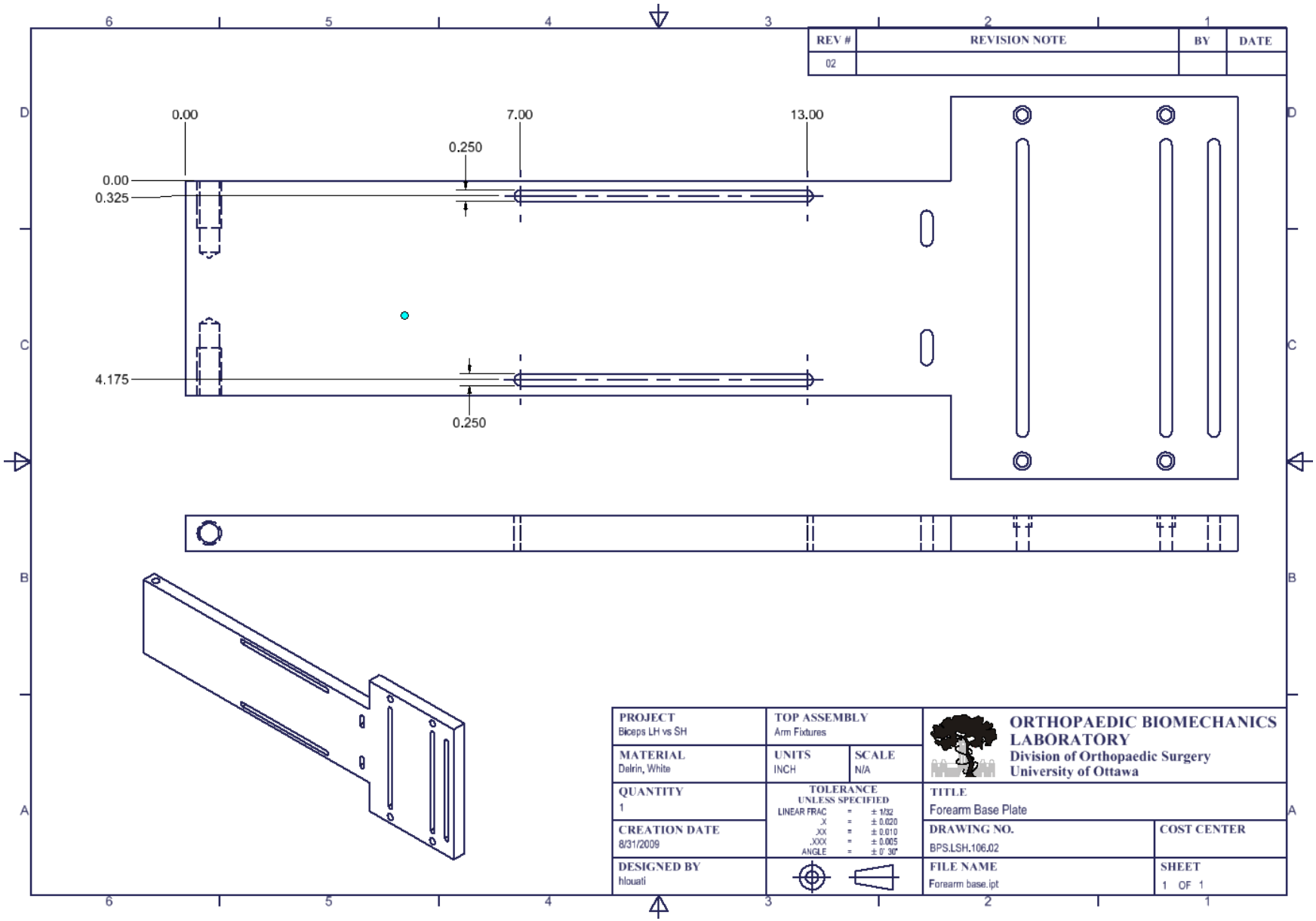
REV # | REVISION NOTE | BY | DATE
02
0.00
7.00
13.00
0.250
0.00
0.325
4.175
0.250
PROJECT
Biceps LH vs SH
TOP ASSEMBLY
Arm Fixtures
MATERIAL
Delrin, White
UNITS
INCH
SCALE
N/A
QUANTITY
1
TOLERANCE
UNLESS SPECIFIED
LINEAR FRAC = ± 1/32
.X = ± 0.020
.XX = ± 0.010
.XXX = ± 0.005
ANGLE = ± 0° 30'
CREATION DATE
8/31/2009
DESIGNED BY
hlouati
ORTHOPAEDIC BIOMECHANICS LABORATORY
Division of Orthopaedic Surgery
University of Ottawa
TITLE
Forearm Base Plate
DRAWING NO.
BPS.LSH.106.02
COST CENTER
FILE NAME
Forearm base.ipt
SHEET
1 OF 1

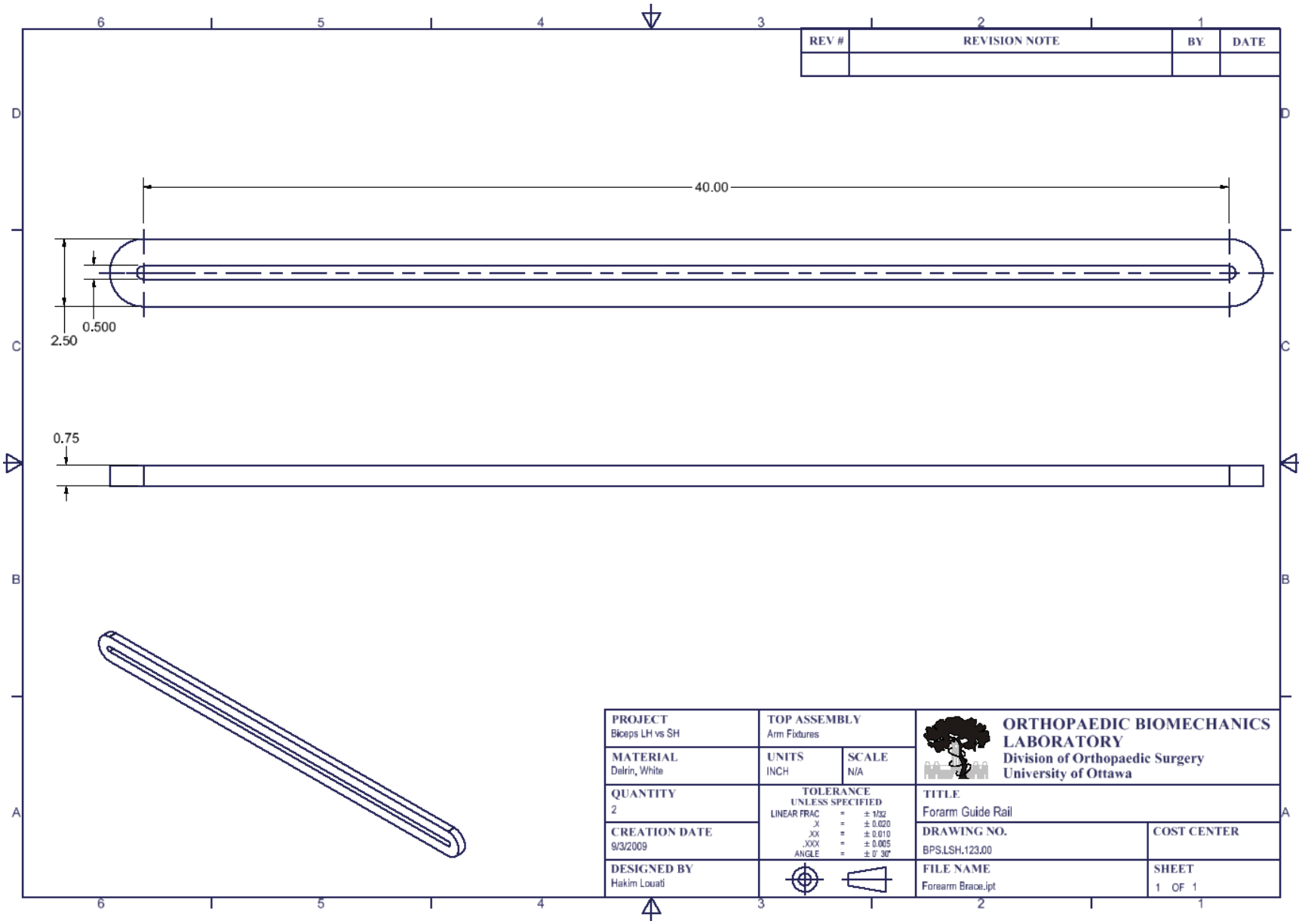
REV #
REVISION NOTE
BY
DATE
40.00
2.50
0.500
0.75
PROJECT
Biceps LH vs SH
TOP ASSEMBLY
Arm Fixtures
MATERIAL
Delrin, White
UNITS
INCH
SCALE
N/A
QUANTITY
2
TOLERANCE
UNLESS SPECIFIED
LINEAR FRAC = ± 1/32
.X = ± 0.020
.XX = ± 0.010
.XXX = ± 0.005
ANGLE = ± 0° 30"
CREATION DATE
9/3/2009
DESIGNED BY
Hakim Louati
ORTHOPAEDIC BIOMECHANICS LABORATORY
Division of Orthopaedic Surgery
University of Ottawa
TITLE
Forarm Guide Rail
DRAWING NO.
BPS.LSH.123.00
COST CENTER
FILE NAME
Forearm Brace.ipt
SHEET
1 OF 1

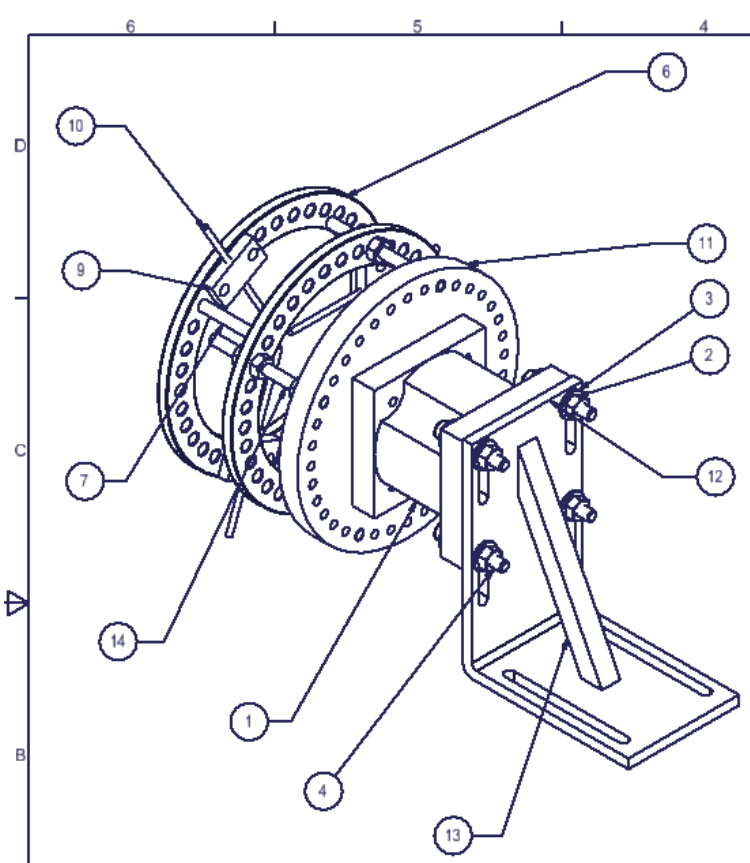

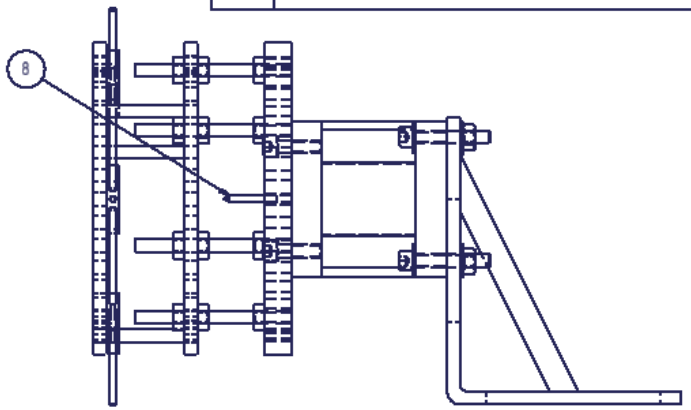

REV #	REVISION NOTE	BY	DATE

Parts List

ITEM	QTY	PART NUMBER	TITLE	DESCRIPTION
1	1	AMTI-MC3-6-100	Six Axis Load Cell	PROVIDED
2	16	ANSI B18.2.2 - 1/4 - 20		Hex Nut
3	8	ANSI B18.22.1 - 1/4 - narrow - Type A		Washer A
4	4	ANSI B18.3 - 1/4 - 20 - 1 1/2		Hexagon Socket Head Cap Screw
5	4	ANSI B18.3 - 1/4 - 20 - 7/8		Hexagon Socket Head Cap Screw
6	2	BPS.LSH.005.00	External Fixator Ring	PROVIDED
7	3	BPS.LSH.006.00	Fixator Cross-member	PROVIDED
8	1	BPS.LSH.007.00	Ulna Guide Pin	PROVIDED
9	3	BPS.LSH.101.01	Ulna Alignment Clamp	Ulna Alignment Clamp
10	3	BPS.LSH.102.00	Ulna Alignment Rod	Ulna Alignment Rod
11	1	BPS.LSH.103.00	External Fixator Adapter	External Fixator Adapter
12	1	BPS.LSH.104.00	Load Cell L-Bracket	Load Cell L-Bracket
13	1	BPS.LSH.105.00	L-Bracket Brace	L-Bracket Brace
14	4	BPS.LSH.125.00	1/4-20 Threaded Rod	1/4-20 threaded rod

PROJECT: Biceps LH vs SH	TOP ASSEMBLY: Biceps LH vs SH Assembly	ORTHOPAEDIC BIOMECHANICS LABORATORY Division of Orthopaedic Surgery University of Ottawa	
MATERIAL	UNITS: INCH / SCALE: N/A		
QUANTITY: 1	TOLERANCE UNLESS SPECIFIED LINEAR FRAC = ± 1/32 .X = ± 0.020 .XX = ± 0.010 .XXX = ± 0.005 ANGLE = ± 0° 30'	TITLE: Load Cell Assembly	
CREATION DATE: 8/30/2009		DRAWING NO.: BPS.LSH.201.00	COST CENTER
DESIGNED BY: Hakim Louati		FILE NAME: Load Cell Assembly.iam	SHEET: 1 OF 1

REV #	REVISION NOTE	BY	DATE

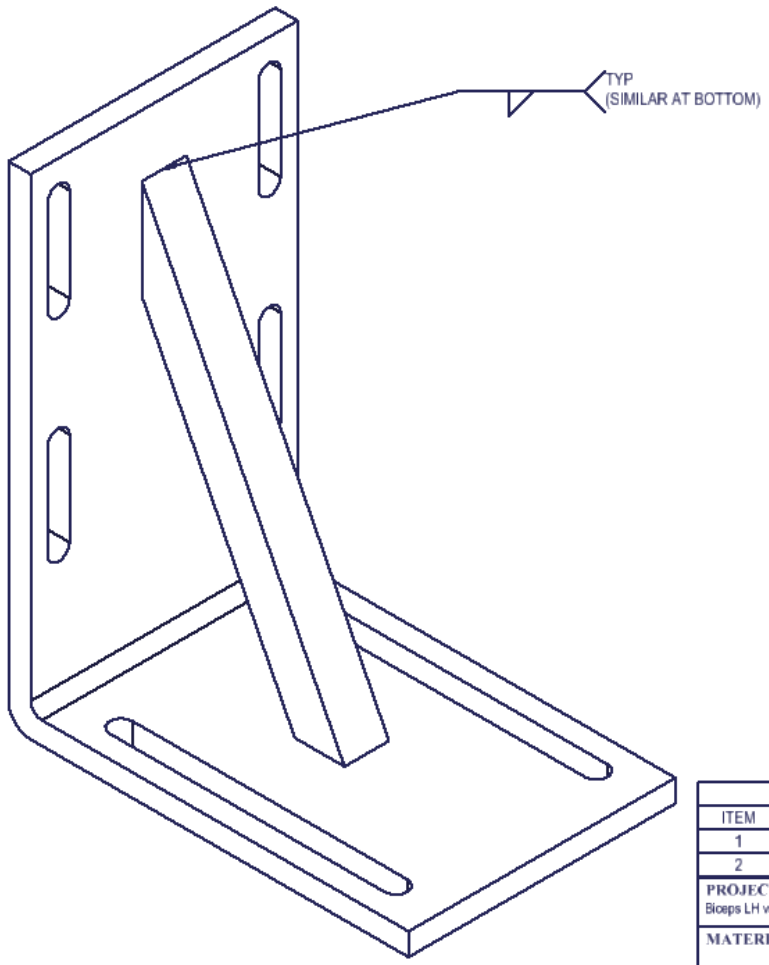

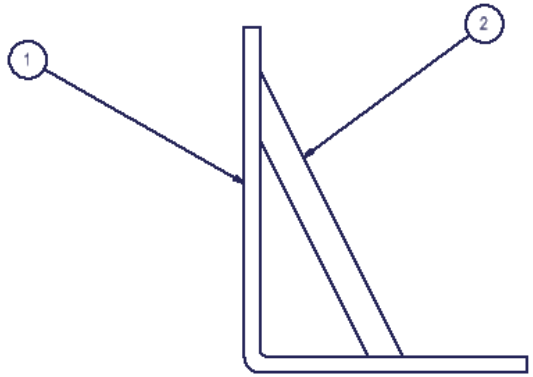

Parts List

ITEM	QTY	PART NUMBER	TITLE	DESCRIPTION
1	1	BPS.LSH.104.00	Load Cell L-Bracket	Load Cell L-Bracket
2	1	BPS.LSH.105.00	L-Bracket Brace	L-Bracket Brace

PROJECT: Biceps LH vs SH	TOP ASSEMBLY: L-Bracket Assembly	ORTHOPAEDIC BIOMECHANICS LABORATORY Division of Orthopaedic Surgery University of Ottawa
MATERIAL	UNITS: INCH / SCALE: N/A	
QUANTITY: 1	TOLERANCE UNLESS SPECIFIED: LINEAR FRAC = ± 1/32; .X = ± 0.020; .XX = ± 0.010; .XXX = ± 0.005; ANGLE = ± 0° 30'	TITLE: L-Bracket Assembly
CREATION DATE: 8/30/2009		DRAWING NO.: BPS.LSH.202.00 / COST CENTER
DESIGNED BY: Hakim Louati		FILE NAME: Load Cell Bracket Assembly Welded.iam / SHEET: 1 OF 1

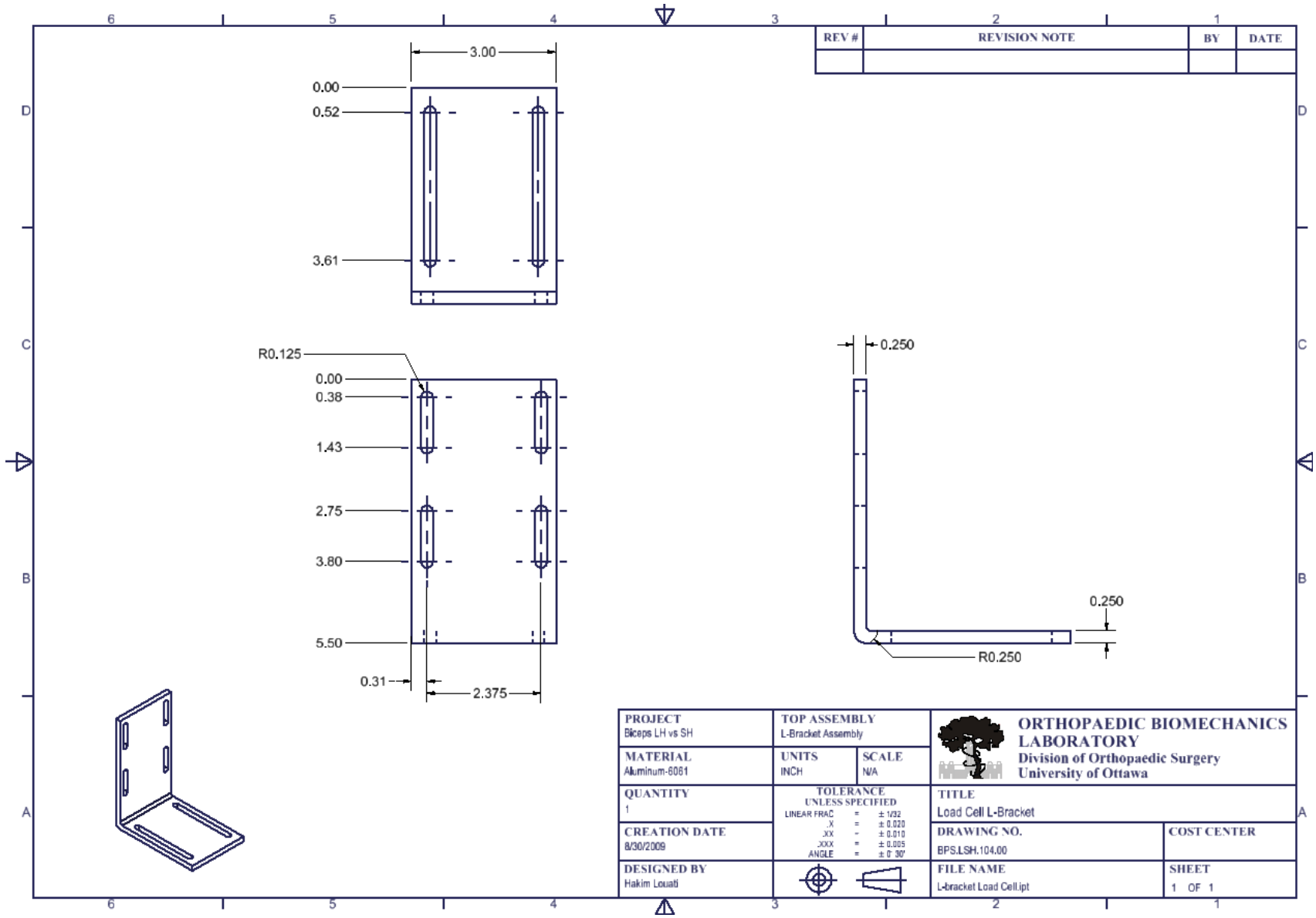
REV #
REVISION NOTE
BY
DATE
3.00
0.00
0.52
3.61
R0.125
0.00
0.38
1.43
2.75
3.80
5.50
0.31
2.375
0.250
0.250
R0.250
PROJECT
Biceps LH vs SH
TOP ASSEMBLY
L-Bracket Assembly
MATERIAL
Aluminum-6061
UNITS
INCH
SCALE
N/A
QUANTITY
1
TOLERANCE
UNLESS SPECIFIED
LINEAR FRAC = ± 1/32
.X = ± 0.020
.XX = ± 0.010
.XXX = ± 0.005
ANGLE = ± 0° 30'
CREATION DATE
8/30/2009
DESIGNED BY
Hakim Louati
ORTHOPAEDIC BIOMECHANICS LABORATORY
Division of Orthopaedic Surgery
University of Ottawa
TITLE
Load Cell L-Bracket
DRAWING NO.
BPS.LSH.104.00
COST CENTER
FILE NAME
L-bracket Load Cell.ipt
SHEET
1 OF 1

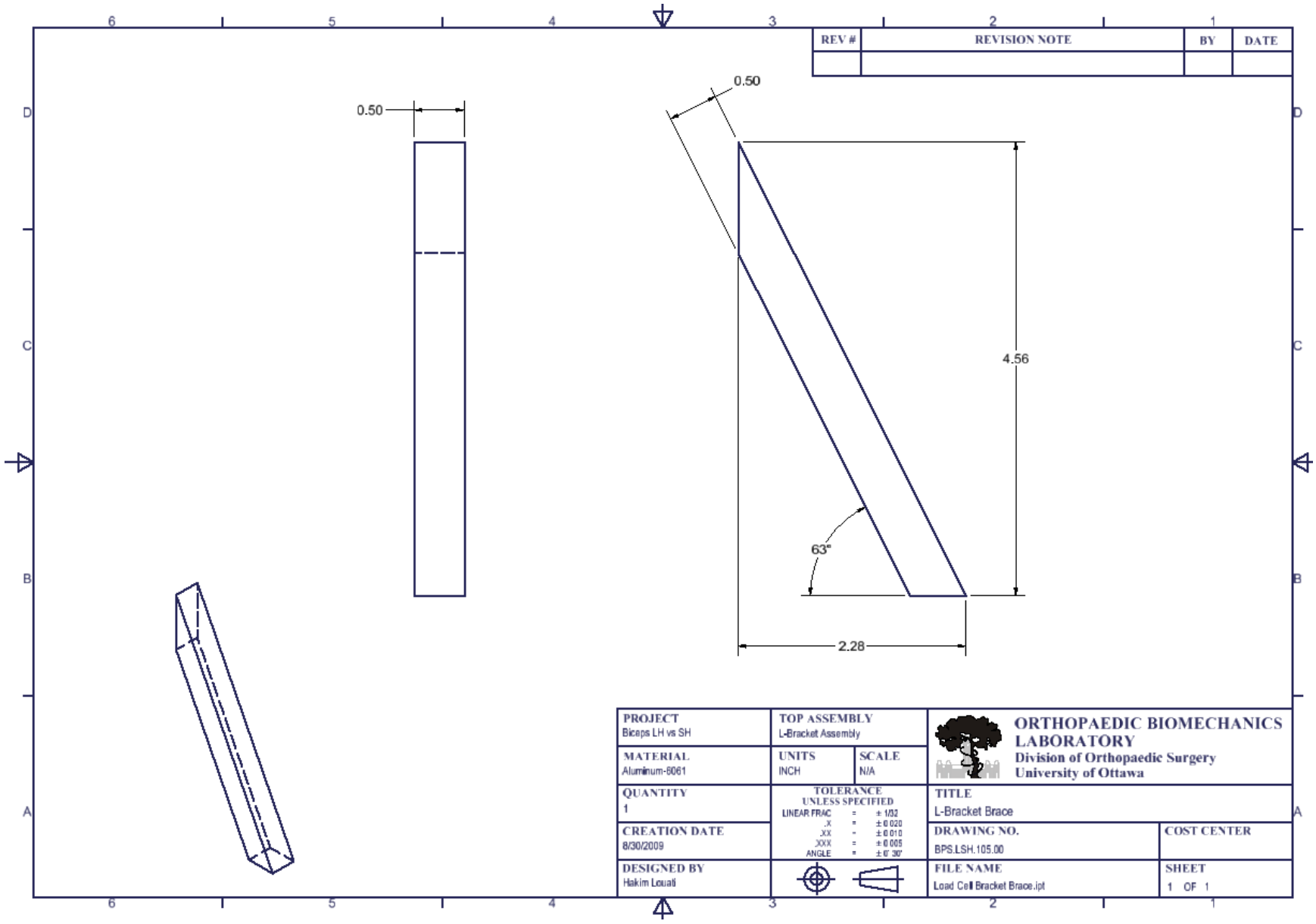
REV #
REVISION NOTE
BY
DATE
0.50
0.50
4.56
63°
2.28
PROJECT
Biceps LH vs SH
TOP ASSEMBLY
L-Bracket Assembly
MATERIAL
Aluminum-6061
UNITS
INCH
SCALE
N/A
QUANTITY
1
TOLERANCE
UNLESS SPECIFIED
LINEAR FRAC = ± 1/32
.X = ± 0.020
.XX = ± 0.010
.XXX = ± 0.005
ANGLE = ± 0° 30'
CREATION DATE
8/30/2009
DESIGNED BY
Hakim Louati
ORTHOPAEDIC BIOMECHANICS LABORATORY
Division of Orthopaedic Surgery
University of Ottawa
TITLE
L-Bracket Brace
DRAWING NO.
BPS.LSH.105.00
COST CENTER
FILE NAME
Load Cell Bracket Brace.ipt
SHEET
1 OF 1

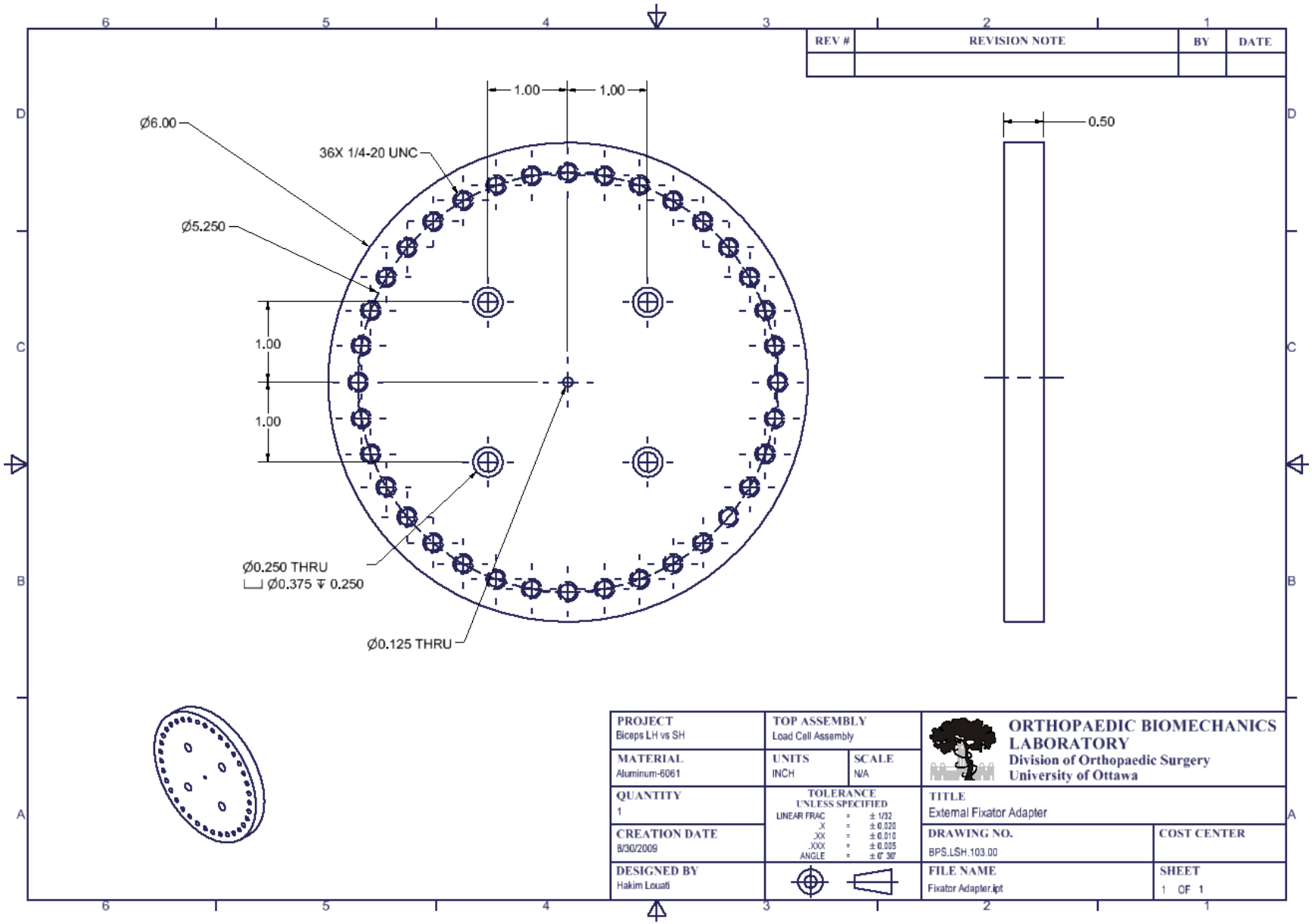
REV #
REVISION NOTE
BY
DATE
1.00
1.00
Ø6.00
36X 1/4-20 UNC
Ø5.250
1.00
1.00
Ø0.250 THRU
⌴ Ø0.375 ∓ 0.250
Ø0.125 THRU
0.50
PROJECT
Biceps LH vs SH
TOP ASSEMBLY
Load Cell Assembly
MATERIAL
Aluminum-6061
UNITS
INCH
SCALE
N/A
QUANTITY
1
TOLERANCE
UNLESS SPECIFIED
LINEAR FRAC = ± 1/32
.X = ± 0.020
.XX = ± 0.010
.XXX = ± 0.005
ANGLE = ± 0° 30'
CREATION DATE
8/30/2009
DESIGNED BY
Hakim Louati
ORTHOPAEDIC BIOMECHANICS LABORATORY
Division of Orthopaedic Surgery
University of Ottawa
TITLE
External Fixator Adapter
DRAWING NO.
BPS.LSH.103.00
COST CENTER
FILE NAME
Fixator Adapter.ipt
SHEET
1 OF 1

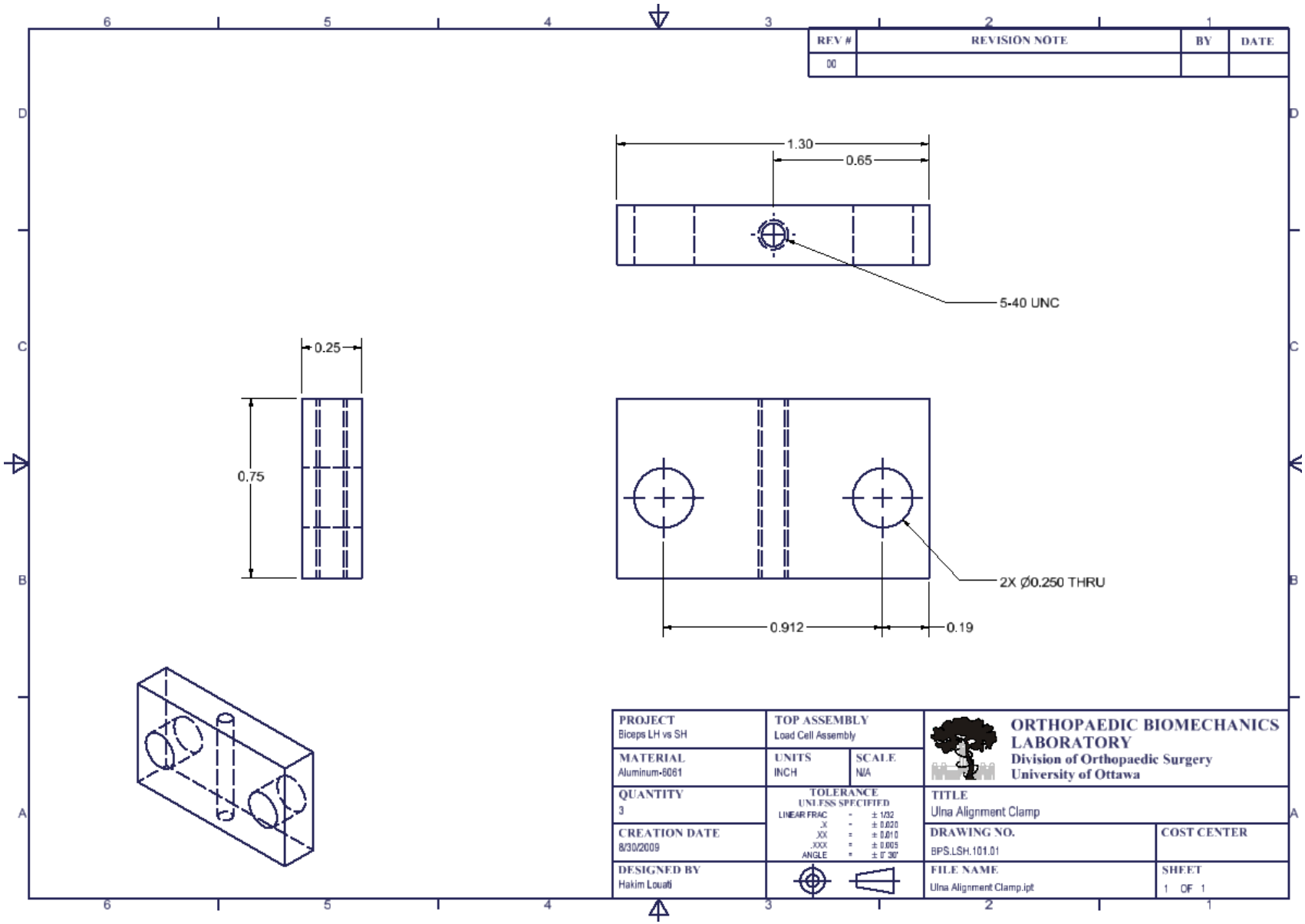
REV #
REVISION NOTE
BY
DATE
00
1.30
0.65
5-40 UNC
0.25
0.75
2X Ø0.250 THRU
0.912
0.19
PROJECT
Biceps LH vs SH
TOP ASSEMBLY
Load Cell Assembly
MATERIAL
Aluminum-6061
UNITS
INCH
SCALE
N/A
QUANTITY
3
TOLERANCE
UNLESS SPECIFIED
LINEAR FRAC - ± 1/32
.X - ± 0.020
.XX - ± 0.010
.XXX - ± 0.005
ANGLE - ± 0° 30'
CREATION DATE
8/30/2009
DESIGNED BY
Hakim Louati
ORTHOPAEDIC BIOMECHANICS LABORATORY
Division of Orthopaedic Surgery
University of Ottawa
TITLE
Ulna Alignment Clamp
DRAWING NO.
BPS.LSH.101.01
COST CENTER
FILE NAME
Ulna Alignment Clamp.ipt
SHEET
1 OF 1

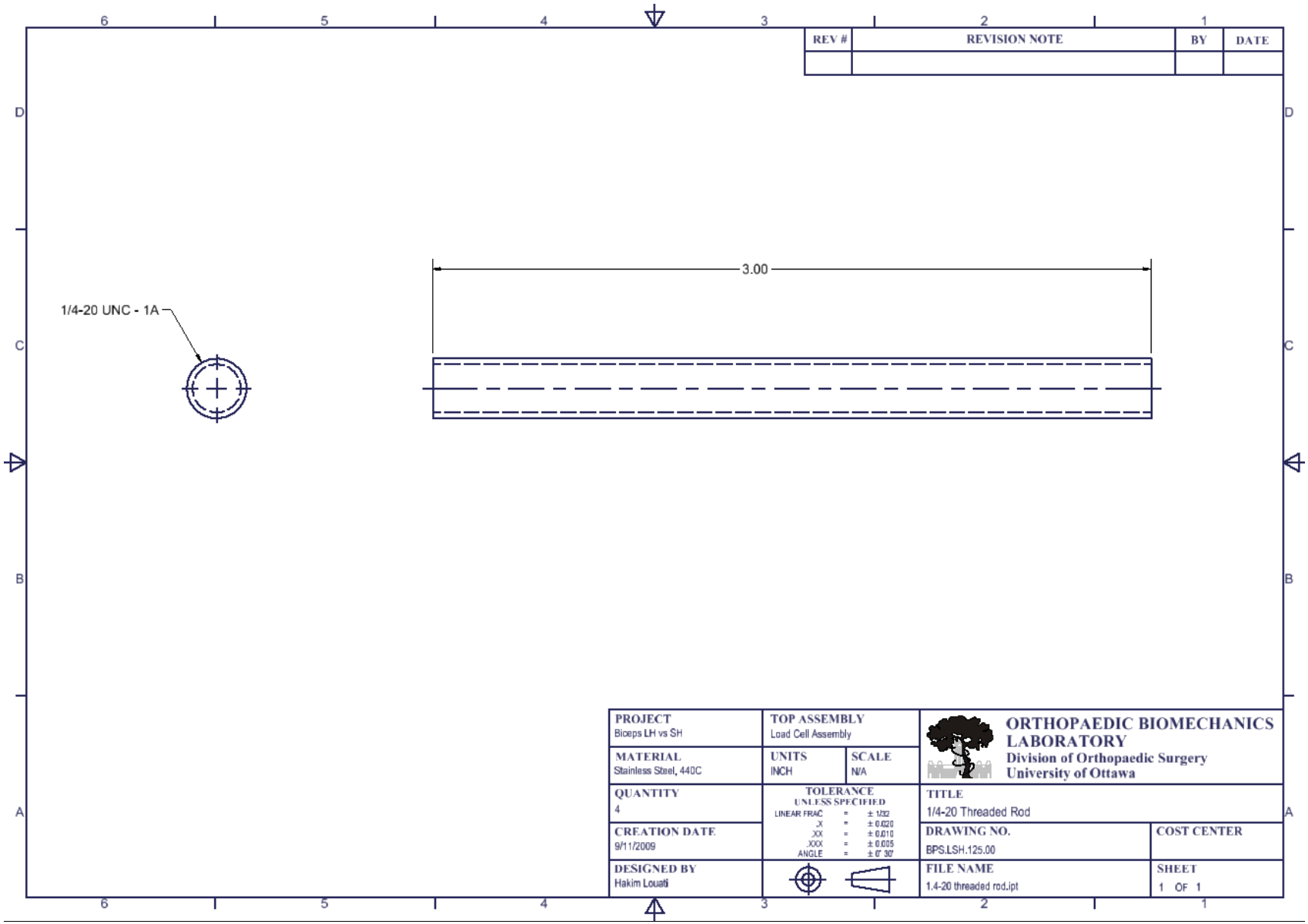
REV #
REVISION NOTE
BY
DATE
1/4-20 UNC - 1A
3.00
PROJECT
Biceps LH vs SH
TOP ASSEMBLY
Load Cell Assembly
MATERIAL
Stainless Steel, 440C
UNITS
INCH
SCALE
N/A
QUANTITY
4
TOLERANCE
UNLESS SPECIFIED
LINEAR FRAC = ± 1/32
.X = ± 0.020
.XX = ± 0.010
.XXX = ± 0.005
ANGLE = ± 0° 30'
ORTHOPAEDIC BIOMECHANICS LABORATORY
Division of Orthopaedic Surgery
University of Ottawa
TITLE
1/4-20 Threaded Rod
CREATION DATE
9/11/2009
DRAWING NO.
BPS.LSH.125.00
COST CENTER
DESIGNED BY
Hakim Louati
FILE NAME
1.4-20 threaded rod.ipt
SHEET
1 OF 1